MOLECULAR MECHANISMS OF MUTANT CARD11 SIGNALING TO NF-κB IN HUMAN DIFFUSE LARGE B CELL LYMPHOMA

by
Waipan Chan

A dissertation submitted to Johns Hopkins University in conformity with the requirements for the degree of Doctor of Philosophy

Baltimore, Maryland
March 2014

Abstract

Upon antigen receptor stimulation in both B and T lymphocytes, the signaling adapter CARD11 transforms from a closed inactive state to an open active scaffold that assembles into a multiprotein complex, leading to the activation of NF-κB, a critical pleiotropic transcription factor of the immune system. This scaffold transition is dysregulated by diffuse large B cell lymphoma (DLBCL)-associated oncogenic CARD11 mutations in humans that induce constitutive NF-κB activation and allow for the uncontrolled proliferation of cancer cells. Since these mutations had only been discovered within the Coiled-coil domain of CARD11, according to the existing signaling model, we speculate that similar oncogenic mutations also exist within the CARD domain. Using PCR-based domain random mutagenesis and a high-throughput quantitative signaling screen, we indeed identify 24 novel gain-of-function CARD11 missense mutations in the CARD domain and define a 19-residue mutational hotspot between the CARD and the Coiled-coil domain as the LATCH domain. Further mechanistic studies reveal that these hyperactive CARD11 mutants disrupt inhibitory domain binding, enhance Bcl10 association and its K63-linked ubiquitination, and promote human lymphoma cell survival. We also identify TRAF2 and TAK1 as required cofactors during the induction of K63-linked ubiquitination of Bcl10. When combining the most active CARD11 missense mutations in both the CARD and the Coiled-coil domain, we identify a super mutant that synergizes the signaling activities of two oncogenic CARD11 missense mutations – C49Y and L251P. Protein complex purification of this super mutant

along with mass spectrometry analysis identifies several CARD11 signaling cofactors including Bcl10, Malt1, IKKγ, CK1α and STUB1, in addition to a list of putative cofactors such as USP7, UBE3C, CKIIα, IGBP1, 14-3-3ε and EFHD2. Altogether, our study develops a highly efficient method for the discovery of mutational variants that promote tumorigenesis of NF-κB-dependent lymphomas, establishes a library of hyperactive CARD11 mutations with oncogenic potential, and provides a mechanistic understanding of how these mutants dysregulate the NF-κB signaling pathway. In addition, our data uncover critical components during the assembly of Bcl10 ubiquitination, a novel super-hyperactive CARD11 mutant, and several putative protein regulators of the CARD11 scaffold complex that are potentially dysregulated by oncogenic CARD11 mutations.

Ph.D. DISSERTATION REFEREES

Joel L. Pomerantz, Ph.D., Associate Professor of Biological Chemistry (advisor)

Peter Espenshade, Ph.D., Professor of Cell Biology (reader)

Acknowledgements

I am extremely grateful to my advisor, Joel Pomerantz, for all of his support and guidance throughout my entire graduate career. As a considerate mentor, Joel has been dedicated to offer his graduate students with an excellent nurturing environment. As a patient teacher, Joel has taught me very useful lessons about how to design my experiments with appropriate controls and troubleshooting strategies. As a skillful public speaker, Joel has shown me how to craft a fascinating oral presentation, an ingenious research proposal, and a concise publication manuscript. As a responsible scientist, Joel has always been encouraging about our scientific career, even amid the worst funding environment in decades. I am truly fortunate to be exposed to this remarkable quality of research training from Joel, without whom none of this dissertation work would have been possible.

The Pomerantz lab has been a very comfortable workplace for my studies throughout all these years, thanks to both the former and current lab members. I am particularly grateful to our former lab technician, Thomas Schaffer, for his fantastic pioneering work on the initial screening of novel CARD11 mutations; three former graduate students, Ryan McCully, Rebecca Lamason, and Stefanie Lew, for laying a solid foundation of biochemical assays for me to build upon. I have been especially impressed and inspired by the professional and respectful spirit of Rebecca, with whom I had countless troubleshooting conversations and insightful discussions. I would also like to thank our current lab technicians, Zhaoquan Wang and Julia Tritapoe, for their endless dedication to our routine lab maintenance.

Regarding research tools and reagents, I would like to thank the Synthesis & Sequencing Facility at Hopkins, for over hundreds of plasmid sequencing requests; Rakhi Jattani, for her assistance in generating the KD-CARD11 Jurkat T cell line; Corinne Hamblet, for introducing the Serial Cloner software to our lab; Richard Davis, for providing us the OCI-Ly3 ABC-DLBCL cell line; Hongxia Hu and Gregg Semenza, for sharing the pSUPER.retro.neo+GFP plasmid with us; Shinya Yamanaka, for sharing the pLenti6-Ubc-Slc7a1 ecotropic receptor plasmid via Addgene; Chao Lu, for sharing the Amicon filters and his technical experience in protein complex purification; Yongkang Yang, for his assistance during the final scale-up purification of mutant CARD11 (C49Y+L251P) protein complexes; Ross Tomaino, for the mass spectrometry identification services provided through the Taplin Facility at Harvard.

Having the great fortune to attend Hopkins for graduate studies is a critical step in my research career. This medical campus is always surrounded by various kinds of intellectual-stimulating seminars and discussions, where novel ideas are constantly being generated among physicians and scientists. Therefore, I am very grateful to the Immunology graduate program for recruiting me into this wonderful research environment and providing stipend support for my initial years of studies. Here I would also like to thank my thesis committee members: Ranjan Sen, Stephen Desiderio, Jonathan Powell, and Peter Espenshade, for their critical suggestions and helpful discussions during our meetings.

Finally, I have to thank my parents back in Macau, for sending me to the United States for college education and always being so supportive of my research career. I would also like to thank my wife, Iris, for her love and support.

Table of Contents

List of Tables

List of Figures

Chapter I:

Overview

Antigen Receptor Signaling to NF-κB

The pleiotropic transcription factor NF-κB is an important master regulator of cellular responses to various kinds of intracellular and extracellular stimulations including pro-inflammatory cytokines (such as TNF, IL-1 and IL-17), cellular stresses (such as ROS, UV and DSB), pathogen-associated molecular patterns (PAMPS), and the engagement of immunoreceptors (such as TCR and BCR) (1). In mammalian cells, the NF-κB proteins exist as homodimers or heterodimers consisting of p50/p105 (NF-κB1), p52/p100 (NF-κB2), p65 (RelA), RelB, and c-Rel, all of which contain a conserved N-terminal Rel homology domain (RHD) that mediates dimerization, IκB (inhibitor of NF-κB) and DNA binding (2). In the resting state, NF-κB remains in the cytoplasm due to its binding to IκB; upon cellular stimulation, activated IκB kinase (IKK) complex phosphorylates IκB, leading to its polyubiquitination and subsequent degradation by the 26S proteasome, thereby unmasking the nuclear localization signal (NLS) of NF-κB and allowing for its nuclear translocation (3). Target genes that are exposed to transcriptional regulation by NF-κB include cytokines (such as TNF, IL-1, IL-6 and IL-12), pro-survival and pro-proliferative molecules (such as Cyclin-D1, Bcl-xL, cFLIP and IAPs), antimicrobial products, non-coding micro-RNAs, adhesion and matrix-remodeling molecules (such as VCAM, ICAM and E-selectin), and lymphocyte activation and differentiation markers (such as IL-2, B7, MHC, Foxp3 and ROR) (1). As these transcriptional programs represent important biological functions in both innate

and adaptive immune systems, the molecular details of signaling pathways that lead to IKK and NF-κB activation have been topics of intense investigation.

The adaptive wing of immunity relies on the proper functions of both B and T lymphocytes, which recognize surrounding antigens by their surface expression of B cell receptor (BCR) and T cell receptor (TCR) respectively. Antigen receptor engagement triggers a complex and highly-regulated network of signaling cascades that ultimately lead to the activation of several transcription factors including NF-κB, NFAT and AP-1. Among these, the activation of NF-κB is particularly critical for lymphocytes and a sustained adaptive immune response as this master regulator allows for the survival, activation, growth and proliferation of both B and T lymphocytes. The extent and duration of BCR- and TCR-induced NF-κB activation are controlled by a number of mechanisms including the strength of antigen-receptor interaction with its ligand (antigen or peptide-MHC), the presence or absence of co-stimulatory signals (such as CD28, OX40, PD1 and CTLA4), and the signaling cascade components that are regulated based on cellular states (4, 5).

CARD11 (also known as CARMA1 or BIMP3) is a multidomain scaffold protein that is indispensable in both BCR- and TCR-induced activation of the IKK complex and the canonical NF-κB (p50/p65) (6–12). Conserved protein domains in CARD11 include CARD, Coiled-coil, PDZ, SH3 and GUK, which are separated by four intervening linker regions known as L1, Inhibitory Domain (ID) (13), L3 and L4. During the latent state, CARD11 is held in a closed inactive conformation by intramolecular interactions among the CARD, Coiled-coil and ID domains. Upon antigen receptor signaling, specific serine residues located within the ID are

phosphorylated by Protein Kinase C (PKCβ in B cells vs. PKCθ in T cells) and some other unidentified kinases (14–17). This series of posttranslational modifications transforms CARD11 into an open active conformation and allows CARD11 to recruit multiple positive signaling cofactors including the adapter Bcl10, the paracaspase MALT1, the TRAF6 E3 Ligase, the TAK1 kinase, Caspase-8 and IKKγ (13). Through some unclear mechanism, this complex of signaling molecules together activates the IKK complex, thereby allowing NF-κB to accumulate in the nucleus to regulate target genes. The CARD11-nucleated signaling complex is transient and disassembles following IKK complex activation, presumably returning CARD11 to an inactive state.

Dysregulation of NF-κB Signaling in Lymphoma

While the proper spatiotemporal onset of NF-κB activation can serve as a powerful master regulator to program B and T lymphocytes for mounting a host-protective immune response, it could become detrimental to the host when NF-κB activation is dysregulated and leads to diseases such as immunodeficiency, autoimmunity and various types of cancer (18). Therefore, the activation level of NF-κB must be exquisitely tuned by the immune system in order to prevent chaotic malfunction in either direction. Aberrant NF-κB activity likely contributes to oncogenesis through the unregulated transcriptional induction of pro-proliferative and anti-apoptotic genes that confer a survival advantage to transformed cells. In human lymphomas, somatic mutations often emerge to target signaling pathway components that are normally regulated by antigen receptor signaling.

Diffuse Large B Cell Lymphoma (DLBCL), the most common type of non-Hodgkin's lymphoma, is classified into three subtypes based on gene expression profiles: 1) activated B-cell-like (ABC) subtype; 2) germinal center B-cell-like (GCB) subtype; 3) primary mediastinal B-cell lymphoma (PMBL) (19). Characterized by constitutive activation of NF-κB, ABC-DLBCL is the least curable subtype with a 5-year survival rate of only 30% and poor prognosis. Interestingly, several oncogenic CARD11 mutations, almost exclusively located within the Coiled-coil domain, have been identified in patient-derived cell lines and biopsies from both ABC- and GCB-DLBCL (20). These Coiled-coil domain mutations were thought to dysregulate CARD11 signaling to NF-κB by enhancing the oligomerization state of CARD11, although this mechanism remains controversial and lacks biochemical evidence.

Recently, a more detailed molecular mechanism was elucidated (21) for two oncogenic CARD11 mutations that were identified in human DLBCL: F123I and L225LI (both located within the Coiled-coil domain). Without significant alteration of CARD11 oligomerization state, these two mutations were found to cause hyperactivity by disrupting the autoinhibitory CARD-Coiled-coil-ID binding that normally keeps CARD11 in a closed, inactive conformation in the absence of antigen receptor signaling. In addition, the F123I and L225LI mutations specifically enhance Bcl10 and (Bcl10-mediated) MALT1 recruitment to CARD11, suggesting the spontaneous formation of the CARD11-nucleated signaling complex. Upon TCR stimulation, K63-linked polyubiquitin chains are conjugated to Bcl10 on its K31 and K63 residues, in a process that requires both CARD11 and MALT1 (22). This modified form of Bcl10 occurs transiently and associates with IKKγ, presumably to

relay upstream activation signals to the IKK complex. The F123I and L225LI oncogenic mutations require Bcl10 residues K31 and K63 for hyperactive NF-κB signaling, indicating that Bcl10 ubiquitination is a target of dysregulation in DLBCL.

A critical question that emerged from the above study is whether oncogenic mutations utilizing similar molecular mechanisms could be identified from the CARD or the ID domain, assuming that mutations in these two domains are also sufficient to disrupt the CARD-Coiled-coil-ID autoinhibitory binding. We will address this issue in the next Chapter. Another critical question that remained unclear is whether there are other unidentified protein cofactors that get recruited to these hyperactive CARD11 signaling complexes. This issue will be discussed in more detail in Chapter III.

Chapter II:

A Quantitative Signaling Screen Identifies CARD11 Mutations in the CARD and LATCH Domains That Induce Bcl10 Ubiquitination and Human Lymphoma Cell Survival

This chapter originally appeared as: Chan, W., Schaffer, T.B., Pomerantz, J.L. A Quantitative Signaling Screen Identifies CARD11 Mutations in the CARD and LATCH Domains That Induce Bcl10 Ubiquitination and Human Lymphoma Cell Survival. *Mol Cell Biol*. 33(2):429-443 (2013).

Abstract

Antigen receptor signaling to NF-κB, essential for normal lymphocyte activation, is dysregulated in several types of lymphoma. During normal signaling, the multidomain adapter CARD11 transitions from a closed, inactive state to an open, active scaffold that assembles a multiprotein complex, leading to NF-κB activation. The regulation of CARD11 scaffold function is bypassed by lymphoma-associated oncogenic CARD11 mutations that induce spontaneous signaling. We report an unbiased high-throughput quantitative signaling screen that identifies new CARD11 hyperactive variants and defines a LATCH domain that functions with the CARD to promote CARD11 autoinhibition. Gain-of-function mutations in the LATCH or CARD disrupt Inhibitory Domain binding, promote Bcl10 association, and induce Bcl10 ubiquitination, NF-κB activation, and human lymphoma cell survival. Our results identify CARD11 mutations with oncogenic potential, provide a mechanistic explanation for their signaling potency, and offer a straightforward method for the discovery of variants that promote the tumorigenesis of NF-κB-dependent lymphomas.

Introduction

The activation of the NF-κB transcription factor by antigen receptor signaling is critical for lymphocyte activation during the adaptive immune response (23). NF-κB controls a variety of genes that participate in lymphocyte proliferation, survival, and differentiation, and the induction of NF-κB activity by antigen is tightly

regulated. Prior to antigen receptor engagement, NF-κB is held inactive in the cytoplasm of cells by the IκB family of inhibitory proteins. Antigen receptor signaling results in the activation of the IKK kinase complex, which phosphorylates IκBs, targeting them for ubiquitination and degradation, and allowing NF-κB to accumulate in the nucleus to regulate target genes. The extent and duration of NF-κB activation downstream of antigen recognition at the surface of B and T lymphocytes is controlled by a variety of mechanisms. These include the strength of antigen:receptor interaction, the presence or absence of concomitant costimulatory signaling, and the action of signaling cascade components that control the magnitude of signaling output as it is being induced or that provide negative feedback to terminate signaling (4, 5).

The exquisite regulation of NF-κB activity by the antigen receptor signaling pathway is disrupted in a variety of cancers of the immune system (18). Aberrant NF-κB activity likely contributes to oncogenesis through the unregulated transcriptional induction of pro-proliferative and anti-apoptotic genes that confer a survival advantage to transformed cells. Multiple mechanisms have been described by which lymphoid cancers achieve dysregulated NF-κB activation, including, for example, the overexpression or gain-of-function mutation of proteins that signal upstream of the IKK complex, the deletion or loss-of-function of inhibitory proteins that downmodulate or terminate signaling, and the overexpression of subunits of NF-κB itself (24).

CARD11 (CARMA1, BIMP3) is a multidomain scaffold protein that is required for B cell receptor (BCR) and T cell receptor (TCR)-mediated activation of the IKK

complex (6–12). CARD11 contains CARD, Coiled-coil, PDZ, SH3, and GUK domains, separated by four intervening regions. As a consequence of BCR or TCR engagement, CARD11 undergoes a conformational transition from a closed, inactive state to an open, active scaffold. This transition is controlled by an Inhibitory Domain (ID), located between the Coiled-coil and PDZ domains, that keeps CARD11 in the closed, latent state through interactions that require the CARD and Coiled-coil domains (13–15). Antigen receptor signaling leads to the neutralization of the ID through its phosphorylation at specific serine residues by PKCθ in T cells, PKCβ in B cells, IKKβ, and at least one additional unidentified kinase (14–17, 25). Subsequent to ID neutralization, CARD11 recruits several positive signaling cofactors into a complex, including the adapter Bcl10, the paracaspase MALT1, the TRAF6 E3 ligase, the TAK1 kinase, Caspase-8, and IKKγ (13). The formation of this complex is thought to elicit the activation of IKK kinase activity through the scaffolding and catalytic activities of each complex component, although the exact mechanistic details of how IKK kinase activity is engaged remain poorly defined. The CARD11-nucleated signaling complex is transient; following IKK activation, the complex disassembles, presumably returning CARD11 to the inactive state.

CARD11-dependent signaling is dysregulated in Diffuse Large B Cell Lymphoma (DLBCL), which has been divided into several subtypes based upon gene expression signatures (19). The Activated B Cell-like (ABC) subtype is characterized by constitutive activation of NF-κB, which is required for the proliferation and survival of ABC-derived cell lines in culture (26). An RNAi screen for genes required for this aberrant signaling to NF-κB revealed obligate roles for CARD11, Bcl10 and

MALT1 (27). In addition, approximately 10% of human ABC DLBCL samples examined by Lenz et al. exhibited gain-of-function mutations in CARD11 that conferred the protein with hyperactive signaling ability, thereby explaining in those cases the origin of the unregulated induction of NF-κB activity (28). Interestingly, most of the hyperactive mutations reported in DLBCL occurred in the Coiled-coil domain.

Recently, we characterized two oncogenic CARD11 mutations, F123I and L225LI, found in human DLBCL, and provided evidence that these mutations cause hyperactivity by disrupting the normal autoinhibition by the ID that keeps CARD11 inactive prior to receptor engagement, resulting in the spontaneous conversion of CARD11 from the closed, inactive state, to the open, active state in the absence of receptor triggering or ID phosphorylation (21). The F123I and L225LI mutations partially disrupted intramolecular binding of the ID and specifically enhanced the ability of CARD11 to associate with Bcl10, but not with several other cofactors examined. Signaling downstream of F123I and L225LI required Bcl10, and the ubiquitination of Bcl10 on K31 and K63 (21), a signaling step required for normal TCR signaling (22).

These findings provided a satisfying explanation for how mutations in the Coiled-coil could cause hyperactivity, since the Coiled-coil domain is one of the regions targeted by the ID in the inactive state. The results also predicted that any mutation that disrupts the ability of the ID to auto-inhibit CARD11 signaling should result in gain-of-function hyperactivity. However, most of the described human DLBCL mutations were found in the Coiled-coil domain and not, for example, in the

CARD domain, which has also been shown to be required for the intramolecular ID association that keeps CARD11 in the closed inactive state. The apparent concentration of oncogenic mutations in the Coiled-coil domain raised the question as to how frequently gain-of-function mutations occur outside the Coiled-coil domain, and if so, whether such mutations might confer a signaling potency comparable to those found in human DLBCL and achieve hyperactivity by the same mechanisms. In this report we address these questions by characterizing novel gain-of-function CARD11 mutants that we identified in a quantitative high-throughput signaling screen designed to detect the dysregulated CARD11-initiated activation of NF-κB.

Experimental Procedures

Primary and secondary screens for CARD11 gain-of-function mutations

A library of murine CARD11 variants containing random mutations between amino acid residues 1 and 138 was generated in the context of pc-CARD11 (13) by error-prone PCR under conditions that favored one mutation per clone using the GeneMorph II EZClone Domain Mutagenesis Kit (Stratagene) and primers 5'-GGATCCACTAGTAACGGCCGCC-3' and 5'-GCAGTTTGATGACCTCGTTCATCAG-3' according to the manufacturer's protocol. A total of 2220 individual clones were screened by transiently transfecting 50 ng of each clone, 20 ng of Igκ$_2$-IFN-LUC and 6 ng of CSK-LacZ into HEK293T cells in 24-well plates by the calcium phosphate method and assaying reporter activities as previously described (13). Each clone

that activated the Igκ$_2$-IFN-LUC reporter at least 3-fold more than wild-type CARD11 was considered positive and sequenced to identify its mutation. The region containing the identified mutation was recloned into the parental pc-CARD11 backbone and re-assayed to confirm hyperactivity.

Determination of specific activities in HEK293T and Jurkat T cells

Each verified mutant was titrated at subsaturating levels, between 1.5 and 27 ng, into the Igκ$_2$-IFN-LUC reporter assay in HEK293T cells, and protein concentration was determined by densitometric analysis of western blots as described previously (21). Relative specific activity was determined by taking the fold Igκ$_2$-IFN-LUC reporter activation elicited by a mutant at the same protein expression at which wild-type CARD11 elicited 3-fold activation and dividing by 3. CARD11-KD Jurkat T cells were transfected with Igκ$_2$-IFN-LUC and CSK-LacZ as previously described (13) using 50-90 ng of expression construct for each CARD11 variant to achieve equivalent protein expression level. The relative activity in T cells was determined by taking the fold Igκ$_2$-IFN-LUC reporter activation elicited by a mutant and dividing by the fold achieved by wild-type CARD11 at the comparable level of expression.

Immunoprecipitations in HEK293T cells

One day prior to transfection, 5x10^5 HEK293T cells were plated in each well of a six-well plate. A total of 2 μg DNA per well was transfected using the calcium phosphate method. The medium was changed 22 to 26 h posttransfection, and the

cells were harvested 42 to 46 h posttransfection. Cells were lysed in 300 or 500 µl of immunoprecipitation lysis buffer (IPLB) and debris was removed as described previously (13). 6 or 20 µl of cell lysate was saved for western blot analysis and 264 or 450 µl was incubated with 1 µg of anti-FLAG antibody (Sigma F7425) for 90 to 120 min at 4°C with rotation. 7 or 10 µl bed volume of protein G-Sepharose 4 Fast Flow (GE Healthcare) was added and incubated for 90 to 120 min at 4°C with rotation. The resulting immunocomplex was washed with IPLB four times for 5 min at 4°C with rotation, eluted twice, pooled, and resolved for western blot analysis as described previously (21) using anti-myc (sc-40; Santa Cruz), anti-FLAG (M2; Eastman Kodak IB13026 or Sigma F1804), and anti-Bcl10 (sc-5273; Santa Cruz). The levels of each CARD11 variant in the input and the IP were determined by densitometric analysis of subsaturating exposures of western blots using ImageJ. To quantitate Bcl10 binding for each variant, the ratio of the quantity of the variant in the IP divided by that in the input was determined and then normalized to the ratio achieved by the ΔID.

Glutathione-Sepharose Pull Downs

Gain-of-function mutations were introduced into the context of pc-ΔID (13). pEBB-HA-ID-GST (13), pEBG (13) and each pc-ΔID variant were transfected separately into HEK293T cells and harvested as described above. Cells from each well of a six-well plate were lysed in 500 µl of IPLB and debris was removed as described above. Between 0.2 and 5.4% of lysates was first analyzed by western blot to quantify the protein expression of each ΔID variant. A titration of ΔID

variant-containing extract was mixed with equivalent fractions of extract containing either HA-ID-GST or GST, and extract from pcDNA3-transfected cells to make a total volume of 500 µl. Mixed lysates were precleared twice by incubating with 10 µl bed volume of Protein G Sepharose for 30 to 50 min at 4°C with rotation. From the precleared mixed lysates, 4.4% was saved as input for western blot analysis and the remaining 450 µl was incubated with 10 µl bed volume of Glutathione-Sepharose (GE Healthcare) for 15 to 17 h at 4°C with rotation. Samples were washed and analyzed as described previously (13) using anti-myc (sc-40; Santa Cruz) and anti-GST (sc-459; Santa Cruz). The levels of each CARD11 variant in the input and the pulldown were determined by densitometric analysis of subsaturating exposures of western blots using ImageJ. To quantitate ID binding for each variant, the ratio of the quantity of the variant in the pulldown divided by that in the input was determined and then normalized to the ratio achieved by the ΔID at a comparable level of expression.

Bcl10-deficient HEK293T and CARD11-, MALT1-, and TRAF6-deficient Jurkat T cell lines

The KD-GFP and KD-Bcl10 HEK293T cell lines have been described (13). CARD11 variant and Bcl10 expression was assessed in these lines by western blot using anti-myc (sc-40; Santa Cruz) and anti-Bcl10 (sc-5273; Santa Cruz). To generate the KD-CARD11 Jurkat T cell line, a self-inactivating lentiviral construct based upon the vector pLKO.1 was constructed to express the sihCARD11-2 short hairpin RNA (Sense sequence: 5'-TGGTCAAGAAGCTGACGATTC-3'; loop sequence:

5’-TTCAAGAGA-3’) downstream of the human U6 RNA promoter. Lentiviral particles were packaged as described previously (29). After clearing cell debris by centrifugation at 2300 x g for 5 min, 100 µl of viral supernatant was added to 1.5 x 10^5 Jurkat T cells in a final volume of 300 µl in a 24-well plate. Approximately 24 h post-infection, cells were resuspended in fresh medium containing 0.5 µg/ml puromycin and selected for 1 week. Puromycin-resistant Jurkat T cells were maintained in media containing 0.5 µg/ml puromycin.

To generate the KD-NT, KD-MALT1, and KD-TRAF6 Jurkat T cell lines, pLKO.1-based lentiviruses were constructed to express either shNT (Sigma SHC002; Sense sequence: 5’-CAACAAGATGAAGAGCACCAA-3’; loop sequence: 5’-CTCGAG-3’), shM1 ((13); Sense sequence: 5’-CCTCACTACCAGTGGTTCAAA-3’; loop sequence: 5’-CTCGAG-3’), or shT6 ((30); Sense sequence: 5’-CCACGAAGAGATAATGGAT-3’; loop sequence: 5’-TTCAAGAGA-3’). To package these lentiviruses, HEK293T cells were plated at 5x10^5 cells per well in a 6-well plate and transfected 24 h later using calcium phosphate with 520 ng pMDL-RRE, 182 ng RSV-Rev, 260 ng pCMV-VSVg, and 1040 ng pLKO.1-based vector. The medium was replaced with 2ml RPMI 22 to 24 h posttransfection. Supernatants containing viral particles were harvested 47 to 48 h posttransfection after clearing cell debris by centrifugation at 18,000 x g for 5 min. 1 ml of viral supernatant was added to 6x10^6 Jurkat T cells in a final volume of 12 ml in a 10-cm plate. Approximately 24 h post-infection, cells were resuspended in fresh RPMI medium containing 0.5 µg/ml puromycin and selected for 10 days. Knockdown was assessed by western blot using anti-MALT1 (catalog# 1664-1;

Epitomics), anti-TRAF6 (sc-7221; Santa Cruz), and anti-IKKα (sc-7606; Santa Cruz) antibodies.

TAK1 inhibition assays

(5Z)-7-oxozeaenol was obtained from Calbiochem (product code 499610). Either DMSO vehicle or 500 nM (5Z)-7-oxozeaenol was added to each sample every twelve hours after transfection for a total of three doses and samples were harvested 41 hours after transfection. Some samples were stimulated with anti-CD3/anti-CD28 crosslinking as described (29) for four hours before harvest.

Stable expression of murine CARD11 variants in Jurkat T cells

Gain-of-function mutations were introduced into the context of pCLIP3A-myc-CARD11-mCherry (29), a Moloney murine leukemia virus-based vector. To package viruses, HEK293T cells were plated at $5x10^5$ cells per well in a 6-well plate and transfected 24 h later using calcium phosphate with 430 ng pCL-SIN-Ampho (31), 430 ng pCMV-VSVg (32), and 1140 ng pCLIP3A-myc-CARD11-mCherry-based vector. The medium was replaced with 2 ml RPMI complete medium 22 to 24 h posttransfection. Supernatants containing viral particles were harvested 49 to 50 h posttransfection after clearing cell debris by centrifugation at 200 x g for 5 min. For each sample, 1.8 ml viral supernatant was added to 5.4×10^6 Jurkat T cells in a final volume of 10.8 ml in a 10-cm plate. Approximately 24 h post-infection, cells were resuspended in fresh medium containing 0.5 μg/ml puromycin and selected for 2

weeks. Puromycin-resistant Jurkat T cell lines were maintained in media containing 0.5 μg/ml puromycin.

NF-κB DNA-binding assays

Electrophoretic Mobility Shift Assays (EMSA) were done as described (11).

Endogenous Bcl10 and IKKγ immunoprecipitations in Jurkat T cell lines

The control Jurkat T cell line stably expressing myc-wild-type-CARD11-mCherry was stimulated with 50 ng/ml PMA (Sigma) and 1 μM ionomycin (Sigma) for 20 min at 37°C. Cells (10^8 per sample) were then incubated in an ice water bath for 5 min, spun at 423 x g for 10 min at 4°C, and lysed in a lysis buffer as described previously (33) except that 10% glycerol was added and a different protease inhibitor cocktail (Sigma P8340) was used. Cell lysates were precleared twice with 20 μl bed volume of Protein A-Sepharose (Sigma P9424) or Protein G-Sepharose for 1 to 2 h at 4°C with rotation. To analyze Bcl10 ubiquitination, the precleared lysates were denatured and diluted as described previously (22) and then incubated with 4 μg of anti-Bcl10 (sc-5611; Santa Cruz) antibody for 16 h at 4°C with rotation. A 20-μl bed volume of Protein A-Sepharose was added to each sample and incubated for 20 to 22 h at 4°C with rotation. To analyze the interaction between IKKγ and Ub_n(K63)-Bcl10, the precleared lysates were incubated with 3 μg of anti-IKKγ (sc-8330; Santa Cruz) antibody for 16 h at 4°C with rotation and then incubated with 30 μl bed volume of Protein G-Sepharose for 4 to 5 h at 4°C with rotation. Samples were washed and analyzed as described previously (13). Western blots were

analyzed using anti-Ub-K63 (14-6077-82; eBioscience), anti-Bcl10 (sc-5273; Santa Cruz), anti-myc (sc-40; Santa Cruz), and anti-IKKγ (sc-8032; Santa Cruz).

Stable expression of murine CARD11 variants in OCI-Ly3 cells

The OCI-Ly3 ABC-DLBCL cell line was a kind gift from Dr. R. Eric Davis (M.D. Anderson). Cells were cultured in OCI medium which contains Iscove's modified Dulbecco medium supplemented with 20% human serum (S40110; Atlanta Biologicals), 50 U/ml each of penicillin and streptomycin, and 55 μM of β-mercaptoethanol in humidified 5% CO_2 at 37°C. First, OCI-Ly3 cells stably expressing the ecotropic receptor mCAT-1 were generated by infecting cells with the lentivirus pLenti6/Ubc/mSlc7a1 (Addgene Plasmid 17224) (34). To package this lentivirus, HEK293T cells were plated at $5x10^5$ cells per well in a 6-well plate and transfected 24 h later using calcium phosphate with 1040 ng pLenti6/Ubc/mSlc7a1, 520 ng pMDL-RRE (35), 182 ng RSV-Rev (35), and 260 ng pCMV-VSVg (32). The medium was replaced with 2 ml OCI medium 22 to 24 h posttransfection. Supernatants containing viral particles were harvested 47 to 48 h posttransfection after clearing cell debris by centrifugation at 423 x g for 5 min. 800 μl of viral supernatant was added to 1.2×10^6 OCI-Ly3 cells in a final volume of 4.8 ml in a 6-well plate. Approximately 48 h post-infection, cells were resuspended in fresh OCI medium containing 2 μg/ml blasticidine and selected for 2 weeks.

mCAT-1 expressing OCI-Ly3 cells were then infected with the same panel of CARD11-mCherry-expressing retroviruses as those used to infect Jurkat T cells. pCLIP3A-myc-CARD11-mCherry variants were transfected and packaged as

described above. The medium was replaced with 2 ml OCI medium 22 to 24 h posttransfection. Supernatants containing viral particles were harvested 49 h posttransfection after clearing cell debris by centrifugation at 18000 x g for 5 min. For each sample, 1 ml viral supernatant was added to 1.5 x 10^6 mCAT-1-expressing OCI-Ly3 cells in a final volume of 6 ml in a 10-cm plate. Approximately 25 h post-infection, cells were resuspended in fresh OCI medium containing both 0.5 μg/ml puromycin and 2 μg/ml blasticidine, and selected for 2 weeks. Puromycin and blasticidine double-resistant OCI-Ly3 cell lines were maintained in OCI medium containing both 0.5 μg/ml puromycin and 2 μg/ml blasticidine. Relative levels of CARD11 variants were assessed by western blot using anti-myc (sc-40; Santa Cruz), anti-CARD11 (cat# 3189; ProSci), and anti-IKKα (sc-7606; Santa Cruz) antibodies.

OCI-Ly3 Proliferation and Survival Assay

Retroviral constructs based upon the vector pSUPER.retro.neo+GFP (pSRGN, Oligoengine) were constructed to express either sihCARD11-2 (Sense sequence: 5'-TGGTCAAGAAGCTGACGATTC-3'; loop sequence: 5'-TTCAAGAGA-3') or sihNT control (Sense sequence: 5'-TTCTCCGAACGTGTCACGT-3'; loop sequence: 5'-TTCAAGAGA-3') (36) short hairpin RNAs (shRNAs) downstream of the H1 RNA promoter, and the EGFP gene downstream of the phosphoglycerate kinase promoter. To package retroviruses, HEK293T cells were plated at 5x10^5 cells per well in a 6-well plate, and transfected 24 h later using Lipofectamine 2000 (Invitrogen) with 800 ng pCL-Eco (31) and 3200 ng pSRGN-derived construct. The medium was replaced with 1.25 ml OCI medium 25 h posttransfection. Supernatants containing

viral particles were harvested 55 h posttransfection after clearing cell debris by filtration through a 0.45 mm filter. 500 µl of viral supernatant was added to 2 x 10^5 OCI-Ly3 cells in a final volume of 1 ml in a 12-well plate, followed by the addition of 3 µg/ml polybrene. 12 to 18 h post-infection, cells were resuspended in fresh OCI medium. GFP^+ percentages measured by FACS 3 days post-infection ranged from 26.2 to 42.6% as compared to the uninfected OCI-Ly3 control cell line. Data were processed as described previously (27), except that the initial GFP^+ data were collected 3 days after retroviral transduction.

Results

Identification of novel gain-of-function mutations in CARD11 in a high-throughput signaling screen

Because of the requirement of the CARD domain for intramolecular ID association, we hypothesized that some CARD domain residues would mediate interactions that maintain CARD11 in the inactive state prior to ID neutralization by antigen receptor signaling. To test this hypothesis we adapted screening methodology previously used to identify molecules that signal to NF-κB (11) or that enhance or suppress the signaling activity of CARD11 (29, 37). We generated a library of CARD11 variants in the context of a mammalian expression vector, in which residues between M1 and L138 of murine CARD11 were randomly mutated by error-prone PCR. Library clones were screened using a quantitative reporter assay in HEK293T cells using the $Ig\kappa_2$-IFN-LUC reporter in a transient transfection

to assess NF-κB activation (Figure 2.1A). For normalization of transfection efficiency and extract recovery, each transfection also included CSK-LacZ, which constitutively expresses β-galactosidase. A clone was considered positive if it activated the reporter at least 3-fold more than wild-type CARD11 expressed at a comparable level. Positive clones were sequenced to identify mutations, and back-cloned into an otherwise wild-type CARD11 expression vector to confirm that the mutation identified between residues 1 and 138 was responsible for eliciting the enhanced signaling activity. After screening 2220 clones, we identified 24 gain-of-function mutations in this region of CARD11 (Figure 2.1B). Nine of these mutations resided in the CARD domain, and one mutation was located in the Coiled-coil domain. Surprisingly, fourteen mutations occurred in the nineteen-residue region located between the CARD and Coiled-coil domains (Figure 2.1B and 2.1C). This region of CARD11 has not been extensively characterized in previous studies. The high density of gain-of-function mutations between residues 112 and 130 defines this region as a functional domain that negatively regulates CARD11 activity. We refer to this region as the LATCH domain.

The specific activity of each variant that emerged from the screen was first determined by titrating its expression in the Igκ$_2$-IFN-LUC reporter assay in HEK293T cells. At equivalent levels of protein expression, the collection of variants displayed activities that were between 2.3- and 31-fold more active than wild-type CARD11 (see Figure 2.2A, 2.2B for example titrations and Table 2.1). For comparison, an ID-deleted variant, CARD11 ΔID, was 43.6 fold more active than wild type under these conditions. The collection of variants displayed similar relative

potencies when expressed in a transient transfection assay in CARD11-deficient Jurkat T cells (Figure 2.2C, 2.2D and Table 2.1), indicating hyperactivity in both lymphoid and non-lymphoid cells. The most potent mutations were distributed between the CARD and LATCH domains, and included C49Y and F97Y in the CARD domain, and G123D, V119E, and G126D in the LATCH domain. Many of the mutations had effects on CARD11 activity that were comparable to or greater than those described previously for the F123I and L225LI mutations found in human DLBCL, which were found to increase specific activity by 12.6 and 28.1-fold in previous studies (21). We note that the numbering scheme used previously (21, 28) to describe F123I and L225LI was based on a human CARD11 sequence that did not account for seven N-terminal residues; F123 and L225 correspond to F130 and L232 in our numbering scheme for murine CARD11 (11).

Gain-of function mutations confer a selective ability to associate with Bcl10

We next determined whether the gain-of-function mutations conferred an enhanced ability for CARD11 to interact with the signaling cofactors that have been previously shown to associate with CARD11 in a signal-dependent and ID-regulated manner (13). We co-expressed each variant with FLAG-tagged Bcl10 in HEK293T cells and assessed the degree to which each mutant co-immunoprecipitated with Bcl10, using wild-type CARD11 and the CARD11 ΔID as negative and positive controls, respectively. Eighteen of the gain-of-function mutants displayed enhanced abilities to associate with Bcl10 in this assay, as compared to wild-type CARD11 (Figure 2.3 and Table 2.1). The relative ability to associate with Bcl10 roughly

correlated with the ability of each variant to activate NF-κB, especially in Jurkat T cells (Table 2.1). For example, the mutations that had the strongest effect on Bcl10 association, C49Y, F97Y, G123D, G126D, and V119E, were the same mutations that elicited the greatest enhancements of activity in the Igκ$_2$-IFN-LUC reporter assay. Five mutants did not display any enhanced association with Bcl10 (H31L, M32K, T112I, T117A, and E122D), and these were among the weakest gain-of-function mutants for NF-κB activation in Jurkat T cells. These data clearly indicate that most gain-of-function mutations identified enhance Bcl10 association with CARD11. In addition, the results reveal that the LATCH domain plays a critical role in controlling the CARD11:Bcl10 interaction.

We also tested whether the gain-of-function mutants affected the association of CARD11 with TAK1, TRAF6, Caspase-8, or IKKγ in similar immunoprecipitation studies. Interestingly, none of the mutations enhanced the interaction with any of these proteins (data not shown), indicating a selective effect on the Bcl10:CARD11 interaction. The F123I and L225LI mutations found in human DLBCL have the same cofactor-selective effect on Bcl10 association (21). Since mutation of fourteen out of nineteen residues in the LATCH domain had no effect in these assays, the results suggest that the LATCH domain does not control the interaction between CARD11 and TAK1, TRAF6, Caspase-8, or IKKγ.

MALT1 directly associates with Bcl10 and can be recruited to the F123I and L225LI mutants in a Bcl10-dependent manner (21). We found that none of the gain-of-function mutations identified in the CARD or LATCH domains was able to confer detectable binding to MALT1 in immunoprecipitation studies in the absence of co-

expressed Bcl10 (data not shown). We then tested four of the most active variants isolated in our screen to see if their mutations would allow Bcl10-dependent recruitment of MALT1 to CARD11. As shown in Figure 2.4, FLAG-tagged MALT1 could associate with the C49Y, F97Y, G123D, and G126D mutants when coexpressed in the presence of Bcl10, indicating that when bound to these mutants, Bcl10 is competent to recruit MALT1 to CARD11. The effect of these mutations in this assay was comparable to that achieved by deletion of the ID.

Gain-of function mutations perturb ID binding

We have previously shown that the ID can associate *in trans* with the CARD11 ΔID construct in a manner that depends upon the CARD and Coiled-coil domain (13). The F123I and L225LI oncogenic mutations found in human DLBCL reduce this association (21). To test the hypothesis that the gain-of-function mutations we isolated also disrupt ID binding we introduced each mutation into the context of the CARD11 ΔID construct and tested for their association with an ID-GST fusion protein under subsaturating conditions after expression in HEK293T cells. All 24 mutations reduced ID binding *in trans* in this assay (Figure 2.5 and Table 2.1) to varying degrees. The strongest effects on ID binding were observed for 12 mutants, 7 in the CARD domain (H31L, M32K, C49Y, K50M, N62Y, E93D, F97Y), and 5 in the LATCH domain (T112I, R113Q, R114I, I118V, G123D), all of which displayed 0-20% of the ID binding observed with the unmutated CARD11 ΔID. These data are consistent with the prediction that gain-of-function mutations would impact the ability of the ID to participate in intramolecular inhibitory interactions. In addition,

the results reveal a previously unappreciated role for the LATCH domain in promoting ID binding.

Hyperactive mutants require Bcl10, MALT1, TRAF6, and TAK1 for signaling to NF-κB

Bcl10 is a required signaling cofactor for CARD11 in normal antigen receptor signaling (38) as well as for the F123I and L225LI oncogenic variants that signal independently of receptor triggering (21). To confirm that the novel hyperactive mutants we identified also require Bcl10 for signaling to NF-κB, we tested the effect of knocking down Bcl10 on their activities in the Igκ$_2$-IFN-LUC reporter assay in HEK293T cells. As expected, the activity of all mutants, regardless of their potency, was severely diminished as a result of Bcl10 deficiency (Figure 2.6 and data not shown).

For several of the most active variants, we also tested the dependence of their signaling activity on MALT1, TRAF6, and TAK1. We compared the activities of the G123D, F97Y, C49Y, G126D, V119E, and Y98F in Jurkat T cell lines that stably expressed a control short hairpin RNA (KD-NT) or one that targeted MALT1 (KD-MALT1) or TRAF6 (KD-TRAF6). As shown in Figure 2.7, the 75% and >75% reduction in MALT1 and TRAF6 levels, respectively, reduced the apparent activity of all of the mutants tested, as assessed in the Igκ$_2$-IFN-LUC reporter assay (Figure 2.7A to 2.7C). To test the requirement for TAK1, we treated Jurkat T cells with 5Z-7-oxozeaenol, a specific inhibitor of TAK1 (39, 40), after transient expression of these variants in the reporter assay. As shown in Figure 2.7D, the signaling activity of all

variants tested was inhibited by 5Z-7-oxozeaenol to a level similar to that observed after ΔID expression or treatment with anti-CD3/anti-CD28 antibodies.

Gain-of-function variants induce K63-linked ubiquitination of Bcl10 and the association of Ub_n(K63)-Bcl10 with IKKγ

The K63-linked ubiquitination of the CARD domain of Bcl10 on K31 and K63 is a required step downstream of CARD11 action in the TCR signaling pathway to NF-κB (22). Furthermore, we demonstrated that the F123I and L225LI oncogenic variants fail to activate NF-κB in the presence of a Bcl10 mutant containing arginine substitutions at K31 and K63 (21), suggesting that F123I and L225LI also depend upon Bcl10 ubiquitination for their dysregulated signaling. To test whether gain-of-function mutations in the CARD and LATCH domains spontaneously induce the K63-linked ubiquitination of Bcl10, we used retroviral-mediated infection to establish a panel of Jurkat T cell lines that stably expressed twelve variants with a range of specific activities. Five of these variants harbored mutations in the CARD domain (M32K, C49Y, N62Y, E93D, and Y98F) while 7 contained LATCH domain mutations (T112I, E121G, E122D, G123D, G126D, L127I, and F130Y). To confirm that each variant spontaneously activated NF-κB after stable expression, we transfected each line with the $Igκ_2$-IFN-LUC reporter and compared the fold induction to that observed with a control line expressing wild-type CARD11 in the absence and presence of PMA/ionomycin treatment, which mimics signaling downstream of the TCR. As shown in Figure 2.8A, stable expression of wild-type CARD11 did not induce appreciable reporter activation, while PMA/Iono treatment of this line

resulted in 27-fold reporter activation. As expected, many of the gain-of-function variants spontaneously activated the reporter at levels of expression comparable to the wild-type control (Figure 2.8A). The C49Y and G123D variants were the most potent, achieving levels of activation similar to that observed with PMA/Iono treatment of the control line. The activity of the stably expressed gain-of-function variants also led, as expected, to the spontaneous induction of nuclear NF-κB DNA binding activity, as revealed by EMSA analysis of nuclear extracts using a consensus κB site DNA probe (Figure 2.8B). The extent of induction of NF-κB DNA-binding activity closely correlated with the activities exhibited in the reporter assay.

To probe for K63-linked ubiquitination of Bcl10, Bcl10 was immunoprecipitated from denatured cell lysates from these lines (22), and assessed for the presence of conjugated ubiquitin using K63-linkage-specific antibodies. K63-linked ubiquitinated Bcl10 (Ub_n(K63)-Bcl10) was detected in the presence of ten of the variants, but not in the presence of the two weakest variants (Figure 2.8C and 2.8E). The levels of Ub_n(K63)-Bcl10 correlated remarkably well with the specific activities displayed in the NF-κB reporter and EMSA assays. In addition, the levels of unconjugated Bcl10 inversely correlated with the activity of each variant (Figure 2.8C).

Since Ub_n(K63)-Bcl10 has been shown to associate with IKKγ during TCR signaling (22), we immunoprecipitated IKKγ from lysates from these stable lines and probed for the presence of associated Ub_n(K63)-Bcl10. Indeed, we observed that Ub_n(K63)-Bcl10 associated with IKKγ to an extent that correlated with the degree of NF-κB activation in the reporter and EMSA assays (Figure 2.8D and 2.8F).

These data indicate that several of the gain-of-function variants induce K63-linked ubiquitination of Bcl10 and the association of Ub_n(K63)-Bcl10 with IKKγ, even in the absence of antigen receptor engagement or signaling upstream of CARD11. In addition, they strongly suggest that residues in both the CARD (C49, N62, E93, and Y98) and LATCH (T112, E122, G123, G126, L127, and F130) domains function to prevent spontaneous Bcl10 ubiquitination and the association of Ub_n(K63)-Bcl10 with IKKγ, two critical CARD11-dependent steps in IKK complex activation by antigen receptor signaling.

Gain-of-function mutations in the CARD and LATCH domains can promote the growth of a human DLBCL line in culture

The OCI-Ly3 cell line, which is representative of the ABC subtype of DLBCL harbors the L244P oncogenic variant of CARD11 and relies on CARD11-dependent signaling to NF-κB for survival and proliferation in culture (28). We adapted an assay originally developed by Lenz et al. (28) to assess the potential for hyperactive CARD11 variants to substitute for the L244P variant in this OCI-Ly3 line. We stably introduced ten murine CARD11 variants into the OCI-Ly3 line by retroviral transduction, and then superinfected the stable lines with a retrovirus that coexpressed GFP with an shRNA that could target the endogenous human L244P CARD11 mRNA by RNA interference (shC11). As previously demonstrated (28), the parental OCI-Ly3 line was highly sensitive to CARD11 L244P knockdown, as indicated by the 56% loss of GFP^+ cells over 18 days in culture (Figure 2.9A). The presence of the hairpin-resistant murine L244P oncogenic mutant served as a

positive control for the assay and rescued a significant fraction of the cells, resulting in an increased survival of GFP^+ cells over the same time course (Figure 2.9A). Among the nine gain-of-function mutants tested, the G123D, G126D, C49Y, and L127I mutants showed the best abilities to rescue the OCI-Ly3 cells (Figure 2.9A). The E93D, Y98F and F130Y mutants also displayed significant rescue ability, while the T112I and N62Y mutants only conferred a slight cell survival advantage, as compared to the OCI-Ly3 parental control (Figure 2.9B). An assessment of the expression levels of the different hyperactive variants (Figure 2.9C) indicated that the level of the G123D variant was slightly higher than other variants, while those of L244P, N62Y, and T112I variants were slightly lower. Analysis of GFP^+ cells from four lines revealed that expression of the shC11 hairpin resulted in 50-60% reduction in endogenous CARD11 expression under the conditions of this experiment (Figure 2.9D). Overall, there was a good correlation between the specific activities of the variants for rescue in this assay and their abilities to activate NF-κB when stably expressed in Jurkat T cells (Figure 2.8A), with the exception of the L127I mutant, which had greater relative OCI-Ly3 rescue activity than expected. The results indicate that gain-of-function mutations in both the CARD (C49Y, E93D, Y98F) and the LATCH (G123D, G126D, L127I, F130Y) domains can provide sufficient activity to promote the survival of human DLBCL-derived cells that depend on NF-κB activation for proliferation in culture.

Discussion

The central role that CARD11 serves in relaying signaling from the antigen receptor to NF-κB depends upon its signal-induced transition from a closed inactive state to an open active scaffold that can recruit signaling cofactors to activate the IKK complex. Previous studies established that this transition is regulated by the ID through intramolecular interactions involving the CARD and Coiled-coil domains (13), and that two DLBCL-associated oncogenic mutations achieve hyperactive signaling by disrupting ID-mediated autoinhibition (21). These findings led us to hypothesize that in addition to those described in the Coiled-coil domain, hyperactive mutations should occur in other domains of CARD11 involved in the ID-mediated repression. Our data confirms that this hypothesis is correct. The screen for gain-of-function CARD11 variants yielded several mutations in the CARD domain that disrupt ID binding, as we predicted. Unexpectedly, the screen also identified a strikingly high density of mutations in the LATCH domain, a short nineteen-residue region between the CARD and Coiled-coil that clearly plays a requisite role in autoinhibition by the ID.

Mutations in both the CARD and LATCH domains resulted in the disruption of ID binding, the selective enhanced association with Bcl10, the spontaneous ubiquitination of Bcl10, and the subsequent activation of the IKK complex and NF-κB (Figure 2.10). These mutants cause hyperactivity by the same mechanisms ascribed to the F123I and L225LI mutants that were identified in human DLBCL.

The chief conclusion that emerges from our data is that the intramolecular regulation of CARD11 that allows for its signal-dependent activation by antigen receptor signaling also results in a vulnerability to mutation that can be exploited by lymphoid cancers to bypass normal controls and induce NF-κB and its pro-proliferative and anti-apoptotic target genes.

All of the gain-of-function mutations in the CARD and LATCH domains reduce ID binding to the CARD11 ΔID variant *in trans*. The effects on ID binding likely account for the enhanced ability of eighteen of the mutants to associate with Bcl10. It is clear, however, that there is not an absolute quantitative correlation for all mutants between the positive effect on Bcl10 binding and the degree to which a mutation disrupted ID binding. This is probably due to the fact that the ID and Bcl10 bind to partially overlapping determinants in the CARD-LATCH-Coiled-coil region such that some mutations that deleteriously affect ID binding may also partially interfere with Bcl10 association. The net effect of such mutations would still be expected to increase Bcl10 association as compared to what would occur with the closed, inactive wild-type CARD11.

It is intriguing that among the gain-of-function mutations that emerged in the screen, eighteen of twenty-three increased Bcl10 binding and none appreciably increased the association of other signaling cofactors whose recruitment to CARD11 is also controlled by the ID. This suggests that selectively enhancing Bcl10 association with CARD11 is sufficient to initiate signaling, presumably by promoting the K63-linked ubiquitination of Bcl10. It is important to point out, however, that the binding of other signaling cofactors that we did not examine, or that remain

unknown could also be affected by some or all of the mutations and may be important in determining signaling output. This possibility is suggested by differences in the specific activity of some mutants in the NF-κB reporter assay that otherwise display very similar abilities to bind Bcl10, and by the five mutants that did not enhance Bcl10 binding in the co-immunoprecipitation assay.

The enhanced association of Bcl10 with CARD11 that is induced by most of the mutations appears to promote the same K63-linked ubiquitination of Bcl10 that transiently occurs during normal antigen receptor signaling and that licenses Bcl10 for its action on the IKK complex through its association with IKKγ. For the twelve mutants analyzed after stable expression in Jurkat T cells, there was a good correlation between their enhancements in Bcl10 binding and the levels of Ub_n(K63)-Bcl10 that were spontaneously produced in these cells. The ability of CARD11 mutations to elicit Bcl10 ubiquitination suggests that during normal antigen receptor signaling, there are no CARD11-independent signaling events upstream of CARD11 activation that are required to induce this modification of Bcl10. The hyperactive CARD11 mutants must be sufficient to directly or indirectly promote the association between Bcl10 and the as yet unidentified E3 ligase that mediates conjugation. The levels of Ub_n(K63)-Bcl10 produced as a result of hyperactive variant expression correlated well with the observed binding of endogenous Ub_n(K63)-Bcl10 to IKKγ, and with the relative degree of NF-κB activation. These data emphasize the importance of K63-linked polyubiquitinated Bcl10 as a signaling intermediate in this pathway that can dictate the extent of signal output. During normal antigen receptor signaling, polyubiquitinated Bcl10 is

produced only transiently (22), and is removed by degradative mechanisms that serve to terminate signaling (41–43). In cells stably expressing the most active hyperactive variants, we readily detect a steady state level of Ub_n(K63)-Bcl10 indicating that its production must override these normal negative feedback mechanisms. It is clear that in order to fully understand how both normal and dysregulated CARD11 signaling occurs, further studies are necessary to identify the E3 ligase that ubiquitinates Bcl10 through K63-linkages, explain how the association with CARD11 promotes this modification, and elucidate how exactly Ub_n(K63)-Bcl10 activates IKK kinase activity.

The six highly active variants tested also required MALT1, TRAF6, and TAK1 for signaling to NF-κB. These factors have been shown by others to be required for IKK kinase induction downstream of antigen receptor engagement. MALT1 is required for K63-linked ubiquitination of Bcl10 (22), and has also been implicated in K63-linked ubiquitination of IKKγ (44). TRAF6 also contributes to IKKγ K63-linked ubiquitination (30), but does not appear to be required for the induction of K63-linked ubiquitination of Bcl10 (data shown in Chapter III). TAK1 has been shown to mediate IKK kinase subunit phosphorylation during signaling (40). Our data indicate that the activities of these factors must function in concert with Ub_n(K63)-Bcl10 to effect maximal NF-κB activation downstream of hyperactive CARD11 variants.

Most of the hyperactive variants that we tested had enough enhanced activity to promote the proliferation and survival of the ABC DLBCL-derived OCI-Ly3 line in culture. There was a good correlation between the ability to activate NF-κB after

stable expression in Jurkat T cells and the ability to protect OCI-Ly3 cells from apoptosis in culture. However, the L127I mutant had more potential to enhance the survival of OCI-Ly3 cells than we would have expected based upon its relative activity after stable expression in Jurkat T cells. This observation may suggest that cell-type specific aspects of the cellular environment in lymphoma can influence the potency of hyperactive CARD11 variants, such as the absence or presence of proteins that modify CARD11 signaling to NF-κB and whose functional interaction with CARD11 could be affected by some mutations and not others. The T112I and N62Y mutants did not provide much protection to OCI-Ly3 cells, but their enhanced abilities to activate NF-κB may be sufficient to contribute to the growth and survival of lymphoid cancers in other settings that have sustained other genetic alterations that could cooperate with weaker CARD11 mutants.

While this work was in progress, several studies reported the presence of CARD11 mutations in the CARD and LATCH domains in human biopsies of DLBCL. Six of these are identical to mutations that we isolated in our screen, including C49Y (45), C49S (46), E93D (46), F115L (46, 47), G123D (48), and G126D (49). Four other reported mutations occur at the same position as those we found in our screen, but mutate to a different residue, including R114I (46), F115I (47), T117P (46), and F130V (49). Although these studies did not demonstrate a functional effect of the mutations in the context of the cancers in which they were sequenced, our data provide a mechanistic characterization that can explain how the substitutions could lead to dysregulated NF-κB activity and promote proliferation and survival.

Our quantitative high-throughput screen could be easily expanded to detect other gain-of-function mutations in other domains of CARD11 including the Coiled-coil domain. A database of such mutations would provide functional insight that would complement the catalog of cancer biopsy-associated CARD11 mutations that is likely to grow as more samples are surveyed. The screening methodology is modular, making it straightforward to substitute the protein that undergoes mutation and screening and therefore easily adaptable to the analysis of other proteins that incur gain-of-function mutations in NF-κB-dependent cancers, such as MyD88, CD79A, or CD79B (18). With the substitution of the NF-κB reporter with that of another transcription factor the screen could readily be applied to molecules that influence the activity of other gene regulators that promote tumorigenesis in other cell types.

Table 2.1: Properties of hyperactive CARD11 variants.

CARD11 variant	Sp act[a]	Relative activity in T cells[b]	Bcl10 binding[c]	ID binding[d]
WT	1.0	1.0	−	
ΔID	43.6	127.3	+++++	+++++
H31L	2.3	2.0	−	+
M32K	12.9	4.6	−	+
C49Y	31.0	79.3	+++++	+
C49S	10.7	6.4	+	+++++
K50M	6.3	2.4	++	+
N62Y	8.5	13.2	++	+
E93D	11.9	17.9	++	+
F97Y	17.5	90.7	+++++	+
Y98F	12.7	18.1	++	+++++
T112I	10.7	3.3	−	+
R113Q	12.4	8.3	++	+
R114I	8.8	7.9	+	+
F115L	15.9	16.8	++	++++
T117A	3.3	2.4	−	+++
I118V	8.5	5.9	++	+
V119E	9.9	36.2	++++	++
E121G	3.6	1.4	+	+++
E122D	6.2	2.0	−	++
G123D	20.9	104.9	+++++	+
G126D	21.0	31.8	++++	+++
L127I	10.8	8.9	+++	++
H129Y	9.3	3.9	++	+++++
F130Y	15.7	6.4	++	++
V135D	4.4	2.1	ND	ND

[a] Specific activity (Sp act) in HEK293T cells was determined as described in Materials and Methods.

[b] Relative activity in T cells was determined as fold activation in KD-CARD11 Jurkat T cells as described for Fig. 2C and D and normalized to that observed for the WT.

[c] Bcl10 binding was determined in coimmunoprecipitation studies as described in Materials and Methods and depicted in Fig. 3. −, no enhancement over the WT level; +, 8% to 20% of that observed with ΔID; ++, 21% to 40% of that observed with ΔID; +++, 41% to 60% of that observed with ΔID; ++++, 61% to 80% of that observed with ΔID; +++++, 81% to 100% of that observed with ΔID. ND, not determined.

[d] ID binding was determined in GST pulldown studies as described in Materials and Methods and depicted in Fig. 4. +, 0% to 20% of the level observed with ΔID; ++, 21% to 40% of that observed with ΔID; +++, 41% to 60% of that observed with ΔID; ++++, 61% to 80% of that observed with ΔID; +++++, 81% to 100% of that observed with ΔID.

Figure Legends

Figure 2.1: A quantitative signaling screen identifies gain-of-function mutations in the CARD and LATCH domains of CARD11.

(A) Example of primary screening in which four clones scored as positives. Clones 1, 5, 34, and 36 encoded C49Y, V119E, H129Y and T117A mutations respectively.

(B) Summary of all mutations identified in the primary sequence at the N-terminus of CARD11. CARD domain residues are depicted in black, LATCH domain residues in blue, and the N-terminal end of the Coiled-coil domain in gray.

(C) Model for CARD11 in the closed inactive state. CARD11 is depicted as a dimer for simplicity but the oligomerization status has not been determined.

Figure 2.1

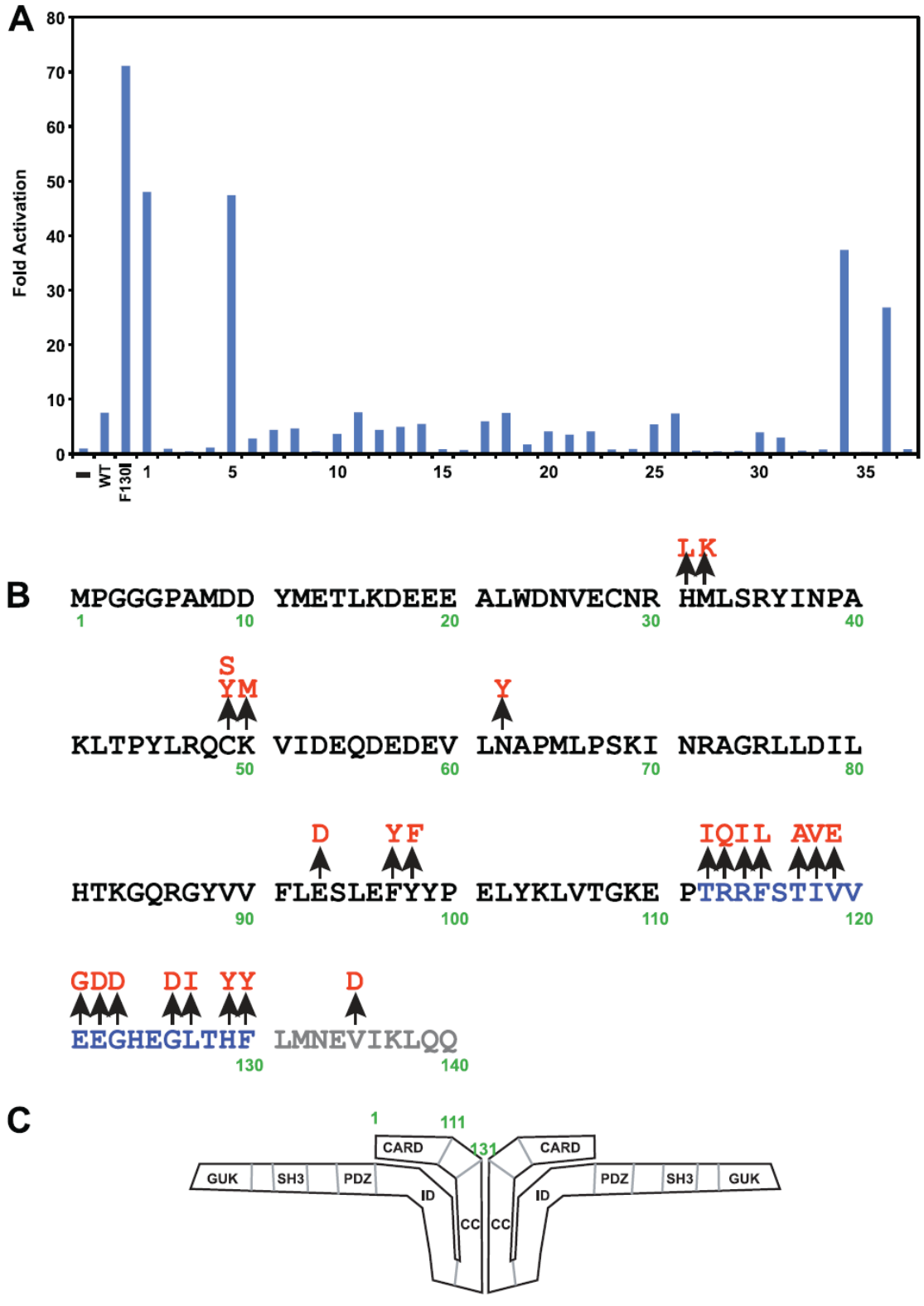
A
Fold Activation
80
70
60
50
40
30
20
10
0
–
WT
F130I
1
5
10
15
20
25
30
35
B
LK
MPGGGPAMDD YMETLKDEEE ALWDNVECNR HMLSRYINPA
1 10 20 30 40
S
YM
Y
KLTPYLRQCK VIDEQDEDEV LNAPMLPSKI NRAGRLLDIL
50 60 70 80
D
YF
IQIL
AVE
HTKGQRGYVV FLESLEFYYP ELYKLVTGKE PTRRFSTIVV
90 100 110 120
GDD
DI
YY
D
EEGHEGLTHF LMNEVIKLQQ
130 140
C
1
111
131
CARD
CARD
GUK
SH3
PDZ
ID
CC
CC
ID
PDZ
SH3
GUK

Figure 2.2: Relative Specific Activity of CARD11 variants in HEK293T and Jurkat T cells.

(A-B) HEK293T cells were transfected with 20 ng of Igκ$_2$-IFN-LUC and 6 ng of CSK-LacZ in the presence of the indicated amounts (in ng) of expression vectors for the indicated myc-tagged CARD11 variants. The panel below each titration displays western blots of corresponding lysates probed with anti-myc primary antibody to indicate the relative expression level of each variant. β-galactosidase activity, driven by CSK-LacZ, was used to normalize luciferase activity and to calculate equivalent amounts of transfected cell-lysate for western analysis.

(C-D) Jurkat T cells in which CARD11 was stably knocked down (KD-CARD11) were transfected with 200 ng of CSK-LacZ and 1500 of ng Igκ$_2$-IFN-LUC in the presence of 50-90 ng of expression vectors for the indicated variants. Vector quantities were adjusted to achieve equivalent protein expression levels for each variant, using the relative expression per ng in HEK293T cells as a guide.

Figure 2.2

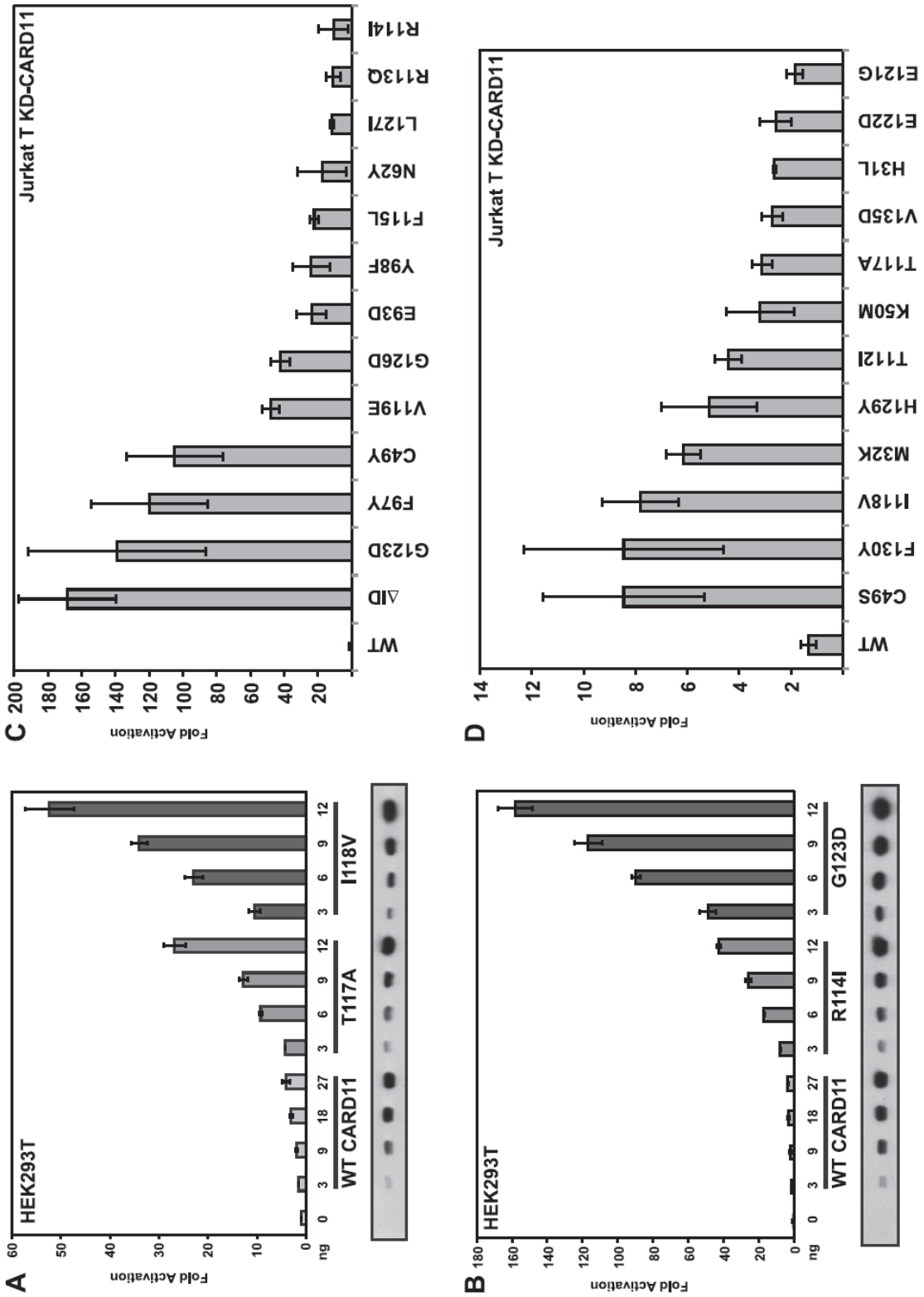
A
HEK293T
Fold Activation
ng
0 3 9 18 27 3 6 9 12 3 6 9 12
WT CARD11
T117A
I118V
B
HEK293T
Fold Activation
ng
0 3 9 18 27 3 6 9 12 3 6 9 12
WT CARD11
R114I
G123D
C
Jurkat T KD-CARD11
Fold Activation
WT
ΔID
G123D
F97Y
C49Y
V119E
G126D
E93D
Y98F
F115L
N62Y
L127I
R113Q
R114I
D
Jurkat T KD-CARD11
Fold Activation
WT
C49S
F130Y
I118V
M32K
H129Y
T112I
K50M
T117A
V135D
H31L
E122D
E121G

Figure 2.3: Mutations in the CARD and LATCH domains enhance the ability of CARD11 to associate with Bcl10.

(A-F) HEK293T cells were transfected with 70-240 ng of expression vectors for the indicated myc-CARD11 variants and 70-225 ng of FLAG-Bcl10, as indicated. Anti-FLAG immunoprecipitations were performed as described in Experimental Procedures and analyzed by western blot with the indicated primary antibodies.

Figure 2.3

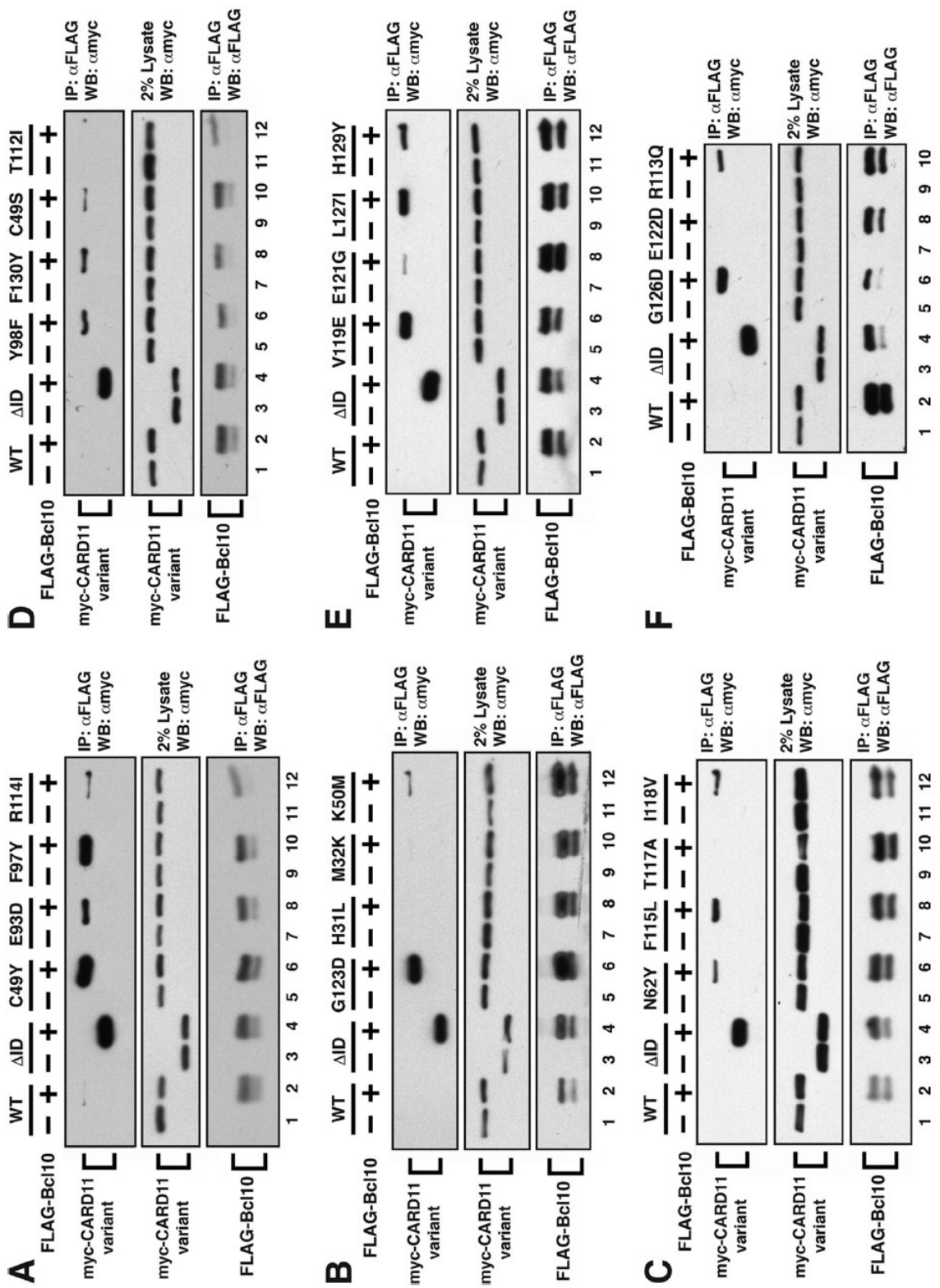
A
FLAG-Bcl10
WT ΔID C49Y E93D F97Y R114I
myc-CARD11 variant
IP: αFLAG WB: αmyc
2% Lysate WB: αmyc
IP: αFLAG WB: αFLAG
1 2 3 4 5 6 7 8 9 10 11 12
B
FLAG-Bcl10
WT ΔID G123D H31L M32K K50M
myc-CARD11 variant
IP: αFLAG WB: αmyc
2% Lysate WB: αmyc
IP: αFLAG WB: αFLAG
1 2 3 4 5 6 7 8 9 10 11 12
C
FLAG-Bcl10
WT ΔID N62Y F115L T117A I118V
myc-CARD11 variant
IP: αFLAG WB: αmyc
2% Lysate WB: αmyc
IP: αFLAG WB: αFLAG
1 2 3 4 5 6 7 8 9 10 11 12
D
FLAG-Bcl10
WT ΔID Y98F F130Y C49S T112I
myc-CARD11 variant
IP: αFLAG WB: αmyc
2% Lysate WB: αmyc
IP: αFLAG WB: αFLAG
1 2 3 4 5 6 7 8 9 10 11 12
E
FLAG-Bcl10
WT ΔID V119E E121G L127I H129Y
myc-CARD11 variant
IP: αFLAG WB: αmyc
2% Lysate WB: αmyc
IP: αFLAG WB: αFLAG
1 2 3 4 5 6 7 8 9 10 11 12
F
FLAG-Bcl10
WT ΔID G126D E122D R113Q
myc-CARD11 variant
IP: αFLAG WB: αmyc
2% Lysate WB: αmyc
IP: αFLAG WB: αFLAG
1 2 3 4 5 6 7 8 9 10

Figure 2.4: Gain-of-function mutations enhance Bcl10-mediated association of MALT1 with CARD11.

(A-B) HEK293T cells were transfected with 400-700 ng of expression vectors for the indicated myc-CARD11 variants, 500-800 ng of FLAG-MALT1 and 300-500 ng of untagged Bcl10, as indicated. Anti-FLAG immunoprecipitations were performed as described in Experimental Procedures and analyzed by western blot with the indicated primary antibodies.

Figure 2.4

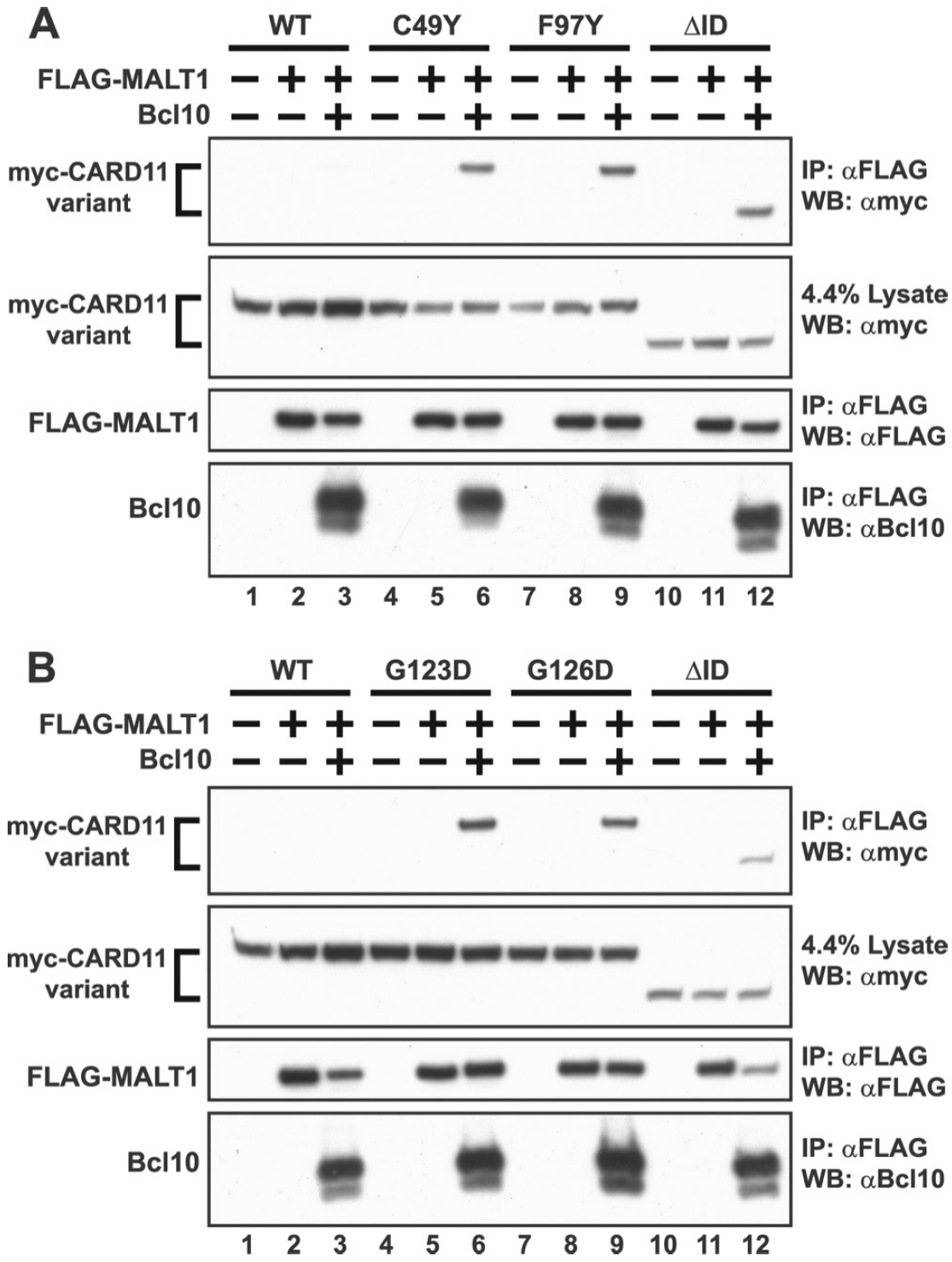
A
WT
C49Y
F97Y
ΔID
FLAG-MALT1
Bcl10
myc-CARD11 variant
IP: αFLAG
WB: αmyc
myc-CARD11 variant
4.4% Lysate
WB: αmyc
FLAG-MALT1
IP: αFLAG
WB: αFLAG
Bcl10
IP: αFLAG
WB: αBcl10
1 2 3 4 5 6 7 8 9 10 11 12
B
WT
G123D
G126D
ΔID
FLAG-MALT1
Bcl10
myc-CARD11 variant
IP: αFLAG
WB: αmyc
myc-CARD11 variant
4.4% Lysate
WB: αmyc
FLAG-MALT1
IP: αFLAG
WB: αFLAG
Bcl10
IP: αFLAG
WB: αBcl10
1 2 3 4 5 6 7 8 9 10 11 12

Figure 2.5: Mutations in the CARD and LATCH domains disrupt ID binding *in trans*.

(A-D) HEK293T cells were transfected with 800-2000 ng of expression vectors for the indicated CARD11 ΔID variants or with 2000 ng or 1500 ng of expression vectors for ID-GST or GST, respectively. Lysates were mixed as indicated, incubated, and glutathione-sepharose pulldowns were performed as described in Experimental Procedures and analyzed by western blot with the indicated primary antibodies.

Figure 2.5

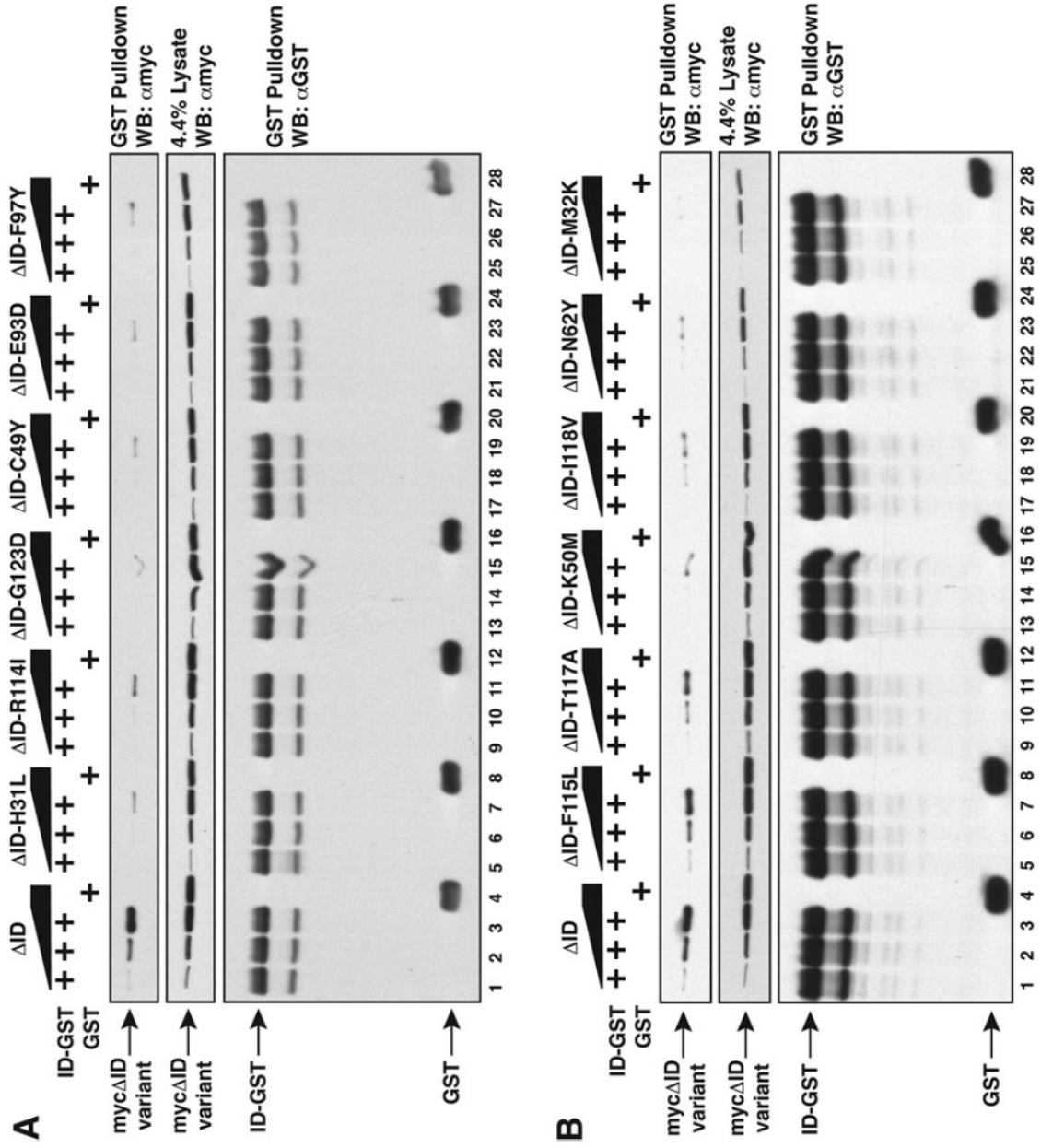
A
ΔID
ΔID-H31L
ΔID-R114I
ΔID-G123D
ΔID-C49Y
ΔID-E93D
ΔID-F97Y
ID-GST
GST
mycΔID variant
mycΔID variant
ID-GST
GST
GST Pulldown WB: αmyc
4.4% Lysate WB: αmyc
GST Pulldown WB: αGST
1 2 3 4 5 6 7 8 9 10 11 12 13 14 15 16 17 18 19 20 21 22 23 24 25 26 27 28
B
ΔID
ΔID-F115L
ΔID-T117A
ΔID-K50M
ΔID-I118V
ΔID-N62Y
ΔID-M32K
ID-GST
GST
mycΔID variant
mycΔID variant
ID-GST
GST
GST Pulldown WB: αmyc
4.4% Lysate WB: αmyc
GST Pulldown WB: αGST
1 2 3 4 5 6 7 8 9 10 11 12 13 14 15 16 17 18 19 20 21 22 23 24 25 26 27 28

Figure 2.5 (continued)

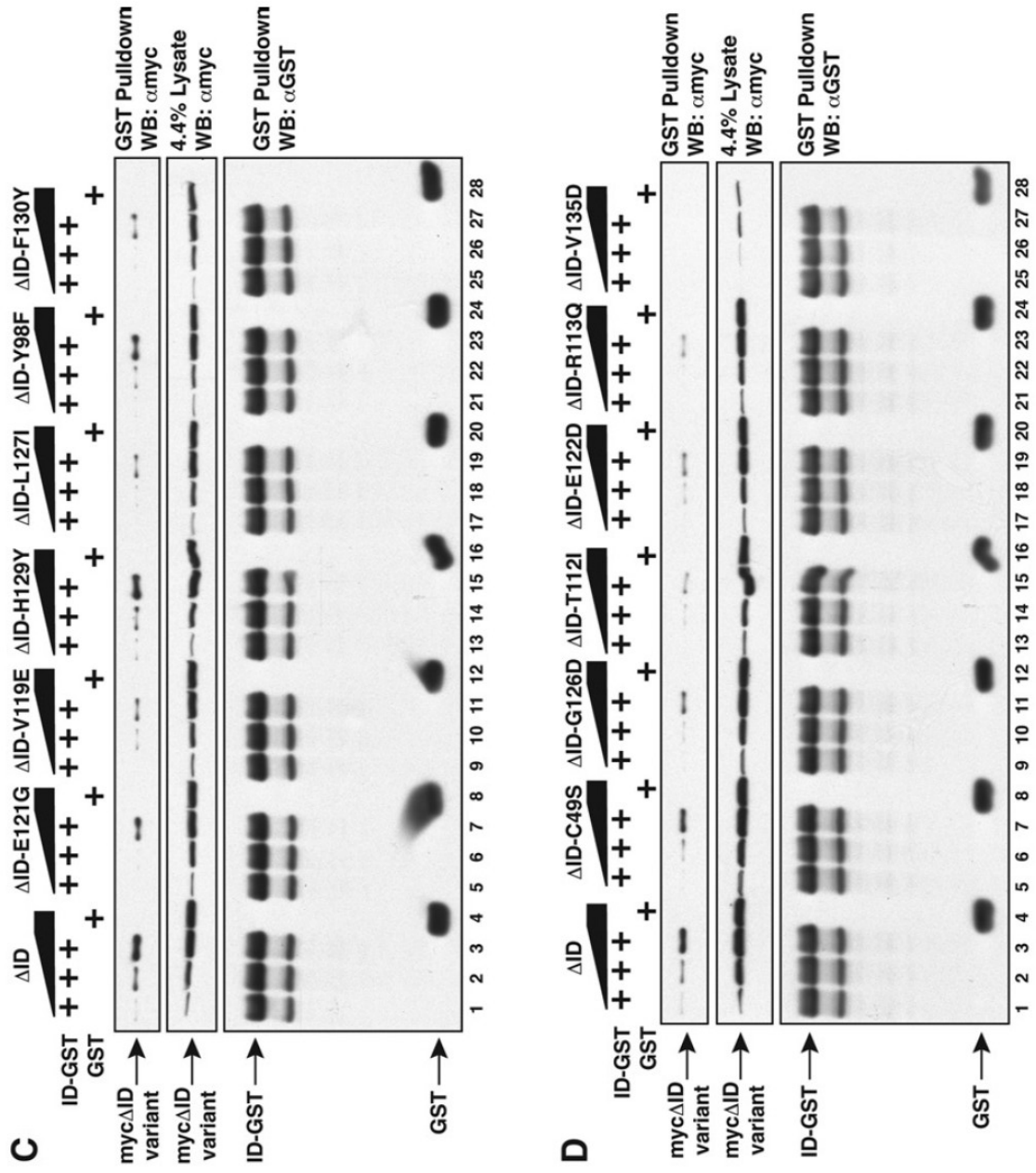

Figure 2.6: Hyperactive CARD11 variants require Bcl10 for NF-κB activation.

(A-D) HEK293T cells stably expressing a shRNA that targets either Bcl10 (KD-Bcl10) or GFP (KD-GFP) as control were transfected with 20 ng of Igκ$_2$-IFN-LUC, 6 ng of CSK-LacZ , and 8-100 ng of expression vectors for the indicated myc-tagged CARD11 variants. The panels below each assay display western blots of corresponding lysates probed with anti-myc or anti-Bcl10 primary antibody to indicate the relative expression level of each variant and Bcl10 in each sample. β-galactosidase activity, driven by CSK-LacZ, was used to normalize luciferase activity and to calculate equivalent amounts of transfected cell-lysate for western blot analysis.

Figure 2.6

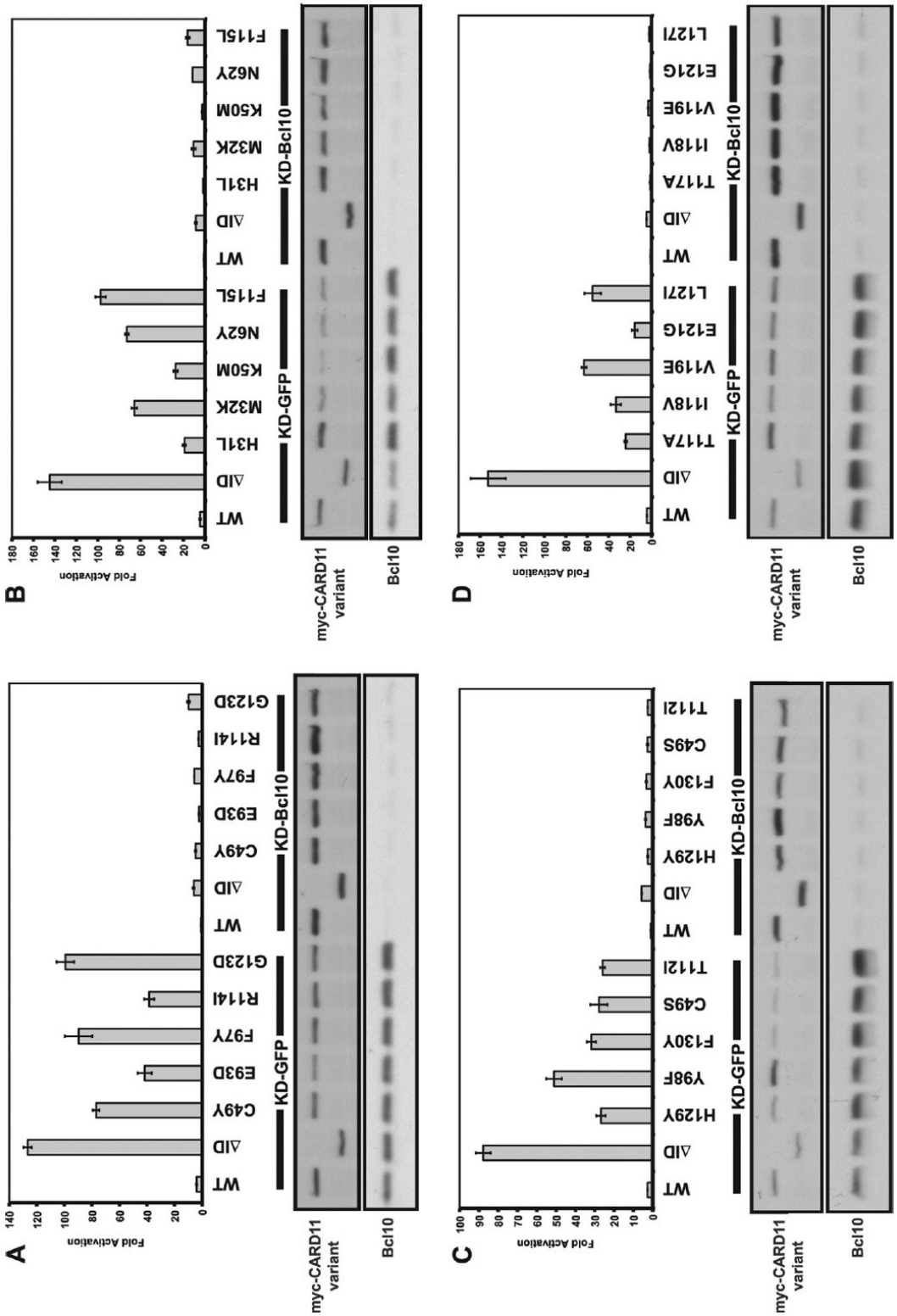
A
Fold Activation
WT
ΔID
C49Y
E93D
F97Y
R114I
G123D
KD-GFP
WT
ΔID
C49Y
E93D
F97Y
R114I
G123D
KD-Bcl10
myc-CARD11 variant
Bcl10
B
Fold Activation
WT
ΔID
H31L
M32K
K50M
N62Y
F115L
KD-GFP
WT
ΔID
H31L
M32K
K50M
N62Y
F115L
KD-Bcl10
myc-CARD11 variant
Bcl10
C
Fold Activation
WT
ΔID
H129Y
Y98F
F130Y
C49S
T112I
KD-GFP
WT
ΔID
H129Y
Y98F
F130Y
C49S
T112I
KD-Bcl10
myc-CARD11 variant
Bcl10
D
Fold Activation
WT
ΔID
T117A
I118V
V119E
E121G
L127I
KD-GFP
WT
ΔID
T117A
I118V
V119E
E121G
L127I
KD-Bcl10
myc-CARD11 variant
Bcl10

Figure 2.7: Hyperactive variants require MALT1, TRAF6, and TAK1 for NF-κB activation.

(A, B) Jurkat T cells stably expressing hairpins that target MALT1 (KD-MALT1) or TRAF6 (KD-TRAF6), or a control hairpin (KD-NT), were transfected with 200 ng of CSK-LacZ and 1500 ng of Igκ$_2$-IFN-LUC in the presence of the indicated amounts of expression vectors for the indicated CARD11 variants and assayed as described in Experimental Procedures.

(C) Lysates from KD-MALT1 and KD-TRAF6 Jurkat T cell lines were assayed by western blot with the indicated primary antibodies.

(D) Jurkat T cells were transfected with 200 ng of CSK-LacZ and 1500 ng of Igκ$_2$-IFN-LUC in the presence of 100 ng of expression vectors for the indicated CARD11 variants. Either DMSO vehicle (-) or 500 nM 5Z-7-oxozeaenol (+) was added to each sample as indicated every 12 hours after transfection for a total of 3 doses. The indicated samples were stimulated with 1 μg/ml anti-CD3/anti-CD28 crosslinking in the absence or presence of 5Z-7-oxozeaenol for 4 hours prior to harvest.

Figure 2.7

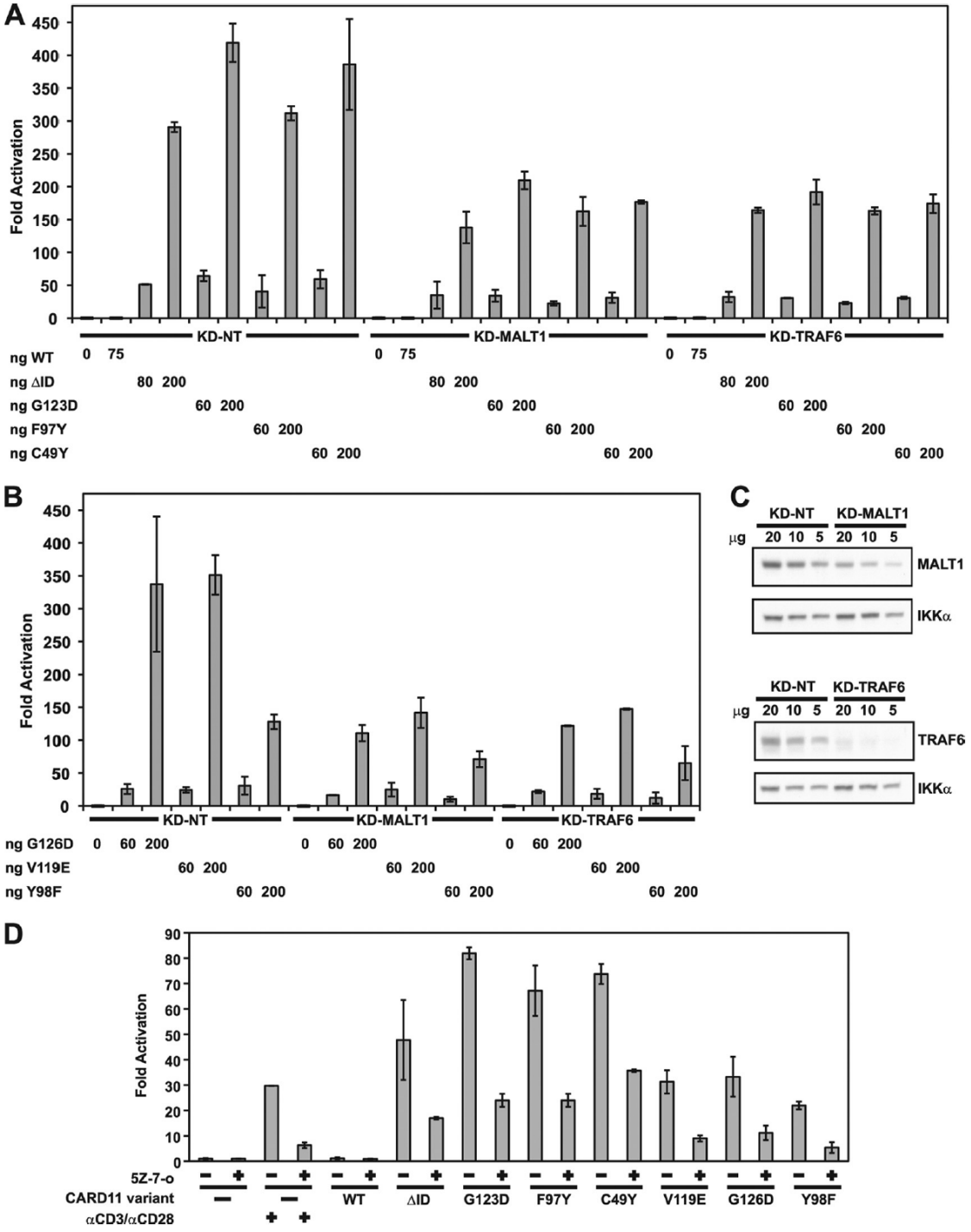
A
Fold Activation
KD-NT
KD-MALT1
KD-TRAF6
ng WT
ng ΔID
ng G123D
ng F97Y
ng C49Y
B
Fold Activation
KD-NT
KD-MALT1
KD-TRAF6
ng G126D
ng V119E
ng Y98F
C
KD-NT
KD-MALT1
μg
MALT1
IKKα
KD-NT
KD-TRAF6
TRAF6
IKKα
D
Fold Activation
5Z-7-o
CARD11 variant
αCD3/αCD28
WT
ΔID
G123D
F97Y
C49Y
V119E
G126D
Y98F

Figure 2.8: Hyperactive CARD11 variants induce K63-linked Ubiquitination of Bcl10 and the association of Ub_n(K63)-Bcl10 with IKKγ.

(A) Jurkat T cell lines stably expressing the indicated CARD11 variants fused to mCherry were generated by retroviral infection and transiently transfected with 200 ng of CSK-LacZ and 1500 ng of Igκ$_2$-IFN-LUC and assayed as described in Experimental Procedures. The line expressing wild-type CARD11 was treated with 50 ng/ml PMA and 1 μM ionomocyin for 4 hours as indicated.

(B) Electrophoretic Mobility Shift Assays were performed using 3 μg of nuclear extracts from the stably expressing Jurkat T cell lines in (A) and a ^{32}P-labelled DNA fragment containing a consensus κB site. The line expressing wild-type CARD11 was treated with 50 ng/ml PMA and 1 μM ionomycin for 30 minutes as indicated.

(C) Immunoprecipitations were performed using denatured lysates from the stably expressing Jurkat T cell lines in (A) using anti-Bcl10 antibodies and analyzed by western blot with anti-Ubiquitin (K63-linkage specific), anti-Bcl10, or anti-myc primary antibodies as indicated. The line expressing wild-type CARD11 was treated with 50 ng/ml PMA and 1 μM ionomocyin for 20 minutes as indicated.

(D) Immunoprecipitations were performed using lysates from the stably expressing Jurkat T cell lines in (A) using anti-IKKγ antibodies and analyzed by western blot with anti-Bcl10, or anti-IKKγ primary antibodies as indicated. The line expressing wild-type CARD11 was treated with 50 ng/ml PMA and 1 μM ionomocyin for 20 minutes as indicated. The relative expression level of CARD11 variants in this experiment is also indicated in the anti-myc western blot in (C) since the same cell lines were used in (C) and (D).

(E) Quantitation of the levels of Bcl10-Ub detected in each sample in (C), divided by the levels of unconjugated Bcl10, normalized to the ratio observed in the WT sample. (F) Quantitation of the levels of Bcl10-Ub detected in the IP with IKKγ in (D), divided by the levels of unconjugated Bcl10, normalized to the ratio observed in the WT sample.

Figure 2.8

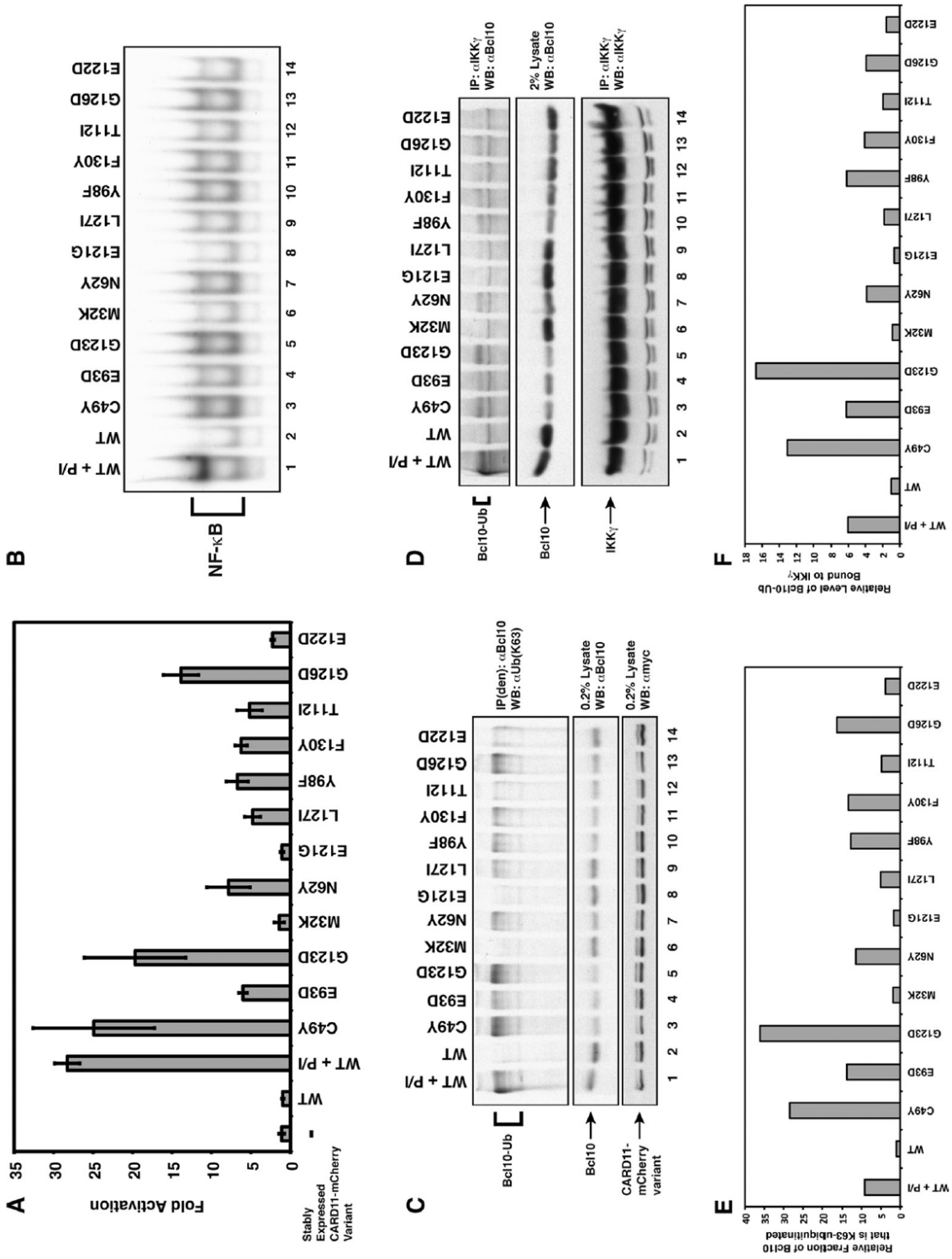
A
Fold Activation
Stably Expressed CARD11-mCherry Variant
-
WT
WT + P/I
C49Y
E93D
G123D
M32K
N62Y
E121G
L127I
Y98F
F130Y
T111I
G126D
E122D
B
NF-κB
WT + P/I
WT
C49Y
E93D
G123D
M32K
N62Y
E121G
L127I
Y98F
F130Y
T111I
G126D
E122D
C
Bcl10-Ub
Bcl10
CARD11-mCherry variant
IP(den): αBcl10 WB: αUb(K63)
0.2% Lysate WB: αBcl10
0.2% Lysate WB: αmyc
D
Bcl10-Ub
Bcl10
IKKγ
IP: αIKKγ WB: αBcl10
2% Lysate WB: αBcl10
IP: αIKKγ WB: αIKKγ
E
Relative Fraction of Bcl10 that is K63-ubiquitinated
F
Relative Level of Bcl10-Ub Bound to IKKγ

Figure 2.9: CARD11 variants containing gain-of-function mutations in the CARD and LATCH domains can promote the survival of OCI-Ly3 human DLBCL-derived cells.

(A-B) OCI-Ly3 cells stably expressing the indicated CARD11 variants were generated by retroviral infection as described in Experimental Procedures. Each line was superinfected with a retrovirus that coexpresses GFP and a shRNA that targets the endogenous human CARD11 mRNA (shC11). The percent GFP^+ cells were normalized to the percentage observed on Day 3 after infection. The survival curves for the parental OCI-Ly3 line and the line rescued with the L244P positive control are depicted in each panel for ease of comparison.

(C) Lysates from the OCI-Ly3 lines stably expressing the indicated CARD11 variants were analyzed by western blot using anti-myc and anti-IKKα antibodies as indicated to reveal the relative expression level of each variant.

(D) OCI-Ly3 cells stably expressing the indicated myc-CARD11-mCherry variants were infected with a retrovirus coexpressing GFP with either a hairpin targeting endogenous human CARD11 (shC11) or a control hairpin (shNT). Seven days after infection, GFP^+ cells were isolated by FACS and lysates were analyzed by western blot with anti-CARD11 or anti-IKKα antibodies.

Figure 2.9

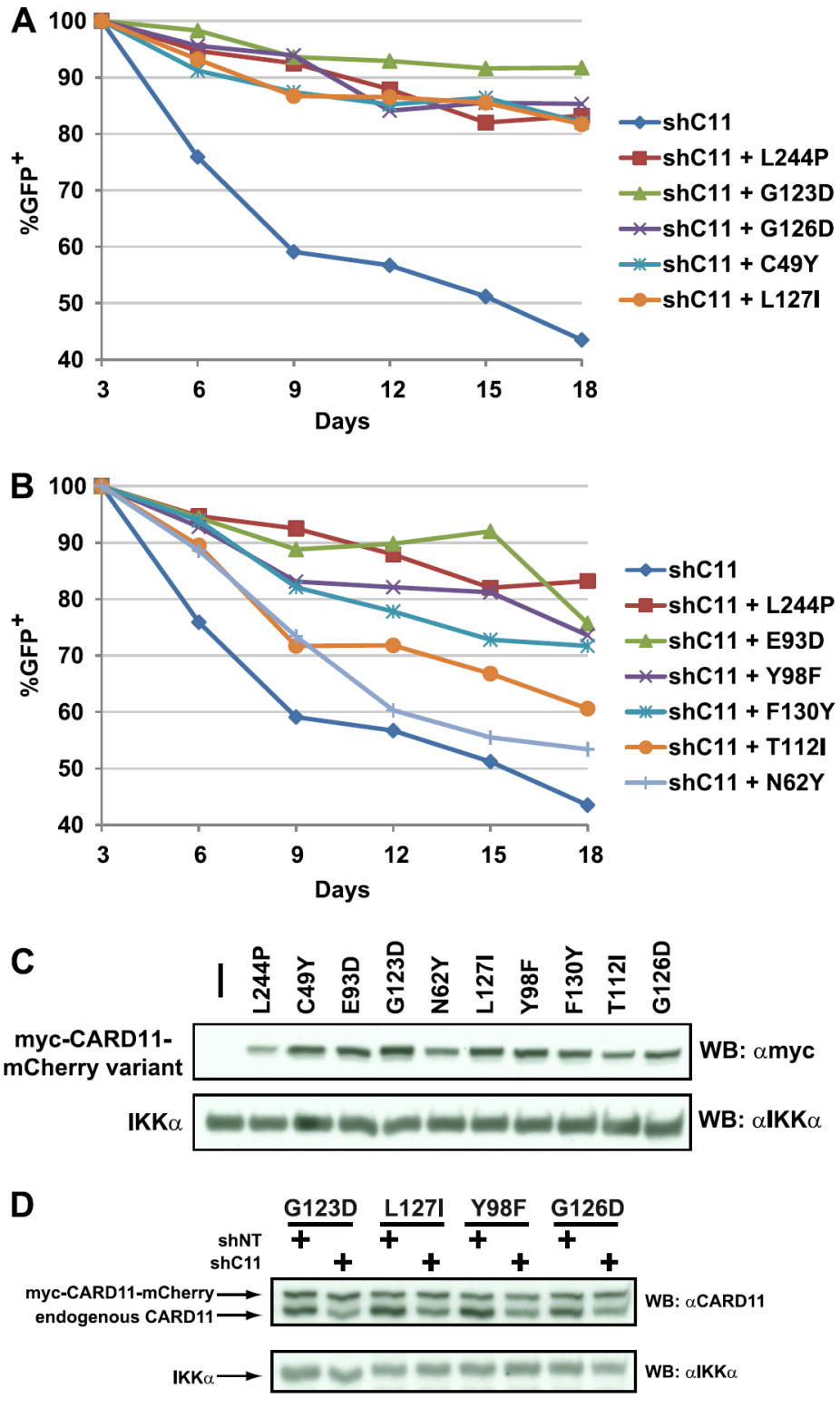
A
100
90
80
70
60
50
40
%GFP+
3
6
9
12
15
18
Days
shC11
shC11 + L244P
shC11 + G123D
shC11 + G126D
shC11 + C49Y
shC11 + L127I
B
100
90
80
70
60
50
40
%GFP+
3
6
9
12
15
18
Days
shC11
shC11 + L244P
shC11 + E93D
shC11 + Y98F
shC11 + F130Y
shC11 + T112I
shC11 + N62Y
C
–
L244P
C49Y
E93D
G123D
N62Y
L127I
Y98F
F130Y
T112I
G126D
myc-CARD11-mCherry variant
WB: αmyc
IKKα
WB: αIKKα
D
G123D
L127I
Y98F
G126D
shNT
shC11
myc-CARD11-mCherry
endogenous CARD11
WB: αCARD11
IKKα
WB: αIKKα

Figure 2.10: Model depicting how gain-of-function mutations in the CARD, LATCH, and Coiled-coil domains spontaneously induce NF-κB activation.

Figure 2.10

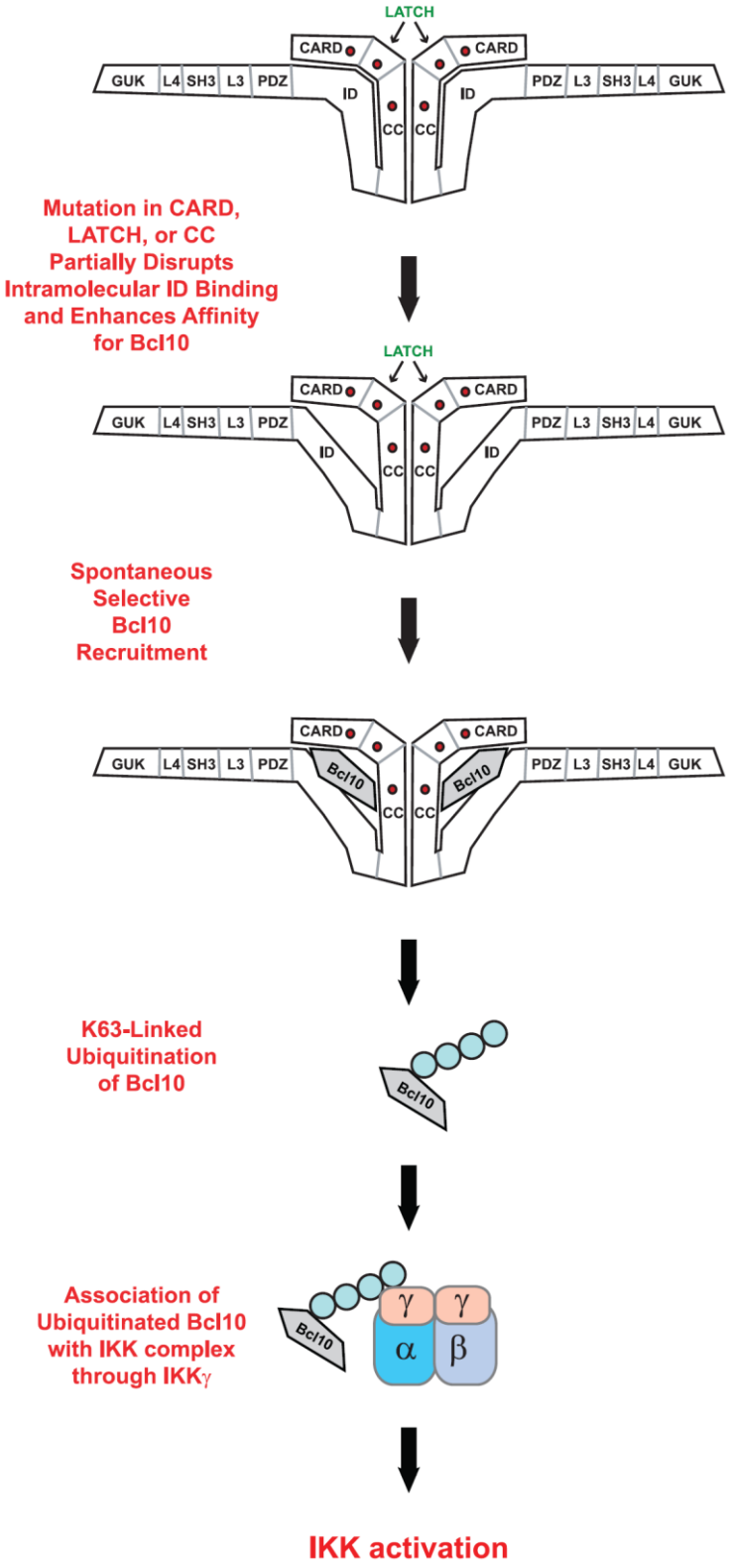
LATCH
CARD
CARD
GUK
L4
SH3
L3
PDZ
ID
CC
CC
ID
PDZ
L3
SH3
L4
GUK
Mutation in CARD, LATCH, or CC Partially Disrupts Intramolecular ID Binding and Enhances Affinity for Bcl10
Spontaneous Selective Bcl10 Recruitment
Bcl10
K63-Linked Ubiquitination of Bcl10
Association of Ubiquitinated Bcl10 with IKK complex through IKKγ
γ
α
β
IKK activation

Chapter III:

Identification of Putative Protein Regulators of the CARD11 Signaling Complex and K63-linked Ubiquitination of Bcl10

Abstract

CARD11-dependent antigen receptor signaling to NF-κB, essential for normal lymphocyte activation, is dysregulated in human diffuse large B cell lymphoma by mutations that exist within the CARD, LATCH, and the Coiled-coil domains. Oncogenic CARD11 mutations evolve to bypass upstream signaling requirements and spontaneously induce K63-linked polyubiquitination of Bcl10, a critical signaling intermediate in IKK complex activation. In this report, we identify two CARD11 signaling cofactors, TRAF2 and TAK1, whose functions are required for the induction of K63-linked ubiquitination of Bcl10 and the hyperactive signaling of oncogenic CARD11 mutations. Furthermore, when combining the most active CARD11 missense mutations in both the CARD and the Coiled-coil domain, we identify a super mutant that synergizes the signaling activities of two oncogenic CARD11 missense mutations, C49Y and L251P, both of which have been identified in human DLBCL patients, although the signaling mechanism of L251P remains poorly understood. The signaling capacity of this super mutant distinctly differs from ΔID in that its activity no longer depends on the presence of the L4 domain and that its hyperactivity is not completely abolished in the absence of the L3, SH3 or GUK domain. Similar to C49Y, this super mutant selectively enhances its association with Bcl10 and MALT1, but not the other signaling cofactors tested. Protein complex purification of this super mutant along with mass spectrometry analysis identifies several CARD11 signaling cofactors including Bcl10, MALT1, IKKγ, CK1α and STUB1, in addition to a list of putative cofactors such as USP7, UBE3C, CKIIα, IGBP1, 14-3-3ε

and EFHD2. Our results identify critical components during the assembly of Bcl10 ubiquitination, a novel super-hyperactive CARD11 mutant for further mechanistic studies, and several putative protein regulators of the CARD11 scaffold complex that are potentially dysregulated by oncogenic CARD11 mutations.

Introduction

In Chapter II, we identified and characterized a collection of hyperactive and potentially oncogenic CARD11 mutations located within the CARD and the LATCH domain that can signal to activate NF-κB even in the absence of antigen receptor signaling. In addition to disrupting the ID autoinhibition against the CARD and the Coiled-coil domains, these mutations specifically enhanced the ability of CARD11 to associate with Bcl10 and spontaneously induce K63-linked polyubiquitination of Bcl10, a signaling step required for normal TCR signaling (22). Although none of these mutations enhances the ability of CARD11 to recruit other signaling cofactors whose association with CARD11 are also controlled by the ID, it is possible that the binding of other signaling cofactors that we did not examine, or that remain unknown could also be affected by some of the mutations and may be important in determining signaling output. Potential candidate cofactors that were not examined by our previous studies but have been shown by the other studies to associate or regulate the CARD11-Bcl10-MALT1 (CBM) complex include CK1α (50), TRAF2 (45, 51), HPK1 (52), PP2A (53), Akt (54), CaMKII (55, 56), CSN (57), MIB2 (58), STUB1 (59) and GAKIN (29).

During regulated antigen receptor signaling, K63-linked polyubiquitinated Bcl10 is produced only transiently (22), and is rapidly removed by degradative mechanisms that serve to terminate signaling (41–43). In cells stably expressing the most active hyperactive variants, we readily detect a steady state level of Ub_n(K63)-Bcl10 (see Chapter II), indicating that its production must override these normal negative feedback mechanisms. These hyperactive CARD11 mutants must be sufficient to directly or indirectly promote the association between Bcl10 and the as yet unidentified E3 ligase that mediates conjugation. In order to fully understand how both normal and dysregulated CARD11 signaling occurs, further studies are necessary to identify the E3 ligase that ubiquitinates Bcl10 through K63-linkages, explain how the association with CARD11 promotes this modification, and elucidate how exactly Ub_n(K63)-Bcl10 activates IKK kinase activity. Several E3 ubiquitin ligases (such as TRAF6, TRAF2, MIB2 and STUB1) have been shown to get recruited to CARD11 or Bcl10 upon antigen receptor signaling, however, there is not yet any evidence to support that any of these E3 ligases serves specifically to conjugate K63-linked polyubiquitination on Bcl10.

The CARD11 variant ΔID has been considered to be the most active mutant, with enhanced ability to recruit multiple signaling cofactors including Bcl10, MALT1, TRAF6, TAK1, IKKγ, and Caspase-8 (13), in the absence of the ID autoinhibition. As shown in Table 2.1, ΔID confers the highest specific activity in both HEK293T and Jurkat T cells when compared to the other hyperactive CARD11 variants. The ability of ΔID to enhance Bcl10 recruitment is also the strongest among the other variants. These data had led us to believe that the ΔID variant represents the maximum

signaling capacity of CARD11. However, a rare double mutant (F115L+I118V) that emerged unexpectedly during our previous study provided data to challenge this belief. With a similar specific activity as the ΔID, this double mutant enhances Bcl10 binding in the same immunoprecipitation assay (Figure 2.3) to an extent that exceeds ΔID by 30 to 50%. This is the first time that we observed a synergistic effect created by the fusion of two relatively less hyperactive CARD11 variants. This accidental discovery led us to wonder whether we could generate even more powerful double, triple or quadruple mutants by combining some of the most active CARD11 variants that have been identified and characterized in previous studies.

In this report, we address these issues by identifying signaling cofactors that are required for the K63-linked polyubiquitination of Bcl10, a novel super-hyperactive CARD11 variant that signals to NF-κB distinctly from ΔID, and several putative protein regulators of the CBM complex that are potentially important for normal antigen receptor signaling and dysregulated by oncogenic CARD11 mutations.

Experimental Procedures

MALT1-, TRAF6-, and TRAF2-deficient Jurkat T cell lines

To generate the KD-NT, KD-MALT1, KD-TRAF6, and KD-TRAF2 Jurkat T cell lines, pLKO.1-based lentiviruses were constructed to express either shNT (Sigma SHC002; Sense sequence: 5'-CAACAAGATGAAGAGCACCAA-3'; loop sequence: 5'-CTCGAG-3'), shM1 ((13); Sense sequence: 5'-CCTCACTACCAGTGGTTCAAA-3'; loop

sequence: 5'-CTCGAG-3'), shT6 ((30); Sense sequence: 5'-CCACGAAGAGATAATGGAT-3'; loop sequence: 5'-TTCAAGAGA-3'), or shT2 ((60); Sense sequence: 5'-GATGTGTCTGCGTATCTACCT-3'; loop sequence: 5'-CTCGAG-3'). Lentiviral packaging, infection condition and puromycin selection were performed as described previously (61). Knockdown was assessed by western blot using anti-MALT1 (catalog# 1664-1; Epitomics), anti-TRAF6 (sc-7221; Santa Cruz), and anti-TRAF2 (sc-876; Santa Cruz) antibodies.

Endogenous Bcl10 immunoprecipitations in Jurkat T cell lines

Wild-type Jurkat or Jurkat T cell line stably expressing pLKO.1-based shNT, shM1, shT6, or shT2 was stimulated with 50 ng/ml PMA (Sigma) and 1 μM ionomycin (Sigma) for 20 min at 37°C. Cells (10^8 per sample) were then incubated in an ice water bath for 5 min, spun at 423 x g for 10 min at 4°C, and lysed in a lysis buffer as described previously (61). Cell lysates were precleared twice with 20 μl bed volume of Protein A-Sepharose (Sigma P9424) for 1 to 2 h at 4°C with rotation. To analyze Bcl10 ubiquitination, the precleared lysates were treated as described previously (61). (5Z)-7-oxozeaenol was obtained from Calbiochem (product code 499610). Jurkat T cells were pretreated with either DMSO vehicle (-) or 2 μM (5Z)-7-oxozeaenol (5Z-7-o) (+) for 30 min prior to PMA/ionomycin treatment and lysis as described above. Western blots were analyzed using anti-Ub-K63 (14-6077-82; eBioscience), anti-Bcl10 (sc-5273; Santa Cruz), anti-MALT1 (catalog# 1664-1; Epitomics), anti-TRAF6 (sc-7221; Santa Cruz), and anti-TRAF2 (sc-876; Santa Cruz) antibodies.

Reporter assays of Jurkat T cells

Jurkat T cells were transfected with Igκ$_2$-IFN-LUC and CSK-LacZ as described previously (13) using 30-280 ng of expression construct for each CARD11 variant.

Immunoprecipitations in HEK293T cells

One day prior to transfection, 5x10^5 HEK293T cells were plated in each well of a six-well plate. A total of 2 μg DNA per well was transfected using the calcium phosphate method. The medium was changed approximately 24 h posttransfection, and the cells were harvested 42 to 46 h posttransfection. Cells were lysed in 500 μl of immunoprecipitation lysis buffer (IPLB) and debris was removed as described previously (13). 20 μl of cell lysate was saved for western blot analysis and 450 μl was incubated with 1 μg of anti-FLAG antibody (Sigma F7425) for 2 h at 4°C with rotation. 10 μl bed volume of protein G-Sepharose 4 Fast Flow (GE Healthcare) was added and incubated for 2 h at 4°C with rotation. The resulting immunocomplex was washed with IPLB four times for 5 min at 4°C with rotation, eluted twice, pooled, and resolved for western blot analysis as described previously (21) using anti-myc (sc-40; Santa Cruz), anti-FLAG (M2; Sigma F1804), and anti-Bcl10 (sc-5273; Santa Cruz) antibodies.

Biotin pulldowns and elutions

CARD11 variants with C-terminal Biotag, a biotin acceptor peptide, was constructed as described previously (62). One day prior to transfection, 15x10^6 or 150x10^6 HEK293T cells were plated in two or twenty 15-cm tissue culture plates

per condition. A total of 30 μg DNA per plate was transfected using the calcium phosphate method. The medium was changed and 50 μM of biotin was added approximately 24 h posttransfection, and the cells were harvested 42 to 46 h posttransfection. Cells per two 15-cm plates were trypsinized, pooled, washed twice with warm PBS, and lysed in 1.2 ml IPLB for 20 min at 4°C. Cell debris was removed by centrifugation at 16,000 xg for 10 min. 1.3 ml of cell lysate was incubated with 100 μl bed volume of NeutrAvidin Agarose Resins (Thermo Scientific) for 2 h at 4°C with rotation. The Neutravidin Beads were washed with IPLB four times for 5 min at 4°C with rotation and eluted sequentially for 30 min at room temperature with: 1) 1 ml elution buffer containing 10 mM TRIS (pH 7.4), 150 mM NaCl and protease inhibitor cocktail (PIC, Sigma P8340); 2) 1 ml elution buffer containing 10 mM TRIS (pH 7.4), 300 mM NaCl and PIC; 3) 1 ml elution buffer containing 10 mM TRIS (pH 7.4), 300 mM NaCl, 0.06% SDS, 50 mM DTT and PIC. Each elution was concentrated with Amicon Ultra 3K device (Millipore) to a final volume of approximately 60 μl and resolved by 10% SDS-PAGE.

Protein staining and mass spectrometry

Protein bands resolved on SDS-PAGE gel were analyzed by Silver Stain Plus Kit (BioRad) or homemade colloidal blue stain (for mass spectrometry) prepared as described previously (63). In-gel digestion, micro-capillary LC/MS/MS analysis, protein database searching, and data analysis were performed by Taplin Mass Spectrometry Facility at Harvard Medical School.

Results

TRAF2 and TAK1 are required for K63-linked ubiquitination of Bcl10

Since RNAi of TRAF6, TRAF2, and TAK1 have been shown previously (30) to inhibit TCR-induced IKK activation and IL-2 production in T cells, we wondered whether the absence of these CARD11 signaling cofactors could also inhibit the induction of K63-linked ubiquitination of Bcl10, a critical signaling intermediate required for TCR-induced IKK activation. To probe for Ub_n(K63)-Bcl10, Bcl10 was immunoprecipitated from denatured cell lysates of wild-type or pLKO.1-transduced Jurkat cell lines and assessed for the presence of conjugated ubiquitin using K63-linkage-specific antibodies. As shown in Figure 3.1A, the >90% knockdown of TRAF6 protein in Jurkat T cells via expression of hairpin shT6 clearly did not affect the amount of K63-linked ubiquitination of Bcl10 induced by PMA/ionomycin treatment, as compared to that observed in control cells expressing the control hairpin shNT. However, the approximately 50% knockdown of TRAF2 protein in Jurkat T cells via expression of hairpin shT2 showed significant reduction of the amount of Ub_n(K63)-Bcl10, similar to the reduction level shown in the control MALT1-knockdown cells (Figure 3.1B). These data strongly suggest that TRAF2, but not TRAF6, plays a critical role upstream of the conjugation of K63-linked ubiquitin chain on Bcl10, although both ubiquitin E3 ligases are required for IKK activation.

In order to test whether TAK1 kinase function is also required for Ub_n(K63)-Bcl10, similar immunoprecipitation assay was performed with Jurkat T cells that were pretreated with 2 μM of (5Z)-7-oxozeaenol, a TAK1-specific inhibitor, for 30

min prior to PMA/ionomycin stimulation. As shown in Figure 3.1C, inhibiting TAK1 kinase activity significantly reduced the induction level of Ub_n(K63)-Bcl10 by PMA/ionomycin treatment, as compared to the level of ubiquitination shown in the DMSO vehicle control. This result suggests that the kinase function of TAK1 also plays a role upstream of Bcl10 ubiquitination, although further analysis with specific silencing of TAK1 protein expression is necessary to confirm this conclusion.

For several of the most active CARD11 variants that were identified and characterized previously, we also tested the dependence of their signaling activity on TRAF2. We compared the activities of the G123D, F97Y, C49Y, V119E, G126D, and Y98F mutants in Jurkat T cell lines as described above that stably expressed a control short hairpin RNA (KD-NT) or one that targeted TRAF2 (KD-TRAF2). As shown in Figure 3.1D, knockdown of TRAF2 protein level reduced the apparent activity of all of the mutants tested, as assessed in the Igκ_2-IFN-LUC reporter assay. This result is consistent with our previous findings that these hyperactive CARD11 mutants dysregulate IKK activation via spontaneously accumulation of K63-linked ubiquitination of Bcl10, whose induction relies on normal TRAF2 expression.

Identification of a novel super-hyperactive CARD11 mutant C49Y+L251P

In order to generate a novel hyperactive mutant whose signaling to NF-κB is even more potent than ΔID for further mechanistic studies of oncogenic CARD11 mutations, we combined the most active mutations (C49Y, F97Y and G123D) from both the CARD and the LATCH domain that were identified and characterized in our previous study. These double mutants (C49Y+F97Y, C49Y+G123D, F97Y+G123D)

were tested along with the control double mutant F115L+I118V using the Igκ2-IFN-LUC reporter assay in a transient transfection in wild-type Jurkat T cells. As shown in Figure 3.2A, these double mutants were slightly more active than F115L+I118V, with activities ranging from 95.7 to 142.0 fold (WT control = 1.5 fold). Next, we generated and tested two triple mutants (C49Y+F97Y+G123D and C49Y+F115L+I118V), however, the activities of these two triple mutants did not differ significantly from the four double mutants tested, indicating that these mutations from both the CARD and the LATCH domains dysregulate CARD11 with overlapping molecular mechanisms.

The OCI-Ly3 cell line, which is representative of the ABC-subtype of DLBCL, harbors the L251P (also known as L244P due to a different numbering scheme) oncogenic variant of CARD11 and relies on the dysregulated L251P signaling to NF-κB for survival and proliferation in culture (28). However, the detailed molecular mechanism of the L251P Coiled-coil domain mutant remains poorly understood. We therefore hypothesized that a more potent CARD11 mutant could be generated by combining the unknown signaling mechanisms of L251P with those of the CARD or the LATCH domain mutants. In order to test this hypothesis, we combined L251P with C49Y, an oncogenic CARD11 mutation in the CARD domain that was previously reported to exist in human DLBCL patient (45). As shown in Figure 3.2A, indeed the double mutant C49Y+L251P emerged as an extremely potent NF-κB activator with its activity reaching up to an unforeseen 1890.5 fold (WT control = 1.2 fold), an order of magnitude higher than the average fold change of C49Y (121.1 fold) and L251P (221.9 fold). Further addition of other CARD or LATCH domain mutations to

the super-hyperactive mutant C49Y+L251P clearly did not further enhance its signaling capacity, again indicating the use of overlapping molecular mechanisms among these mutations.

The hyperactivity of the ΔID variant has been shown to depend strictly on the presence of all the C-terminal domains of CARD11 (L3, SH3, L4 and GUK) except for the PDZ domain (13). In order to examine whether the novel super-hyperactive mutant C49Y+L251P is also subjected to similar restrictions, we constructed several C49Y+L251P variants in which the PDZ, L3, SH3, L4 or GUK domain was deleted respectively, and assessed their activities in a transient transfection assay using the Igκ$_2$-IFN-LUC reporter in wild-type Jurkat T cells. As expected, deleting the PDZ domain did not significantly alter the activity of C49Y+L251P, however, deleting the L4 domain also did not significantly alter the activity of C49Y+L251P (Figure 3.2B). Although deleting the L3, SH3 or GUK domain did reduce the activity of C49Y+L251P by approximately 60 to 80%, in every case the original activity is almost completely restored by higher expression level. On the contrary, higher expression level clearly did not restore any activity of the ΔID domain deletion variants except for the ΔIDΔPDZ variant (Figure 3.2B). Collectively, these data suggest that the novel super-hyperactive CARD11 variant C49Y+L251P probably employs other different signaling mechanisms that are not utilized by ΔID. Therefore, it is likely that novel dysregulation mechanisms can be uncovered by studying this synergistic super mutant.

Super-hyperactive mutant C49Y+L251P selectively confers the ability to associate with Bcl10 and MALT1

We next determined whether the novel super-hyperactive mutant conferred to CARD11 an enhanced ability to interact with the signaling cofactors that have been previously shown to associate with CARD11 in a signal-dependent and ID-regulated manner (13). We coexpressed the C49Y+F97Y+G123D+L251P variant with FLAG-tagged Bcl10, MALT1, TRAF6, TAK1, IKKγ, or Capase-8 C360S in HEK293T cells and assessed the degree to which this mutant coimmunoprecipitated with each FLAG-tagged cofactor, using the CARD11 ΔID as positive controls. As shown in Figure 3.3A, this super-hyperactive mutant selectively enhanced the recruitment of Bcl10 and MALT1, but not the other ID-regulated signaling cofactors TRAF6, TAK1, IKKγ and Caspase-8. We then coexpressed the C49Y+L251P variant with FLAG-tagged Bcl10, MALT1, TRAF2 or GAKIN, in the presence or absence of untagged Bcl10, in HEK293T cells and performed similar coimmunoprecipitation assay as described above. As shown in Figure 3.3B, the super-hyperactive mutant C49Y+L251P also selectively enhanced the recruitment of Bcl10 and MALT1, but not TRAF2 and GAKIN. Since the levels of Bcl10 and MALT1 recruitment were not significantly different between the ΔID and the C49Y+L251P variants, these data strongly suggest that other unexamined or unknown signaling cofactors of CARD11 whose recruitments depend on the presence of certain ID domain residues could be specifically dysregulated by the C49Y+L251P super mutant.

Identification of putative CARD11 signaling cofactors through protein complex purification of the C49Y+L251P super mutant

In order to identify unknown signaling components of the CBM complex, we attempted to purify protein cofactors that associate with the C49Y+L251P super-hyperactive mutant from HEK293T cells. To maximize protein complex recovery from cell lysates, we created CARD11 variants with C-terminal Biotag, a specific biotin acceptor peptide that has been described previously (62). Using the calcium phosphate transfection method, we then coexpressed either wild-type CARD11 or the C49Y+L251P super mutant with the biotin ligase BirA (62) in HEK293T cells. Biotinylated CARD11 complexes were pulled-down efficiently, as indicated by more than 95% of CARD11 protein depletion after 2 h of incubation with the Neutravidin beads, which is difficult to achieve by other epitope tags after prolonged incubation. To further purify the associated proteins, we fractionated them by three differential elutions performed as described in Experimental Procedures and in Figure 3.4. For small-scale purification, silver staining was used to analyze each elution fraction on SDS-PAGE gel as shown in Figure 3.4A. We readily observed several extra protein bands that get recruited to the C49Y+L251P variant at higher levels, as compared to the wild-type CARD11 and the negative controls. Using the same approach, we scaled-up the purification by 10 fold and stained the SDS-PAGE gel with colloidal blue (Figure 3.4B). Protein bands of interest were identified by mass spectrometry and the results were analyzed and summarized as shown in Figure 3.4B.

Among these identified proteins, the Casein kinase CK1α emerged as the most significant protein cofactor whose recruitment to the C49Y+L251P variant is at

a much higher level as compared to that observed in the wild-type CARD11 control. These data also suggest that CK1α binds so tightly to the C49Y+L251P variant that the interaction can only be disrupted by denaturating elution condition. Consistent with this finding, CK1α has been shown to play a critical role in lymphoma cell survival as shRNA-mediated knockdown of CK1α in several ABC-DLBCL cell lines including OCI-Ly3 (which harbors the L251P variant) was toxic to these lymphoma cells (50). CK1α has also been shown to rely on both the Coiled-coil and the ID domains of CARD11 for its association (50), suggesting that the ΔID variant is missing certain CK1α binding sites in the ID domain, which could potentially explain why the ΔID variant is much less active than the C49Y+L251P super mutant.

In addition to CK1α, we have also identified other known cofactors of CARD11 including Bcl10, MALT1 and IKKγ (Figure 3.4B), although the abundance of these proteins was much lower than that of CK1α, indicating a low steady-state level of the CBM complex using our purification method in HEK293T cells. From almost all elution fractions in protein bands between 25 to 35 kDa, we also identified an ubiquitin E3 ligase STUB1, which has been shown to be required for TCR-induced NF-κB activation and IL-2 production (59). Interestingly, CARD11 has been shown to be a substrate of STUB1 for K27-linked ubiquitination, although the significance of such modification on CARD11 is not clear. Collectively, the presence of these known signaling cofactors of CARD11 in our purification and mass spectrometry identification strengthened our confidence about the validity of the other putative protein cofactors that were also isolated and identified in this screen.

Among all the putative protein cofactors identified, the ubiquitin-specific-processing protease USP7 was the most promising candidate. As shown in Figure 3.4B, the protein band that contained a relatively abundant amount of USP7 was clearly absent from the wild-type CARD11 control lane, indicating the dysregulated recruitment of USP7 to the C49Y+L251P variant. Another promising candidate that emerged from this study was the phosphoserine-binding signaling adapter 14-3-3 ε (YWHAE), which was coincidently isolated from another protein-protein interaction screen in which the truncated L251P CARD11 variant was used as bait protein. As shown in Figure 3.4B, the protein bands that contained 14-3-3 ε were clearly much more intense than those corresponding bands in the wild-type CARD11 control lane, indicating dysregulated recruitment of 14-3-3 ε to the C49Y+L251P variant. We also identified previously uncharacterized ubiquitin E3 ligases in this study, including UBE3C, UBE3D and RNF114. Among these E3 ligases, our mass spectrometry data suggest that UBE3C is probably the most significant candidate, as supported by the presence of an abundant amount of representative peptides in the indicated gel band shown in Figure 3.4B.

Discussion

Although it is clear that oncogenic CARD11 mutations can elicit intracellular accumulation of the K63-linked ubiquitination of Bcl10, the specific E3 ligase that catalyzes this process remains unidentified. Our data suggest that TRAF2 and TAK1 are required cofactors for the induction of Ub_n(K63)-Bcl10 upon antigen receptor

signaling. Similar to TRAF6, TRAF2 has been shown previously (30) to associate with the C-terminal domain of MALT1 (residues 334-824), however, our data clearly showed that TRAF6 could be dispensable for the induction of Ub_n(K63)-Bcl10 upon PMA/ionomycin stimulation. Furthermore, a role for TRAF2 in Ub_n(K63)-Bcl10 is supported by the finding that TRAF2 is associated with Bcl10 and a MALT1 fusion protein found in MALT lymphoma (64, 65). Our finding is supported by another previous study that identified mutations in both TRAF2 and TAK1 as the culprits of NF-κB dysregulation in human diffuse large B-cell lymphoma (45). It will be interesting and informative to examine whether these TRAF2 and TAK1 oncogenic mutations could also function to spontaneously induce the accumulation of Ub_n(K63)-Bcl10. Our data do not exclude the possibility that TRAF2 and TAK1 are required for the activation of another unidentified ubiquitin E3 ligase that directly catalyzes the conjugation of K63-linked ubiquitin chain on Bcl10 during normal antigen receptor signaling.

Our study identified an extremely potent double mutant of CARD11 that synergizes the signaling potentials of both the C49Y (CARD) and the L251P (Coiled-coil) oncogenic variants. According to protein expression data obtained in transient transfection in HEK293T cells, the protein expression level (per ng of transfected plasmid) of this super mutant is actually lower than that of wild-type CARD11 or the C49Y variant. Therefore, it is unlikely that the hyperactivity of this super mutant emerged as a result of protein overexpression in Jurkat T cells. Interestingly, adding the LATCH domain mutations to the C49Y+L251P variant did not further enhance its signaling capacity, indicating that the LATCH domain function has already been

dysregulated by the presence of both C49Y and L251P mutations. It is currently unclear whether a complete deletion of the LATCH domain will have an impact on the hyperactive signaling of the C49Y+L251P variant. We were surprised to find that deleting any one of the C-terminal domains of CARD11 (L3, SH3, L4 and GUK) in the context of the C49Y+L251P super mutant failed to completely abolish its hyperactivity. However, it is still unclear whether all of these C-terminal domains are dispensable for the hyperactive signaling of this super mutant.

The quadruple mutant C49Y+F97Y+G123D+L251P, which is approximately 10 fold more active than ΔID for NF-κB signaling, clearly did not enhance the recruitment of TRAF6, TAK1, IKKγ or Caspase-8 to CARD11, as compared to the ΔID variant. The discrepancy between signaling activity and cofactor binding suggests that the ID domain probably harbors critical activation and cofactor association domains that are both deleted in the ΔID variant. It would be interesting to perform similar cofactor binding studies with a ΔID variant in which the C49Y and L251P mutations are incorporated, and test whether this ID-deleted super mutant could maintain its signaling capacity to NF-κB even in the absence of the ID domain.

A major finding of our protein complex purification using the biotinylated C49Y+L251P variant was the identification of CK1α as a dysregulation target of oncogenic CARD11 mutations. It remains to be seen whether this enhanced binding of CK1α is dysregulated specifically by the L251P Coiled-coil mutation and not by the C49Y CARD mutation. It is also unclear whether CK1α is required for the induction of K63-linked ubiquitination of Bcl10 upon antigen receptor or oncogenic CARD11 signaling. Furthermore, the detailed molecular mechanism of how CK1α

regulates the function of the CBM complex during normal antigen receptor signaling remains poorly understood. In Jurkat T cells stably expressing the C49Y+L251P variant, we also observed enhanced CK1α recruitment to mutant CARD11, as compared to the wild-type CARD11 control (data not shown). Interestingly, our recent data have confirmed that the enhanced CK1α recruitment to the C49Y+L251P variant occurred even in Bcl10 knocked-out Jurkat T cells, suggesting that CK1α is capable of interacting with CARD11 in a different CARD11 complex upstream of or independent of the formation of the CBM complex. Our mass spectrometry data also suggest a potential dysregulation of CKIIα recruitment to CARD11 by the C49Y+L251P variant. Although CKIIα has not been linked to CARD11 during normal antigen receptor signaling, recently the Casein kinase-2 interacting protein-1 (CKIP-1), which was originally identified as an interacting protein of CKIIα, has been shown to interact with CARD11 and negatively regulate T cell activation (66). It remains to be seen whether CKIIα is an essential regulator of CARD11 during antigen receptor signaling.

Although we have identified a list of putative protein binding partners using CARD11 as the major bait, it is important to point out that some of these identified protein cofactors may not be directly interacting with CARD11. Instead, their association with CARD11 could be mediated through the dysregulated binding of other protein cofactors such as CK1α, Bcl10, MALT1 and IKKγ. A secondary screen using some recently emerging genetic tools such as CRISPR and TALEN to knock out the expression of these candidates in Jurkat T cells would be necessary to confirm the significance of these proteins during antigen receptor signaling to NF-κB.

Figure Legends

Figure 3.1: An E3 ubiquitin ligase TRAF2 and TAK1 kinase are required for PMA/ionomycin-induced K63-linked ubiquitination of Bcl10.

(A) Knockdown of TRAF6 in Jurkat T cells via expression of hairpin shT6 did not affect the induction of Ub_n(K63)-Bcl10 by PMA/ionomycin treatment, as compared to that observed in control cells expressing the control hairpin shNT. Cells were treated with or without 50 ng/ml PMA and 1 μM ionomycin for 20 minutes before lysis and assayed for Ub_n(K63)-Bcl10 levels as described in Experimental Procedures.

(B) Knockdown of TRAF2 or MALT1 via expression of hairpin shT2 or shM1 respectively reduced induction of Ub_n(K63)-Bcl10 by PMA/ionomycin treatment. Cells were treated as described in (A).

(C) Inhibition of TAK1 kinase activity reduced induction of Ub_n(K63)-Bcl10 by PMA/ionomycin treatment. Jurkat T cells were pretreated with either DMSO vehicle (-) or 2 μM (5Z)-7-oxozeaenol (5Z-7-o) (+) for 30 min prior to PMA/ionomycin treatment and lysis as described in (A).

(D) Hyperactive CARD11 variants require TRAF2 for NF-κB activation. Jurkat T cells stably expressing hairpin that targets TRAF2 (KD-TRAF2) or a control hairpin (KD-NT), were transfected with 200 ng of CSK-LacZ and 1,500 ng of Igκ$_2$-IFN-LUC in the presence of the indicated amounts of expression vectors for the indicated CARD11 variants and assayed as described in Experimental Procedures.

Figure 3.1

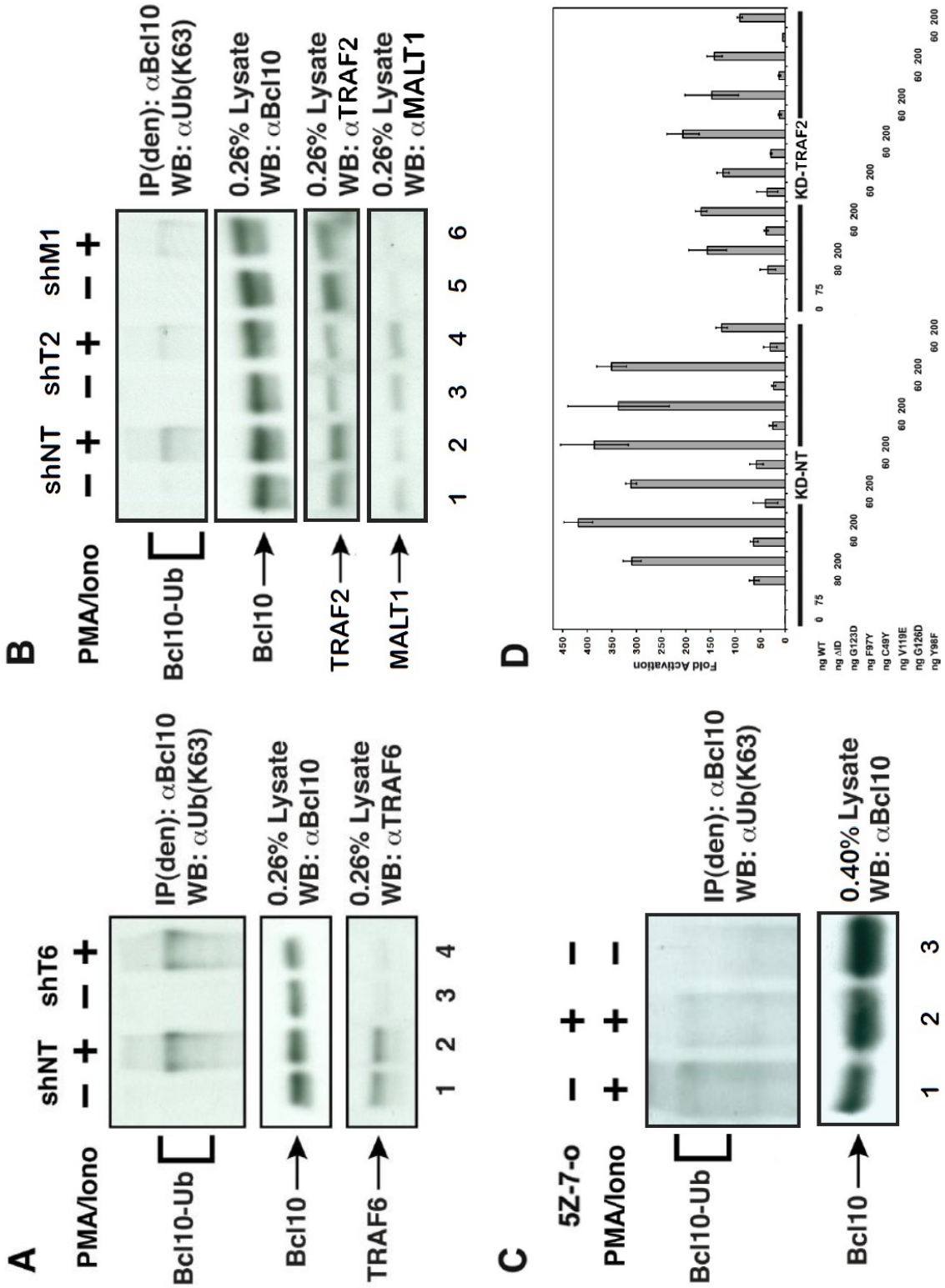
A
shNT shT6
PMA/Iono - + - +
Bcl10-Ub
IP(den): αBcl10
WB: αUb(K63)
Bcl10
0.26% Lysate
WB: αBcl10
TRAF6
0.26% Lysate
WB: αTRAF6
1 2 3 4
B
shNT shT2 shM1
PMA/Iono - + - + - +
Bcl10-Ub
IP(den): αBcl10
WB: αUb(K63)
Bcl10
0.26% Lysate
WB: αBcl10
TRAF2
0.26% Lysate
WB: αTRAF2
MALT1
0.26% Lysate
WB: αMALT1
1 2 3 4 5 6
C
5Z-7-o - + -
PMA/Iono + + -
Bcl10-Ub
IP(den): αBcl10
WB: αUb(K63)
Bcl10
0.40% Lysate
WB: αBcl10
1 2 3
D
Fold Activation
KD-NT
KD-TRAF2
ng WT
ng ΔID
ng G123D
ng F97Y
ng C49Y
ng V119E
ng G126D
ng Y98F

Figure 3.2: Oncogenic CARD11 mutations C49Y (CARD) and L251P (Coiled-coil) synergize their respective signaling capacity to generate a super-hyperactive mutant that no longer requires PDZ, L3, SH3, L4 or GUK for signaling to NF-κB. (A and B) Jurkat T cells were transfected with 200 ng of CSK-LacZ and 1,500 ng of Igκ$_2$-IFN-LUC in the presence of the indicated amounts of expression vectors for the indicated CARD11 variants.

Figure 3.2A

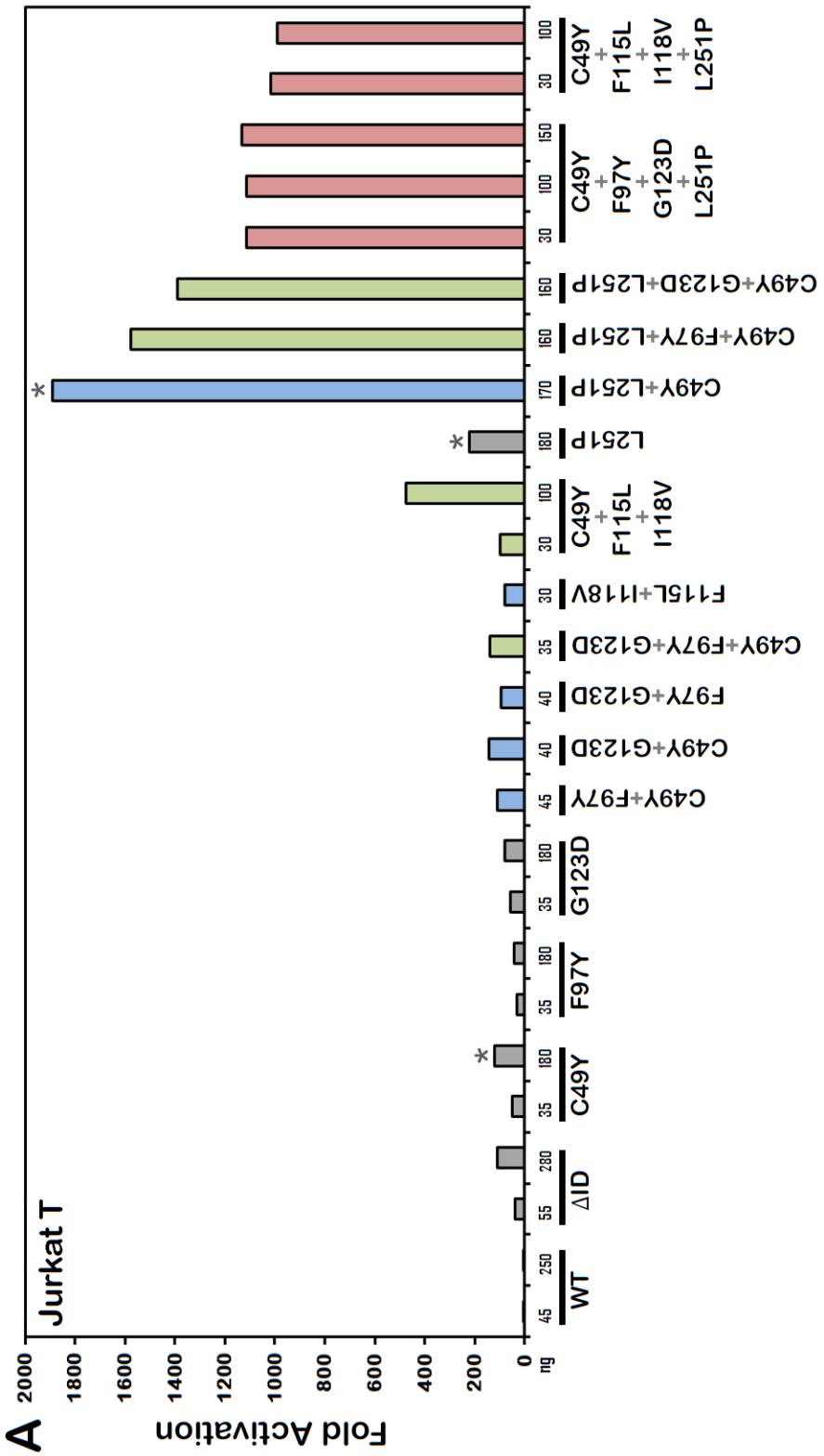
A
Fold Activation
Jurkat T
2000
1800
1600
1400
1200
1000
800
600
400
200
0
ng
WT
ΔID
C49Y
F97Y
G123D
C49Y+F97Y
C49Y+G123D
F97Y+G123D
C49Y+F97Y+G123D
F115L+I118V
C49Y+F115L+I118V
L251P
C49Y+L251P
C49Y+F97Y+L251P
C49Y+G123D+L251P
C49Y+F97Y+G123D+L251P
C49Y+F115L+I118V+L251P
*
*
*

Figure 3.2B

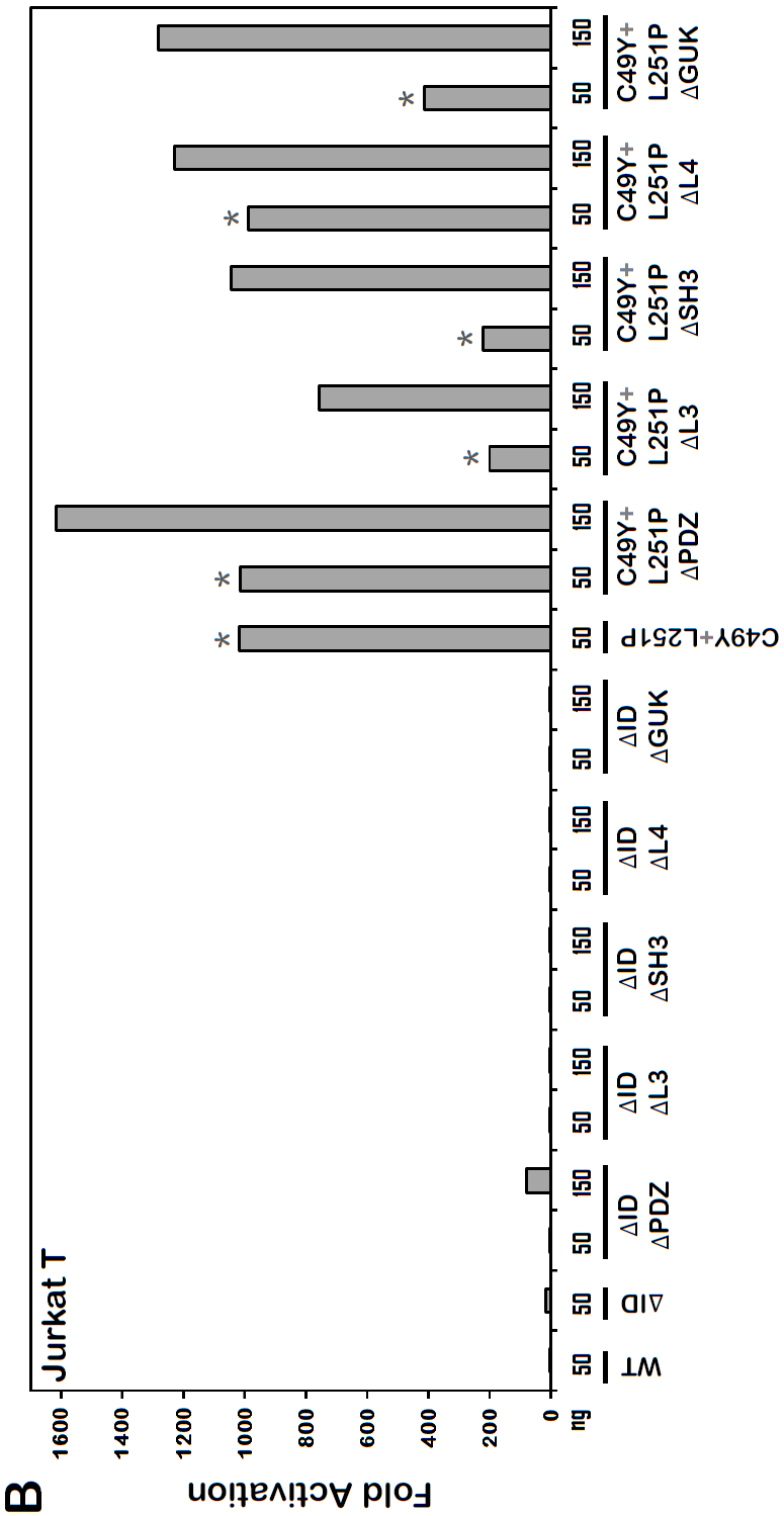
B
Jurkat T
Fold Activation
0
200
400
600
800
1000
1200
1400
1600
ng
WT
ΔID
ΔID ΔPDZ
ΔID ΔL3
ΔID ΔSH3
ΔID ΔL4
ΔID ΔGUK
C49Y+L251P
C49Y+ L251P ΔPDZ
C49Y+ L251P ΔL3
C49Y+ L251P ΔSH3
C49Y+ L251P ΔL4
C49Y+ L251P ΔGUK
50
150
*

Figure 3.3: Super-hyperactive mutant C49Y+L251P enhances the ability of CARD11 to associate with Bcl10 and MALT1, but not other signaling cofactors.

(A) HEK293T cells were transfected with 30 to 55 ng of expression vectors for the indicated myc-CARD11 variants and either 25 to 30 ng of FLAG-Bcl10, 250 to 300 ng of FLAG-MALT1, 50 to 60 ng of FLAG-TRAF6, 50 to 60 ng of FLAG-TAK1, 250 to 300 ng of FLAG-IKKγ, or 250 to 300 ng of FLAG-Caspase-8-C360S, as indicated. Anti-FLAG immunoprecipitations were performed as described in Experimental Procedures and analyzed by western blot with the indicated primary antibodies.

(B) HEK293T cells were transfected with 40 to 60 ng of expression vectors for the indicated myc-CARD11 variants and either 25 to 30 ng of FLAG-Bcl10, 250 to 300 ng of FLAG-MALT1, 250 to 300 ng of FLAG-TRAF2, 300 to 400 ng of untagged Bcl10 along with 500 to 600 ng of FLAG-MALT1 or FLAG-TRAF2, or 250 to 300 ng of FLAG-GAKIN, as indicated. Anti-FLAG immunoprecipitations were performed as described in Experimental Procedures and analyzed by western blot with the indicated primary antibodies.

Figure 3.3A

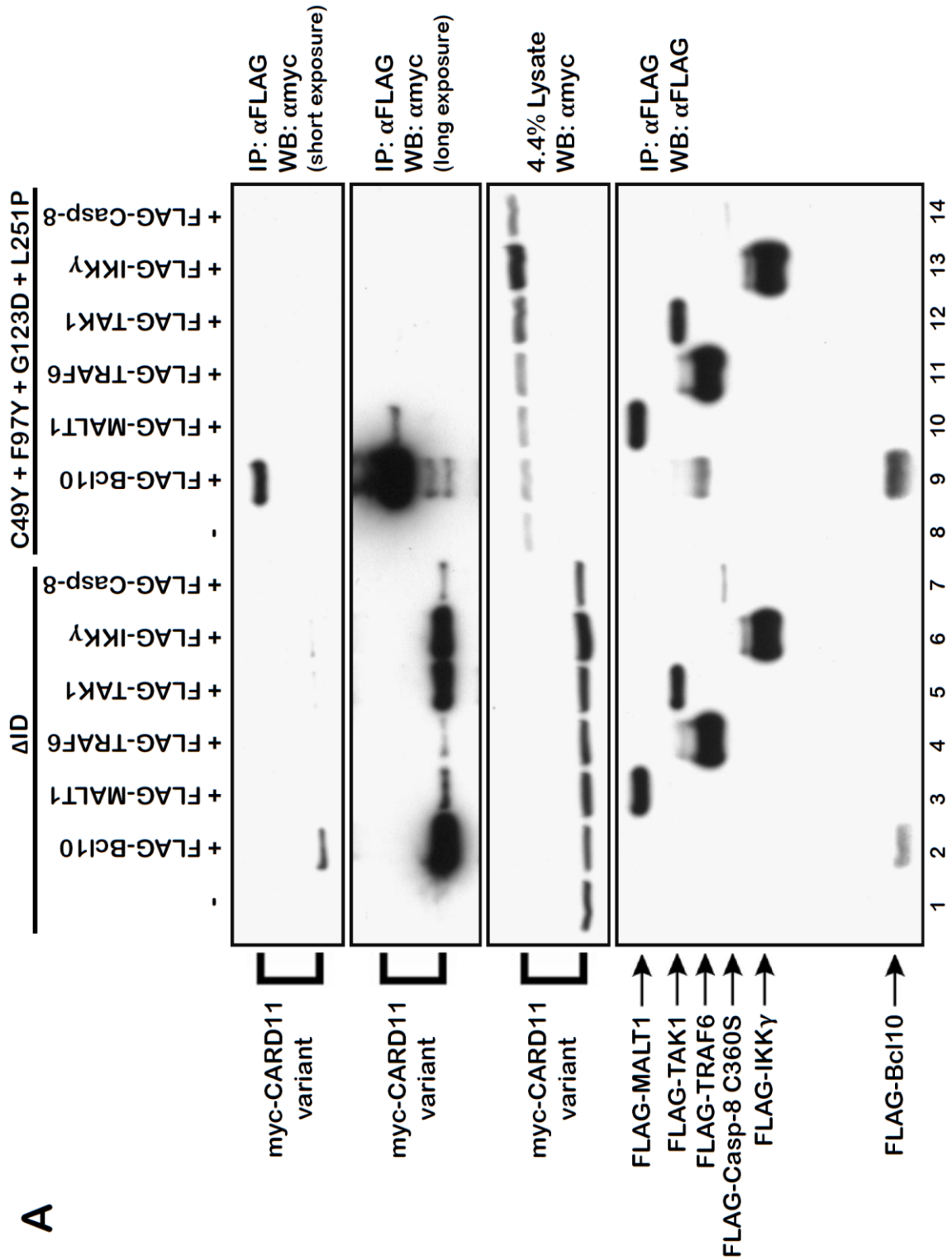
A
ΔID
C49Y + F97Y + G123D + L251P
- + FLAG-Bcl10 + FLAG-MALT1 + FLAG-TRAF6 + FLAG-TAK1 + FLAG-IKKγ + FLAG-Casp-8
- + FLAG-Bcl10 + FLAG-MALT1 + FLAG-TRAF6 + FLAG-TAK1 + FLAG-IKKγ + FLAG-Casp-8
IP: αFLAG WB: αmyc (short exposure)
IP: αFLAG WB: αmyc (long exposure)
4.4% Lysate WB: αmyc
IP: αFLAG WB: αFLAG
myc-CARD11 variant
myc-CARD11 variant
myc-CARD11 variant
FLAG-MALT1
FLAG-TAK1
FLAG-TRAF6
FLAG-Casp-8 C360S
FLAG-IKKγ
FLAG-Bcl10
1 2 3 4 5 6 7 8 9 10 11 12 13 14

Figure 3.3B

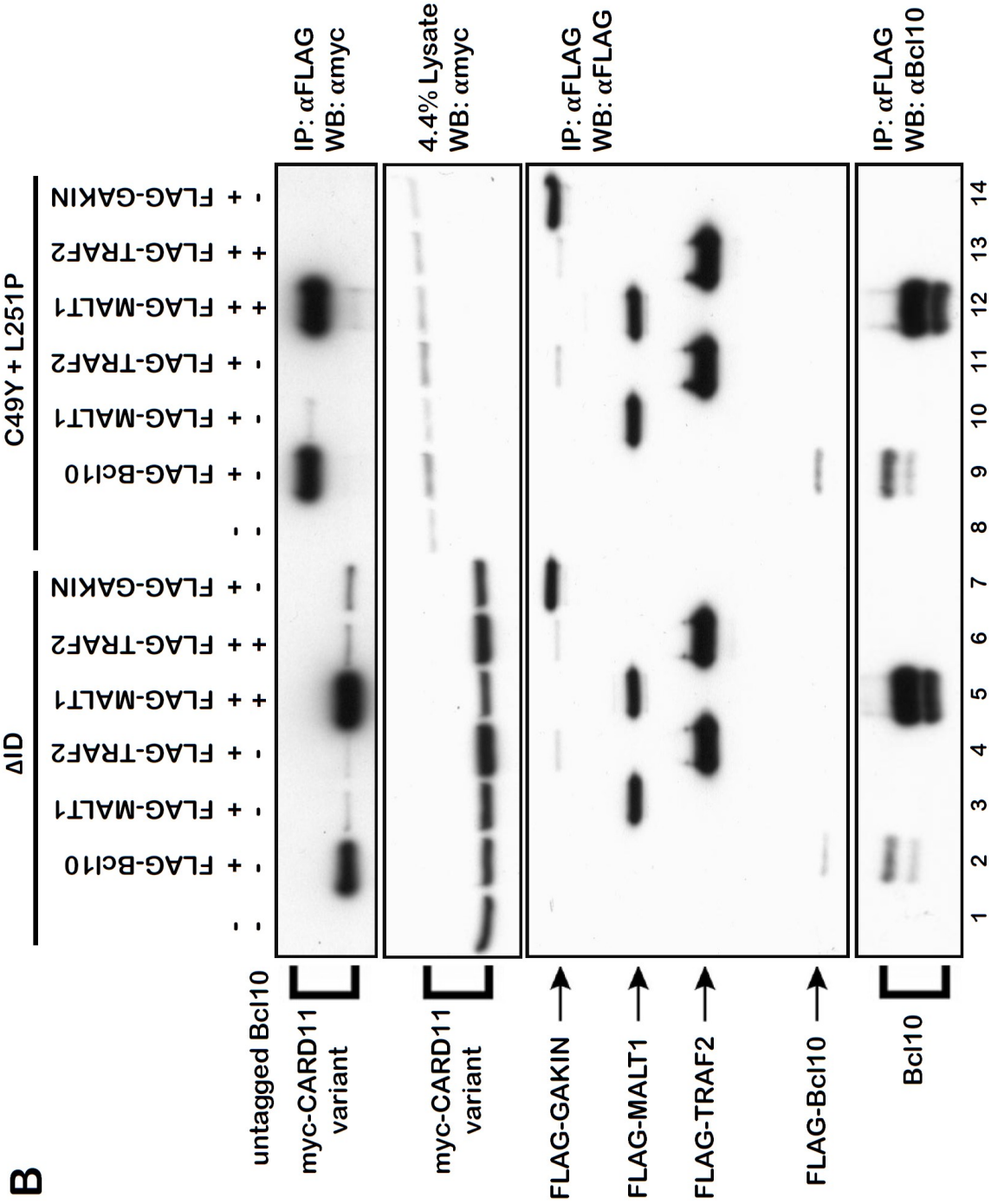
B
ΔID
C49Y + L251P
- - FLAG-Bcl10
- + FLAG-Bcl10
- + FLAG-MALT1
- + FLAG-TRAF2
+ + FLAG-MALT1
+ + FLAG-TRAF2
- + FLAG-GAKIN
- -
- + FLAG-Bcl10
- + FLAG-MALT1
- + FLAG-TRAF2
+ + FLAG-MALT1
+ + FLAG-TRAF2
- + FLAG-GAKIN
IP: αFLAG WB: αmyc
4.4% Lysate WB: αmyc
IP: αFLAG WB: αFLAG
IP: αFLAG WB: αBcl10
untagged Bcl10
myc-CARD11 variant
myc-CARD11 variant
FLAG-GAKIN
FLAG-MALT1
FLAG-TRAF2
FLAG-Bcl10
Bcl10
1 2 3 4 5 6 7 8 9 10 11 12 13 14

Figure 3.4: Several putative CARD11 signaling cofactors were identified through protein complex purification of the super-hyperactive CARD11 mutant C49Y+L251P.

HEK293T cells were transfected with 5 to 12 μg per 15-cm plate of expression vectors for the indicated myc-CARD11-Biotag variants and 1.2 μg per 15-cm plate of FLAG-BirA biotin ligase. Biotin pulldowns were performed as described in Experimental Procedures. NaCl and SDS elutions were collected sequentially as indicated, resolved by 10% SDS-PAGE, and detected by (A) silver stain or (B) colloidal blue stain. Gel slices containing protein bands of interest were identified by mass spectrometry. Data were analyzed as described in Experimental Procedures.

Figure 3.4A

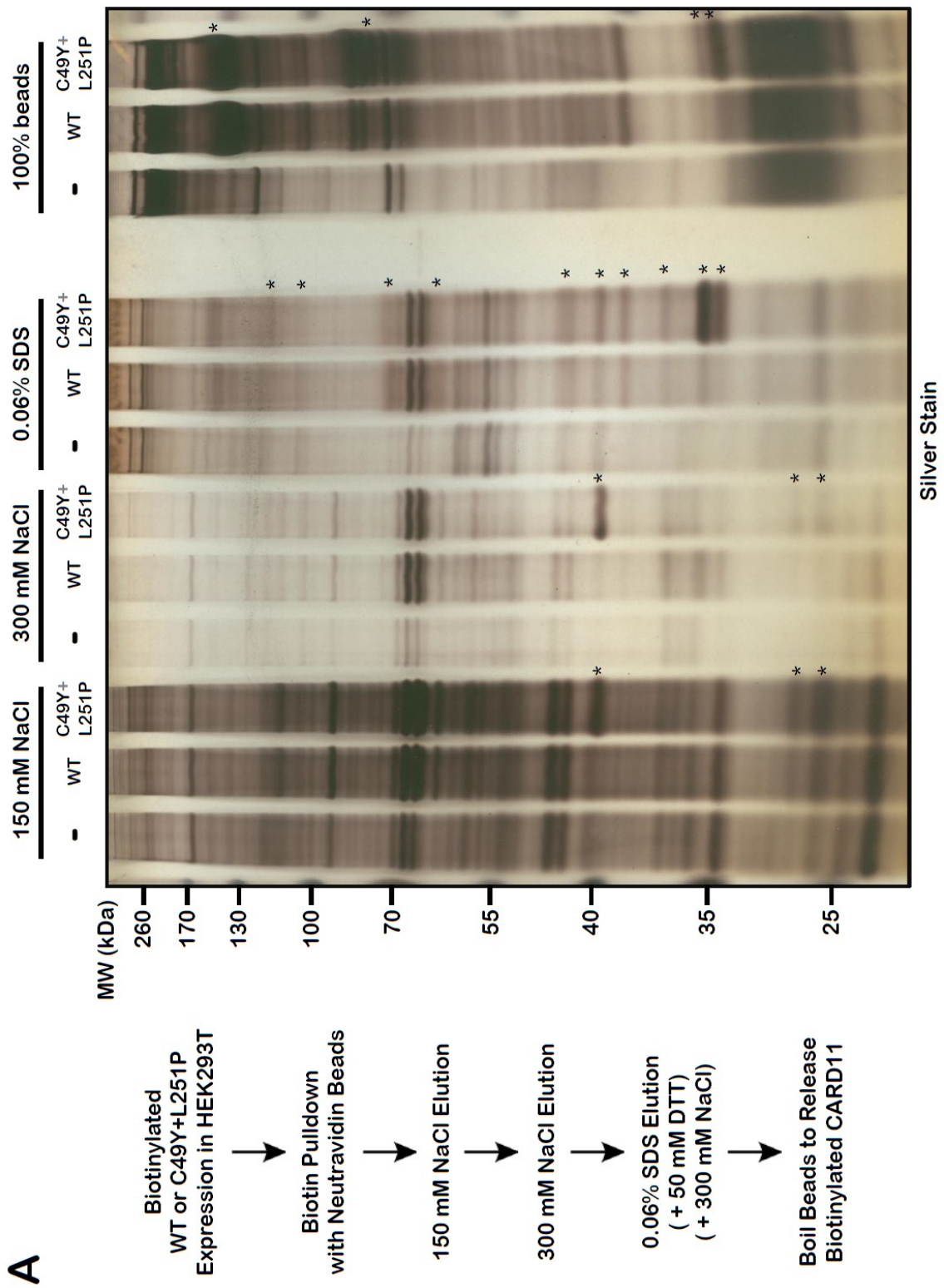
A
Biotinylated WT or C49Y+L251P Expression in HEK293T
Biotin Pulldown with Neutravidin Beads
150 mM NaCl Elution
300 mM NaCl Elution
0.06% SDS Elution (+ 50 mM DTT) (+ 300 mM NaCl)
Boil Beads to Release Biotinylated CARD11
MW (kDa)
260
170
130
100
70
55
40
35
25
150 mM NaCl
300 mM NaCl
0.06% SDS
100% beads
-
WT
C49Y+ L251P
Silver Stain

Figure 3.4B

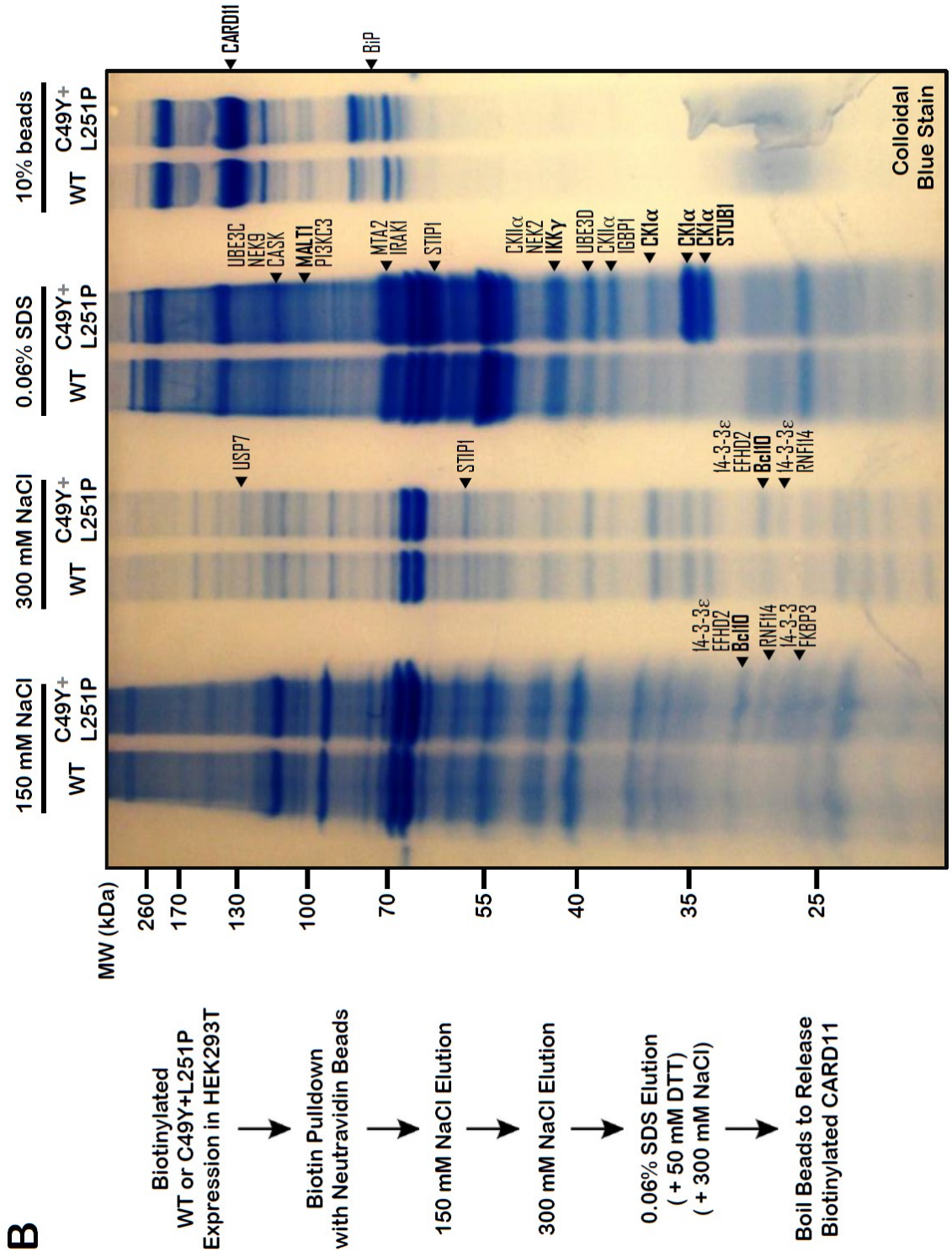
B
Biotinylated
WT or C49Y+L251P
Expression in HEK293T
Biotin Pulldown
with Neutravidin Beads
150 mM NaCl Elution
300 mM NaCl Elution
0.06% SDS Elution
(+ 50 mM DTT)
(+ 300 mM NaCl)
Boil Beads to Release
Biotinylated CARD11
MW (kDa)
260
170
130
100
70
55
40
35
25
150 mM NaCl
300 mM NaCl
0.06% SDS
10% beads
WT
C49Y+
L251P
CARD11
BiP
USP7
STIP1
UBE3C
NEK9
CASK
MALT1
PI3KC3
MTA2
IRAK1
CKIIα
NEK2
IKKγ
UBE3D
IGBP1
CKIα
STUBI
14-3-3ε
EFHD2
Bcl10
RNF114
14-3-3
FKBP3
Colloidal
Blue Stain

Chapter IV:

Discussion

Hyperactive CARD11 Mutations in the CARD and LATCH Domains

CARD11-mediated antigen receptor signaling to NF-κB is a critical pathway for normal lymphocyte activation and proliferation. As the activation level of NF-κB needs to be exquisitely tuned by the immune system in order to prevent chaotic malfunction in either direction, an intricate network of both positive and negative regulation has evolved to protect the host from diseases. During normal signaling, CARD11 is regulated by its conformational transition between a closed, inactive state and an open, active scaffold. This transition of CARD11 is dysregulated by lymphoma-associated CARD11 mutations that induce spontaneous signaling. Since almost all of the identified mutations were located within the Coiled-coil domain, we conducted a high-throughput quantitative signaling screen and identified new CARD11 hyperactive variants in both the CARD and LATCH domains. Mechanistic characterization suggest that these gain-of-function mutations disrupt the autoinhibitory ID domain binding, promote Bcl10 association and K63-linked polyubiquitination, NF-κB activation, and human lymphoma cell survival.

The main conclusion that emerges from our data is that the intramolecular regulation of CARD11 that allows for its signal-dependent activation by antigen receptor signaling also results in a vulnerability to mutation that can be exploited by lymphomas to bypass normal controls and induce NF-κB and its pro-proliferative and anti-apoptotic target genes. Our data clearly suggest that hyperactive CARD11 mutations can also emerge in domains outside of the Coiled-coil domain by disrupting the CARD-Coiled-coil-ID autoinhibitory binding. Based on our current working model of the CARD11 scaffold transition, we should be able to identify

hyperactive mutations within the ID domain by the same token. However, we have not yet been able to identify any missense mutation in the ID domain by the random mutagenesis approach, and lymphoma-associated oncogenic ID mutation has never been identified there either. The absence of hyperactive ID domain mutations conflicts with our current model of CARD11 scaffold transition and suggests that a major revision of this simple model is necessary.

Unexpectedly, our screening also identified a surprisingly high density of mutations in the LATCH domain, a short nineteen-residue region between the CARD and Coiled-coil that plays a significant role in autoinhibition by the ID. It is currently unclear how the LATCH domain participates in the CARD-Coiled-coil-ID intramolecular interaction and autoinhibitory function. Interestingly, the S116 and T117 residues within the LATCH domain have been shown to serve as substrates for phosphorylation by CaMKII (55) and PKCβ (25) respectively.

Our data emphasize the importance of K63-linked polyubiquitinated Bcl10 as a signaling intermediate whose accumulation is dysregulated by hyperactive CARD11 mutants and correlates with the enhanced recruitment of unconjugated Bcl10 to hyperactive CARD11 mutants. During normal antigen receptor signaling, K63-linked polyubiquitinated Bcl10 is induced only transiently (22), and is rapidly removed by negative feedback mechanisms that serve to terminate signaling (41–43). It is clear that in order to fully understand how both normal and dysregulated CARD11 signaling occurs, further studies are necessary to identify the E3 ligase that ubiquitinates Bcl10 through K63-linkages, explain how the association with CARD11

promotes this modification, and elucidate how exactly Ub_n(K63)-Bcl10 activates IKK kinase activity.

Although none of the hyperactive CARD or LATCH domain mutations showed enhanced recruitment of MALT1, TRAF6, and TAK1 cofactors to CARD11, the six most hyperactive variants tested did require MALT1, TRAF6, and TAK1 for signaling to NF-κB. These cofactors have been shown by other groups to be required for IKK kinase induction downstream of antigen receptor engagement. MALT1 is required for K63-linked ubiquitination of Bcl10 (22), and has also been implicated in K63-linked ubiquitination of IKKγ (44). TRAF6 also contributes to IKKγ K63-linked ubiquitination (30), but does not appear to be required for the induction of K63-linked ubiquitination of Bcl10. TAK1 has been shown to mediate IKK kinase subunit phosphorylation during signaling (40). An alternative dysregulation mechanism of hyperactive CARD11 variants can be achieved through reduced association with inhibitory cofactors such as GAKIN (29). Preliminary data suggest that several hyperactive CARD11 variants tested did indeed reduce their association with GAKIN, as compared to the wild-type CARD11 control in a coimmunoprecipitation assay in HEK293T cells. This observation is consistent with our previous finding that GAKIN can compete with Bcl10 for binding sites in both the CARD and Coiled-coil domains upon PMA/ionomycin stimulation.

Most of the hyperactive variants that we tested had enough enhanced activity to promote the proliferation and survival of the ABC DLBCL-derived OCI-Ly3 line in culture, indicating their oncogenic potential in human lymphoma cells. In fact, while our work was in progress, several studies reported the presence of CARD11

mutations in the CARD and LATCH domains in human biopsies of DLBCL, which provide further validation of our screening approach. Interestingly, six of these are identical to mutations that we isolated in our screen, and four other reported mutations occur at the same position as those we found in our screen, but mutated to different residues. Although these studies did not demonstrate a functional effect of the mutations in the context of the cancers in which they were sequenced, our data provide a mechanistic characterization that can explain how the substitutions could lead to dysregulated NF-κB activity and promote proliferation and survival.

We can easily expand our quantitative high-throughput screen to detect other hyperactive variants in other domains of CARD11 such as the Coiled-coil domain. Our modular screening approach makes it straightforward to substitute the target protein that undergoes mutation and screening, which allows for the efficient discovery of hyperactive variants that emerge in the other proteins (such as MyD88, CD79A or CD79B) and contribute to the oncogenesis of NF-κB-dependent cancers. By replacing the NF-κB reporter with that of another transcription factor, the screen could readily be adopted to identify variants of other gene regulators that promote tumorigenesis in other cell types.

In summary, our results identify hyperactive CARD11 mutations with oncogenic potential, provide a mechanistic explanation for their signaling potency, and offer a straightforward method for the discovery of variants that promote the tumorigenesis of NF-κB-dependent lymphomas.

Super-hyperactive Mutant and Putative Regulators of the CBM Complex

In order to fully understand how both normal and dysregulated CARD11 signaling occurs, we conducted further studies to identify the specific E3 ligase that ubiquitinates Bcl10 through K63-linkages. Several E3 ubiquitin ligases including TRAF6, TRAF2, MIB2, and STUB1 have previously been shown to associate with CARD11 or Bcl10 upon antigen receptor signaling. Our data suggest that TRAF2 and TAK1, but not TRAF6, are required for the induction of K63-linked ubiquitination of Bcl10. However, we have not yet examined the requirement of MIB2 and STUB1 for the induction of Ub_n(K63)-Bcl10. According to previous reports, TRAF2 could associate with the CARD domain of Bcl10 and the C-terminal domain of MALT1, although it is unclear whether these interactions were direct or mediated by other endogenous bridging factors. As MALT1 is required for the induction of Ub_n(K63)-Bcl10 and constitutively associated with Bcl10, it is possible that MALT1 could serve as a bridging cofactor that helps recruit TRAF2 to Bcl10. Nevertheless, it remains possible that TRAF2 and TAK1 function to activate another unidentified ubiquitin E3 ligase that functions directly to catalyze the conjugation of K63-linked ubiquitin chain on Bcl10 during normal antigen receptor signaling.

The identification of an extremely potent double oncogenic CARD11 mutant C49Y+L251P suggests that the hyperactivity of ΔID is far below the maximum potential of CARD11. However, we are aware that the hyperactivity of this super mutant is transient and subjected to strong negative feedback mechanisms in Jurkat T cells, as indicated by much less NF-κB activation in cells stably expressing the C49Y+L251P variant. Imaging data show that the localization of this super mutant

tends to adopt a punctate pattern with lower protein expression, as compared to the wild-type, C49Y, and L251P controls. Interestingly, cytosolic CK1α has been shown to reorganized into punctate structures that colocalized with CD3 clusters upon TCR activation (50). Our cofactor purification data also identified CK1α as the major dysregulation target of the C49Y+L251P super mutant. As CK1α has been shown to confer a dual 'gating' function which first promotes and then terminates receptor-induced NF-κB activation, this kinase could serve as a negative feedback mechanism to downmodulate the super-hyperactive signaling of the C49Y+L251P variant in the long run, presumably to protect lymphocytes from the toxic side effects of over-activation. Further studies are necessary to clarify the molecular details of CK1α action on CARD11 during normal antigen receptor and dysregulated lymphoma signaling to NF-κB.

Although deleting any one of the C-terminal domains of CARD11 (L3, SH3, L4 and GUK) in the context of the C49Y+L251P super mutant failed to completely abolish its hyperactivity, it is unclear whether all of these C-terminal domains are simply dispensable for the hyperactive signaling of this super mutant. If that turns out to be true, it would suggest that a C-terminal truncated mini-CARD11 could still assemble into an active scaffold for signal relay. Further study is also needed to determine whether the LATCH domain, the CARD-Coiled-coil linker, is absolutely required for the hyperactive signaling of the C49Y+L251P variant.

Even with much weaker activity as compared to the C49Y+L251P super mutant, the ΔID variant remains to be better at recruiting signaling cofactors. The discrepancy between signaling activity and cofactor binding suggests that the ID

domain probably harbors critical activation and cofactor association domains that are both deleted in the ΔID variant. It would be interesting to perform similar cofactor binding studies with a ΔID variant in which the C49Y and L251P mutations are incorporated, and test whether this ID-deleted super mutant could maintain its signaling capacity to activate NF-κB even in the absence of the ID domain.

It remains to be seen whether the enhanced binding of CK1α is dysregulated specifically by the L251P Coiled-coil mutation and not by the C49Y CARD mutation. As CK1α depends on the Coiled-coil and ID domain for association with CARD11, it would be more consistent that the L251P but not the C49Y mutation could function to expose CK1α binding sites within the Coiled-coil domain for association, possibly through disruption of the Coiled-coil-ID autoinhibitory binding. This would be in parallel with the C49Y mutation which is known to enhance Bcl10 association through disrupting the CARD-ID autoinhibitory binding. This would also help explain the synergy between the C49Y and the L251P mutations, since they may combine at least two positive non-overlapping mechanisms to maximize the signaling capacity of CARD11. Interestingly, our recent data have confirmed that the enhanced CK1α recruitment to the C49Y+L251P variant occurred even in Bcl10 knocked-out Jurkat T cells, suggesting that CK1α is capable of interacting with CARD11 in a different CARD11 complex upstream of the formation of the CBM complex. It would be informative to examine whether CK1α recruitment to CARD11 during normal antigen receptor signaling requires the activity of PKCθ or PKCβ.

Our protein complex purification method from mammalian cell lysates is highly efficient as the Biotag peptide allows for almost complete recovery of the bait

protein during a short incubation time with the Neutravidin resin. The method also does not require the addition of excessive amount of antibodies and therefore helps eliminate some interfering protein bands in the background and results in more sensitive detection of differential protein bands. The strong interaction between biotin and Neutravidin ($K_d = 10^{-15}$ M) makes the biotinylated bait protein resistant to harsh elution conditions and thereby enables the separation of prey proteins from the abundant biotinylated bait proteins on the resin.

In summary, our results identify critical components during the assembly of K63-linked polyubiquitination of Bcl10, a novel super-hyperactive CARD11 mutant that synergizes dysregulation mechanisms from both the CARD and the Coiled-coil domains, and several putative protein regulators of the CARD11 scaffold complex that are potentially dysregulated by oncogenic CARD11 mutations in human DLBCL.

References

1. Ghosh S, Hayden M. Celebrating 25 years of NF-κB research. Immunol Rev. 2012;246(1):5–13.

2. Ghosh G, Wang VY-F, Huang D-B, Fusco A. NF-κB regulation: lessons from structures. Immunol Rev. 2012 Mar;246(1):36–58.

3. Liu F, Xia Y, Parker AS, Verma IM. IKK biology. Immunol Rev. 2012 Mar;246(1):239–53.

4. Jiang C, Lin X. Regulation of NF-κB by the CARD proteins. Immunol Rev. 2012 Mar;246(1):141–53.

5. Kaileh M, Sen R. NF-κB function in B lymphocytes. Immunol Rev. 2012 Mar;246(1):254–71.

6. Egawa T, Albrecht B, Favier B, Sunshine M-J, Mirchandani K, O'Brien W, et al. Requirement for CARMA1 in antigen receptor-induced NF-κB activation and lymphocyte proliferation. Curr Biol. 2003;13:1252–8.

7. Gaide O, Favier B, Legler DF, Bonnet D, Brissoni B, Valitutti S, et al. CARMA1 is a critical lipid raft–associated regulator of TCR-induced NF-κB activation. Nat Immunol. 2002;3(9):836–43.

8. Hara H, Wada T, Bakal C, Kozieradzki I, Suzuki S, Suzuki N, et al. The MAGUK Family Protein CARD11 Is Essential for Lymphocyte Activation. Immunity. 2003;18:763–75.

9. Jun JE, Wilson LE, Vinuesa CG, Lesage S, Blery M, Miosge LA, et al. Identifying the MAGUK Protein Carma-1 as a Central Regulator of Humoral Immune Responses and Atopy by Genome-Wide Mouse Mutagenesis. Immunity. 2003;18:751–62.

10. Newton K, Dixit V. Mice lacking the CARD of CARMA1 exhibit defective B lymphocyte development and impaired proliferation of their B and T lymphocytes. Curr Biol. 2003;13:1247–51.

11. Pomerantz J, Denny E, Baltimore D. CARD11 mediates factor-specific activation of NF-κB by the T cell receptor complex. EMBO J. 2002;21(19):5184–94.

12. Wang D, You Y, Case SM, McAllister-Lucas LM, Wang L, DiStefano PS, et al. A requirement for CARMA1 in TCR-induced NF-kappa B activation. Nat Immunol. 2002 Sep;3(9):830–5.

13. McCully R, Pomerantz J. The protein kinase C-responsive inhibitory domain of CARD11 functions in NF-κB activation to regulate the association of multiple signaling cofactors that differentially depend on Bcl10 and MALT1 for association. Mol Cell Biol. 2008;28(18):5668–86.

14. Matsumoto R, Wang D, Blonska M, Li H, Kobayashi M, Pappu B, et al. Phosphorylation of CARMA1 Plays a Critical Role in T Cell Receptor-Mediated NF-κB Activation. Immunity. 2005;23:575–85.

15. Sommer K, Guo B, Pomerantz JL, Bandaranayake AD, Ovechkina YL, Moreno-garcı ME, et al. Phosphorylation of the CARMA1 Linker Controls NF-κB Activation. Immunity. 2005;23:561–74.

16. Thome M, Charton JE, Pelzer C, Hailfinger S. Antigen receptor signaling to NF-kappaB via CARMA1, BCL10, and MALT1. Cold Spring Harb Perspect Biol. 2010 Sep;2(9):a003004.

17. Wegener E, Oeckinghaus A, Papadopoulou N, Lavitas L, Schmidt-Supprian M, Ferch U, et al. Essential role for IkappaB kinase beta in remodeling Carma1-Bcl10-Malt1 complexes upon T cell activation. Mol Cell. 2006 Jul 7;23(1):13–23.

18. Lim K, Yang Y, Staudt L. Pathogenetic importance and therapeutic implications of NF-κB in lymphoid malignancies. Immunol Rev. 2012;246:359–78.

19. Rosenwald A, Staudt LM. Gene Expression Profiling of Diffuse Large B-Cell Lymphoma. Leuk Lymphoma. 2003 Nov;44(S3):S41–S47.

20. Lenz G, Davis RE, Ngo VN, Lam L, George TC, Wright GW, et al. Oncogenic CARD11 mutations in human diffuse large B cell lymphoma sup. Science. 2008 Mar 21;319(5870):1676–9.

21. Lamason R, McCully R, Lew S, Pomerantz J. Oncogenic CARD11 mutations induce hyperactive signaling by disrupting autoinhibition by the PKC-responsive inhibitory domain. Biochemistry. 2010;49(38):8240–50.

22. Wu C, Ashwell J. NEMO recognition of ubiquitinated Bcl10 is required for T cell receptor-mediated NF-κB activation. Proc Natl Acad Sci U S A. 2008;105(8):3023–8.

23. Schulze-Luehrmann J, Ghosh S. Antigen-receptor signaling to nuclear factor kappa B. Immunity. 2006 Nov;25(5):701–15.

24. Staudt L. Oncogenic activation of NF-κB. Cold Spring Harb Perspect Biol. 2010;2:a000109.

25. Shinohara H, Maeda S, Watarai H, Kurosaki T. IkappaB kinase beta-induced phosphorylation of CARMA1 contributes to CARMA1 Bcl10 MALT1 complex formation in B cells. J Exp Med. 2007;204(13):3285–93.

26. Davis RE, Brown KD, Siebenlist U, Staudt LM. Constitutive nuclear factor kappaB activity is required for survival of activated B cell-like diffuse large B cell lymphoma cells. J Exp Med. 2001 Dec 17;194(12):1861–74.

27. Ngo V, Davis R, Lamy L, Yu X, Zhao H. A loss-of-function RNA interference screen for molecular targets in cancer. Nature. 2006;441(May):1–5.

28. Lenz G, Davis RE, Ngo VN, Lam L, George TC, Wright GW, et al. Oncogenic CARD11 mutations in human diffuse large B cell lymphoma. Science. 2008;319(5870):1676–9.

29. Lamason RL, Kupfer A, Pomerantz JL. The Dynamic Distribution of CARD11 at the Immunological Synapse Is Regulated by the Inhibitory Kinesin GAKIN. Mol Cell. 2010;40(5):798–809.

30. Sun L, Deng L, Ea C-K, Xia Z-P, Chen ZJ. The TRAF6 ubiquitin ligase and TAK1 kinase mediate IKK activation by BCL10 and MALT1 in T lymphocytes. Mol Cell. 2004 May 7;14(3):289–301.

31. Naviaux RK, Costanzi E, Haas M, Verma IM. The pCL vector system: rapid production of helper-free, high-titer, recombinant retroviruses. J Virol. 1996 Aug;70(8):5701–5.

32. Naldini L, Blömer U, Gage FH, Trono D, Verma IM. Efficient transfer, integration, and sustained long-term expression of the transgene in adult rat brains injected with a lentiviral vector. Proc Natl Acad Sci U S A. 1996 Oct 15;93(21):11382–8.

33. Wu C, Conze DB, Li T, Srinivasula SM, Ashwell JD. Sensing of Lys 63-linked polyubiquitination by NEMO is a key event in NF-κB activation. Nat Cell Biol. 2006;8(4):398–406.

34. Takahashi K, Tanabe K, Ohnuki M, Narita M, Ichisaka T, Tomoda K, et al. Induction of pluripotent stem cells from adult human fibroblasts by defined factors. Cell. 2007 Nov 30;131(5):861–72.

35. Dull T, Zufferey R, Kelly M, Mandel RJ, Nguyen M, Trono D, et al. A third-generation lentivirus vector with a conditional packaging system. J Virol. 1998 Nov;72(11):8463–71.

36. Luo W, Wang Y, Reiser G. p24A, a type I transmembrane protein, controls ARF1-dependent resensitization of protease-activated receptor-2 by influence on receptor trafficking. J Biol Chem. 2007 Oct 12;282(41):30246–55.

37. Lamason RL, Lew SM, Pomerantz JL. Transcriptional target-based expression cloning of immunoregulatory molecules. Immunol Res. 2010 Jul;47(1-3):172–8.

38. Ruland J, Duncan GS, Elia a, del Barco Barrantes I, Nguyen L, Plyte S, et al. Bcl10 is a positive regulator of antigen receptor-induced activation of NF-kappaB and neural tube closure. Cell. 2001 Jan 12;104(1):33–42.

39. Ninomiya-Tsuji J, Kajino T, Ono K, Ohtomo T, Matsumoto M, Shiina M, et al. A resorcylic acid lactone, 5Z-7-oxozeaenol, prevents inflammation by inhibiting the catalytic activity of TAK1 MAPK kinase kinase. J Biol Chem. 2003 May 16;278(20):18485–90.

40. Shambharkar P, Blonska M, Pappu B. Phosphorylation and ubiquitination of the IκB kinase complex by two distinct signaling pathways. EMBO J. 2007;26(7):1794–805.

41. Lobry C, Lopez T, Israël A, Weil R. Negative feedback loop in T cell activation through IκB kinase-induced phosphorylation and degradation of Bcl10. Proc Natl Acad Sci U S A. 2007;104(3):908–13.

42. Scharschmidt E, Wegener E, Heissmeyer V, Rao A, Krappmann D. Degradation of Bcl10 induced by T-cell activation negatively regulates NF-κB signaling. Mol Cell Biol. 2004;24(9):3860–73.

43. Zeng H, Di L, Fu G, Chen Y, Gao X, Xu L, et al. Phosphorylation of Bcl10 negatively regulates T-cell receptor-mediated NF-kappaB activation. Mol Cell Biol. 2007 Jul;27(14):5235–45.

44. Zhou H, Wertz I, Rourke KO, Ultsch M, Seshagiri S, Eby M, et al. Bcl10 activates the NF-κB pathway through ubiquitination of NEMO. Nature. 2004;427:167–71.

45. Compagno M, Lim WK, Grunn A, Nandula S V., Brahmachary M, Shen Q, et al. Mutations of multiple genes cause deregulation of NF-κB in diffuse large B-cell lymphoma. Nature. 2009;459:717–21.

46. Lohr JG, Stojanov P, Lawrence MS, Auclair D, Chapuy B, Sougnez C, et al. Discovery and prioritization of somatic mutations in diffuse large B-cell lymphoma (DLBCL) by whole-exome sequencing. Proc Natl Acad Sci U S A. 2012 Feb 17;109:3879–84.

47. Montesinos-rongen M, Schmitz R, Brunn A, Gesk S, Richter J, Hong K, et al. Mutations of CARD11 but not TNFAIP3 may activate the NF-κB pathway in primary CNS lymphoma. Acta Neuropathol. 2010;120:529–35.

48. Bu R, Bavi P, Abubaker J, Jehan Z, Al-Haqawi W, Ajarim D, et al. Role of nuclear factor-κB regulators TNFAIP3 and CARD11 in Middle Eastern diffuse large B-cell lymphoma. Leuk Lymphoma. 2012 Oct;53(10):1971–7.

49. Dong G, Chanudet E, Zeng N, Appert A, Chen Y-W, Au W-Y, et al. A20, ABIN-1/2, and CARD11 mutations and their prognostic value in gastrointestinal diffuse large B-cell lymphoma. Clin Cancer Res. 2011 Mar 15;17(6):1440–51.

50. Bidère N, Ngo VN, Lee J, Collins C, Zheng L, Wan F, et al. Casein kinase 1alpha governs antigen-receptor-induced NF-kappaB activation and human lymphoma cell survival. Nature. 2009 Mar 5;458(7234):92–6.

51. So T, Soroosh P, Eun S-Y, Altman A, Croft M. Antigen-independent signalosome of CARMA1, PKCθ, and TNF receptor-associated factor 2 (TRAF2) determines NF-κB signaling in T cells. Proc Natl Acad Sci U S A. 2011 Feb 15;108(7):2903–8.

52. Brenner D, Brechmann M, Rohling S, Tapernoux M, Mock T, Winter D, et al. Phosphorylation of CARMA1 by HPK1 is critical for NF-κB activation in T cells. Proc Natl Acad Sci U S A. 2009;106(34):14508–13.

53. Eitelhuber AC, Warth S, Schimmack G, Düwel M, Hadian K, Demski K, et al. Dephosphorylation of Carma1 by PP2A negatively regulates T-cell activation. EMBO J. 2011 Feb 2;30(3):594–605.

54. Narayan P, Holt B, Tosti R, Kane LP. CARMA1 Is Required for Akt-Mediated NF-κB Activation in T Cells. Mol Cell Biol. 2006;26(6):2327–36.

55. Ishiguro K, Green T, Rapley J, Wachtel H, Giallourakis C, Landry A, et al. Ca2+/calmodulin-dependent protein kinase II is a modulator of CARMA1-mediated NF-kappaB activation. Mol Cell Biol. 2006 Jul;26(14):5497–508.

56. Ishiguro K, Ando T, Goto H, Xavier R. Bcl10 is phosphorylated on Ser138 by Ca2+/calmodulin-dependent protein kinase II. Mol Immunol. 2007 Mar;44(8):2095–100.

57. Welteke V, Eitelhuber A, Düwel M, Schweitzer K, Naumann M, Krappmann D. COP9 signalosome controls the Carma1-Bcl10-Malt1 complex upon T-cell stimulation. EMBO Rep. 2009 Jun;10(6):642–8.

58. Stempin CC, Chi L, Giraldo-vela JP, High AA, Redecke V. The E3 Ubiquitin Ligase Mind Bomb-2 (MIB2) Protein Controls B-cell CLL / Lymphoma 10 (BCL10) -dependent NF-κB. J Biol Chem. 2011;286(43):37147–57.

59. Wang S, Li Y, Hu Y-H, Song R, Gao Y, Liu H-Y, et al. STUB1 is essential for T-cell activation by ubiquitinating CARMA1. Eur J Immunol. 2013 Apr;43(4):1034–41.

60. Zhang W, Zhang X, Wu X, He L, Zeng X, Grammer AC, et al. Competition between TRAF2 and TRAF6 Regulates NF-κB Activation in Human B Lymphocytes. Chinese Med Sci J. Chinese Academy Medical Sciences; 2010 Mar;25(1):1–12.

61. Chan W, Schaffer TB, Pomerantz JL. A quantitative signaling screen identifies CARD11 mutations in the CARD and LATCH domains that induce Bcl10 ubiquitination and human lymphoma cell survival. Mol Cell Biol. 2013 Jan;33(2):429–43.

62. Kulman JD, Satake M, Harris JE. A versatile system for site-specific enzymatic biotinylation and regulated expression of proteins in cultured mammalian cells. Protein Expr Purif. 2007 Apr;52(2):320–8.

63. Candiano G, Bruschi M, Musante L, Santucci L, Ghiggeri GM, Carnemolla B, et al. Blue silver: a very sensitive colloidal Coomassie G-250 staining for proteome analysis. Electrophoresis. 2004 May;25(9):1327–33.

64. Yoneda T. Regulatory Mechanisms of TRAF2-mediated Signal Transduction by Bcl10, a MALT Lymphoma-associated Protein. J Biol Chem. 2000 Apr 6;275(15):11114–20.

65. Uren a G, O'Rourke K, Aravind L a, Pisabarro MT, Seshagiri S, Koonin E V, et al. Identification of paracaspases and metacaspases: two ancient families of caspase-like proteins, one of which plays a key role in MALT lymphoma. Mol Cell. 2000 Oct;6(4):961–7.

66. Sakamoto T, Kobayashi M, Tada K, Shinohara M, Io K, Nagata K, et al. CKIP-1 Is an Intrinsic Negative Regulator of T-Cell Activation through an Interaction with CARMA1. PLoS One. 2014 Jan 17;9(1):e85762.

CURRICULUM VITAE FOR Ph.D. CANDIDATES

The Johns Hopkins University School of Medicine

Waipan Chan

March 2014

Educational History

Ph.D.	2014	Program in Immunology Mentor: Joel Pomerantz, Ph.D.	Johns Hopkins School of Medicine
B.S.	2007	Biochemistry	Binghamton University – SUNY

Other Professional Experience

Research Rotation	2008	Lab of Jonathan Powell, M.D., Ph.D. Johns Hopkins School of Medicine
Summer Scholars Program	2006	Lab of Paul Brookes, Ph.D. University of Rochester Medical Center
Undergraduate Research	2005-2007	Lab of Chuan-Jian Zhong, Ph.D. Binghamton University – SUNY

Scholarships, fellowships, or other external funding

Summer Research Fellowship (University of Rochester Medical Center), 2006, $4000, stipend support

Undergraduate Student Scholarship (DSEJ Macau SAR Government), 2005-2007, $6000, stipend support

Dean's Undergraduate Research Awards (Binghamton University), 2005-2007, $1000, research support

Academic and other honors at Hopkins and elsewhere

2013	The 8th Annual NGSRC Program	National Institute of Health
2007	*summa cum laude*	Binghamton University
2006	Award for Excellence in Biochemistry	Binghamton University
2006	The PHI BETA KAPPA Society	Binghamton University
2004	CRC Freshman Chemistry Award	Binghamton University
2003-2007	Dean's List	Binghamton University

Publications, peer-reviewed

Chan W, Schaffer TB, Pomerantz JL (2013) A quantitative signaling screen identifies CARD11 mutations in the CARD and LATCH domains that induce Bcl10 ubiquitination and human lymphoma cell survival. *Molecular and Cellular Biology* 33(2): 429-443.

Zheng Y, Delgoffe GM, Meyer CF, **Chan W**, Powell JD (2009) Anergic T cells are metabolically anergic. *Journal of Immunology* 183(10): 6095-6101.

Mott D, Luo J, Smith A, **Chan W**, Bozza W, Sarkhel A, Park S, Zhong CJ (2006) Silica-supported Au and Pt nanoparticles and CO adsorption. *MRS Proceedings* 0900: O01-06.1-6.

Posters, abstracts, etc.

Chan W, Pomerantz JL (2013) Molecular mechanisms of mutant CARD11 signaling to NF-κB in human DLBCL. The 8th Annual National Graduate Student Research Conference, Bethesda, MD, October 6-8, 2013.

Chan W, Mott D, Lim SI, Luo J, Zhong CJ (2006) AFM and IRS studies of assembly of amino acids and nanoparticles on surfaces. The 34th Northeast Regional Meeting, Binghamton, NY, October 5-7, 2006.

Chan W, Burwell L, Nadtochiy S, Brookes PS (2006) Protective mechanism of a mitochondrial S-nitrosating agent. GEBS Summer Scholars Program, Rochester, NY, August 3, 2006.

Service and leadership

2011 Teaching Assistant for Cell Physiology, Scientific Foundations of Medicine, Johns Hopkins School of Medicine